

DEVELOPMENT OF NOVEL SURFACES FOR ENHANCEMENT OF SENSITIVITY
AND SELECTIVITY WITH CARBON FIBER ELECTRODES

By

ROBERTO BRAVO

A DISSERTATION PRESENTED TO THE GRADUATE SCHOOL
OF THE UNIVERSITY OF FLORIDA IN PARTIAL FULFILLMENT
OF THE REQUIREMENTS FOR THE DEGREE OF
DOCTOR OF PHILOSOPHY

UNIVERSITY OF FLORIDA

1999

I dedicate this work and dissertation to the memory of my wonderful sister Gloria Inés and to my family and fiancé who have unconditionally encouraged and supported me throughout all these years.

ACKNOWLEDGMENTS

I would like to express my sincere gratitude to my research advisor, Dr. Anna Brajter-Toth, for her guidance and assistance. I would also like to thank my group mates who graduated before me especially Charlie Hsueh, Quan Cheng, Lisa Spurlock, and Merle Regino for their words of hope, their teaching and friendship. Also, I would like to acknowledge the friendship and assistance of my other group members, Tianyi Zhang and Kholoud Mohammed El-Noor. I would like to give my sincere appreciation to Dr. Alonso Jaramillo and Dr. Eder Cavalheiro for their friendship and encouragement in the past few years. I would also like to give my sincere gratitude and appreciation to Dawn Stickle for her enormous assistance on my research and her friendship.

I would like to thank Dr. Jim Winefordner, Dr. Vaneica Young, Dr. John Reynolds, and Dr. Paul Holloway for the time and willingness to serve on my committee. I would also like to thank Jeanne Karably and Donna Balkcom for making my life easier during all these years.

Many thanks to Dr. Kathryn Williams for her support and for sharing with me her philosophy of research and teaching. A special thanks goes to Russ Pierce for all his help fixing and sharing his instruments.

I would like to express my sincere gratitude to Kathryn Kidder, coordinator of the Academic Spoken English program at the University of Florida, for her constant dedication and effort to improve my English when I was taking English classes.

I would like to acknowledge the past and present Colombian chemistry students in this department especially Fernando Gómez, Carlos Martínez, Andres Reyes, Rogelio Ocampo, Rodrigo Abonía, Nora Restrepo, Fernando Larmat, Fabio Zuluaga, for their support and friendship. Having a colombian group away from home has been vital to my sanity during these years. Many thanks to Alvaro Pérez Alvarez (my general chemistry teacher, mentor, and friend in high school in Colombia) for giving and selling me the crazy idea of pursuing a Ph. D. someday.

My greatest appreciation and gratitude goes to my mothers, Maria Teresa Cárdenas, Gloria I. Cárdenas, and Dilia Arciniegas, for always encouraging me to take the next step and for their support. My appreciation to my brothers, Laureano, Humberto, Manuel, and Carlos, and to my sister Beatriz for their moral support.

Finally, I would like to thank my lovely fiancé, María Ospina, for her constant love and total support.

TABLE OF CONTENTS

	<u>page</u>
ACKNOWLEDGMENTS	iii
ABSTRACT.....	ix
CHAPTERS	
1 INTRODUCTION	1
Ultramicroelectrodes.....	1
Properties and Applications of UMEs	2
Mass Transport.....	2
Reduced iR Effects and Small Cell Time Constant.....	4
Fast Scan Voltammetry (FSV).....	6
Carbon Fibers.....	7
Origin and Structure.....	8
Electrode Activation	9
Mechanical polishing of CFEs.....	9
Electrochemical Pretreatment of CFEs.....	10
Thermal Pretreatment of CFEs	11
Chemical Pretreatment of CFEs.....	11
Modification of Carbon Fiber Electrodes	11
Polymer Modified Electrodes	12
Conducting Polymers.....	13
Permselective Polymers	15
Inorganic Polymers	17
Uric Acid (UA)	17
Biological Significance of UA.....	17
Previous Strategies for Detection of UA.....	19
Spectroscopic Methods	20
Chromatographic Methods.....	20
Electrochemical Properties	22
Electrochemical Methods.....	23
Purpose of Work.....	24
2 EXPERIMENTAL	31
Reagents and Solutions	31

Electrodes.....	32
Reference and Auxiliary Electrodes	32
Working Electrodes	32
Instrumentation	34
Instrumental setup for determinations at low scan rate	34
Instrumental setup for determinations at high scan rate	36
Fundamentals of Electrochemical Methods.....	37
Cyclic Voltammetry.....	37
Determination of the Electrode Capacitance	43
Fast Scan Voltammetry (FSV).....	44
Chronocoulometry	45
 3 A HIGHLY ACTIVE CARBON FIBER SURFACE FOR THE DETERMINATION OF URIC ACID IN PHYSIOLOGICAL BUFFERS.....	 53
Background	53
Results and Discussion	57
Effect of Mechanical Polishing.....	57
Activation Potential	59
Effect of Positive Potential Limit	59
Effect of Negative Potential Limit.....	62
Effect of Electrolyte.....	63
Stability of Background Current.....	65
Stability of the Electrode After ECP.....	66
Determination of Uric Acid	67
Proposed Model of Electrode Activation.....	67
Conclusions.....	68
 4 ELECTROCHEMICAL CHARACTERIZATION OF CARBON FIBER SURFACES	 78
Background	78
Results and Discussion	80
Determination of Apparent Geometric Areas at Low Scan Rates	80
Oxidation/Reduction Voltammetry of Carbon Fiber Electrode Surfaces	82
Determination of the Roughness Factor	85
Fe(CN) ₆ ^{3-/4-} and Ru(NH ₃) ₆ ^{3+/2+} as Electrochemical Probes of Activity and	
Structure of carbon fiber surface.....	86
Effect of Solution pH on Electrode Response	88
Ascorbic Acid, Uric Acid and Dopamine Electrochemical Probes of	
Activity and Structure of Carbon Fiber Surface	91
Voltammetry of Ascorbic Acid (AA), Uric Acid (UA), and Dopamine	
(DA) at Low Scan Rates	91
Determination of the Sensitivity Enhancement Factor	94
Conclusions.....	94

5 ELECTROCHEMICAL POLYMERIZATION AND CHARACTERIZATION OF AN ULTRATHIN OVEROXIDIZED POLYPYROLE FILM.....	107
Background	107
Results and Discussion	110
Preparation of Ultrathin OPPy Film Electrodes.....	110
Effect of Polishing in the formation of OPPy films.....	111
Characterization of OPPy film using ferricyanide.....	114
Determination of Surface Coverage.....	115
Characterization of Electrochemical System	117
Morphology of OPPy at Electrochemically Pretreated Carbon Fiber Electrodes (EPCFE)	118
Determination of Diffusion Coefficient of Pyrrole.....	121
Thickness of OPPy Layer	122
Film Stability	123
Background Current Reduction	124
Conclusions.....	125
6 POSSIBILITIES AND LIMITATIONS IN MINIATURIZED SENSOR DESIGN FOR URIC ACID.....	138
Background	138
Results and Discussion	140
Determination of UA absorption on the oxidation peak of UA at FSV...140	
Fast Scan Voltammetry with Signal Averaging.....	141
Determination of UA at FSV in Physiological Buffers	142
Effect of pH in UA determinations at 500 Vs ⁻¹	145
Detection of UA without the interference from AA	146
Determination of UA in perfused heart sample	149
Determination of UA in urine sample.....	150
Determination of UA at OPPy modified CFE	151
Determination of UA in presence of AA at OPPy modified Electrodes..152	
Conclusions.....	153
7 ELECTROCHEMICAL POLYMERIZATION AND CHARACTERIZATION OF PHOSPHOTUNGSTATE FILM.....	174
Background	174
Results and Discussion	176
Experimental conditions for UA Determination Using Colorimetric Method	176
Effect of pH.....	176
Effect of Reagent Concentration.....	177
Electrochemistry of Phosphotungstic Acid at RPG	178

Electrochemistry in Solution.....	178
Electrochemistry of Phosphotungstate at RPG surface.....	179
Formation of Film.....	179
Determination of UA Using a Phosphotungstate Modified RPG	180
Electrochemistry of Phosphotungstic Acid at Electrochemically Treated Carbon Fiber Electrode	180
Electrochemistry in Solution.....	180
Formation of the Film	180
Conclusions	181
8 SUMMARY AND FUTURE DIRECTIONS.....	189
Summary.....	189
Future Directions	191
Instrumental Directions.....	191
Applications and New Modified Electrodes	192
REFERENCES	193
BIOGRAPHICAL SKETCH	206

Abstract of Dissertation Presented to the Graduate School
of the University of Florida in Partial Fulfillment of the
Requirements for the Degree of Doctor of Philosophy

DEVELOPMENT OF NOVEL SURFACES FOR ENHANCEMENT
OF SENSITIVITY AND SELECTIVITY
WITH CARBON FIBER ELECTRODES

By

Roberto Bravo

August 1999

Chairperson: Anna Brajter-Toth
Major Department: Chemistry

The development of novel surfaces for enhancement of sensitivity and selectivity of uric acid (UA) determinations with carbon fiber electrodes (CFE) has been the goal in our research. To achieve this goal, different approaches have been taken. First, a nanostructured CFE was prepared by a combination of mechanical polishing and electrochemical pretreatment, which involves moderate oxidation of the surface, followed by reduction. The effects of the treatment parameters such as polishing time, potential window, composition of the buffer and cycling time at the carbon fiber electrode surface were investigated.

Electrochemical parameters such as capacitance, roughness factor, area of electrode, kinetics of different probes were used to follow and validate structural changes at the CFE surface before and after electrochemical pretreatment.

An ultrathin film of overoxidized polypyrrole (OPPY) was used as another new strategy to increase the signal-to-noise ratio and the sensitivity of nanostructured carbon fiber electrode for UA determination. The film decreased the background current and enhanced sensitivity in fast scan voltammetry (FSV) because the electroactive area is large while the area that undergoes charging decreased. Electrochemical characterization of the film and the polymerization process were studied. Experimental results suggest that the electropolymerization of pyrrole is a diffusion-controlled process.

One of the major problems of *in vivo* determinations of UA comes from electrochemical interferences such as ascorbic acid (AA). We present here the results of fast scan voltammetry (FSV) which show improved selectivity and sensitivity in UA determination in the presence of 100 fold excess of AA at a bare CFE. *Signal-to-noise* (S/N) ratios at bare nanostructured CFE in FSV are improved because high temporal resolution of the technique allows acquisition of a large number of scans that can be averaged in a short period of time.

Preliminary results in biological systems show that the nanostructured CFE can be applied in *in vivo* UA determinations. The pH effect in uric acid determinations at the bare nanostructured CFE was also evaluated. The nanostructured CFE and OPPy modified CFE were used for UA determination in 70 mM phosphate buffer (pH 7.4). The OPPy modified CFE increases the sensitivity and S/N ratios for UA determinations.

Other strategy used to increase the sensitivity in UA detection was the modification of CFE with phosphotungstic acid. Phosphotungstic acid modified electrodes enhance UA response due to catalysis of UA oxidation reaction.

CHAPTER 1 INTRODUCTION

Ultramicroelectrodes

In the historical sense, the use of small electrodes in electrochemistry is an old subject. In 1922, Jaroslav Heyrovsky recorded the current-voltage response for a 1 mol dm⁻³ sodium hydroxide solution and interpreted the current increase between -1.9 and -2.0 V as the result of the deposition of Na⁺ ions, forming an amalgam [Heyrovsky 1925]. The development of polarography gave the small spherical mercury drop electrode world recognition. However, the use of microelectrodes has become widespread only in the past twenty years thanks to advances made in the field of electronics, especially in the measurement of small currents, and the use of special materials such as carbon fiber.

Ultramicroelectrodes (UMEs) can be defined in many different ways [Wightman, et al, 1980; Amatore, 1995]. However in this work, UMEs are defined as electrodes that have a diameter in the order of micrometers, usually lower than 20 μm [Bindra, et al., 1975; Adams 1976; Gonon, et al., 1979]

Ultramicroelectrodes can be constructed in a variety of geometric forms such as rings, arrays, interdigitated structures, and disk. In this work, we used a disk electrode, which is the most widely used geometry, since it is relatively easy to fabricate and maintain, and the current at a disk follows closely the theory [Bond 1991]. A variety of

materials can be used to fabricate UMEs such as gold, platinum, copper, mercury and carbon fibers. Carbon fibers offer many advantages and will be discussed below.

Properties and Applications of Ultramicroelectrodes

Ultramicroelectrodes offer several advantages over electrodes of conventional size. The most obvious advantage is that their small size facilitates their use in small volumes [Unwin and Bard, 1992; Fan, et al., 1996]. The use of UMEs has opened up the possibilities of *in vivo* electrochemistry [Stamford, 1986; Michael, et al., 1987; Leszczyszyn, et al., 1990; Schroeder, et al., 1992; Jankowski, et al., 1993; Nakasato, et al., 1993; Duff and O'Neill, 1994; Chen, et al., 1995]. Additionally, UMEs have the ability to perform electrochemical determinations in poorly conducting media [Bond and Fleischmann, 1984; Bond, et al., 1986; Bond and Man, 1987], can be used in scanning electrochemical microscopy [Kwak and Bard, 1989a; 1989b], and in fast scan voltammetry [Miller, et al., 1981; Kuhr and Wightman, 1986; Hsueh and Brajter-Toth, 1997].

Mass transport at UME

Depending on the geometry of the electrode and the time scales of the experiment, two well-defined cases of diffusion (linear and radial) can be obtained [Bard and Faulkner, 1980]. The diffusion layer thickness, δ , can be used to estimate if the diffusion process is linear or radial. The diffusion layer thickness can be described by the following equation:

$$\delta = (\pi D_o t)^{1/2} \quad (1.1)$$

Where D_0 is the diffusion coefficient of the electroactive species in cm^2s^{-1} and t is time in s. The relative contributions of linear or radial diffusion can be determined by the relative magnitudes of the electrode radius (r) and the diffusion layer thickness. If $\delta \gg r$ then radial diffusion predominates, whereas if $r \gg \delta$, linear diffusion is dominant.

Assuming a typical experimental time of 40 s for a voltammetric determination (potential window from 0 to 1.0 V and scan rate of 50 mVs^{-1}) and a typical value of $1 \times 10^{-6} \text{ cm}^2\text{s}^{-1}$ for the diffusion coefficient of a small electroactive species in aqueous solution [Bard and Faulkner, 1980], a value of $1.12 \times 10^{-2} \text{ cm}$ is obtained for δ . A conventional size disk electrode radius is on the order of $1 \times 10^{-1} \text{ cm}$. The diffusion layer is much smaller than the electrode radius and the diffusion process under these conditions corresponds to mass transfer in a one-dimensional diffusion field (perpendicular to the electrode) as illustrated in Figure 1.1.A.

Figure 1.1.B represents the growth of the diffusion layer as a function of time at a disk UME. At a very short time (t_1) the diffusion layer thickness of the UME is very small compared to the radius of the electrode, thus the UME will behave similarly to a conventional size electrode under this condition. However, at longer times (t_3 , t_4), the dimensions of the diffusion layer exceed the radius of the UME ($\delta \gg r$), and the diffusion becomes radial.

The high efficiency of mass transport at UMEs facilitates steady state electrochemistry, and this steady state behavior can be observed in low scan voltammetric determinations. Figure 1.1.B shows the voltammogram of potassium ferricyanide at the UME surface, the shape of the curve is sigmoidal (steady state response). Figure 1.1.A shows the voltammogram at 50 mVs^{-1} of the same analyte under

the same conditions at a conventional size electrode. A peak-shaped curve is obtained because the initial rate of electrolysis is bigger than the rate at which the analyte from bulk solution can diffuse to the electrode.

Reduced iR Effects and Small Cell Time Constant

Ohmic drops in conventional size electrodes can severely distort the data obtained in electrochemical experiments. This drop occurs as the current that flows through the cell generates a potential that opposes the applied potential. The true potential of the working electrode (E_w) in V can be determined by subtracting the product of the current from the applied potential (E_{appl}) as illustrated in Equation 1.6:

$$E_w = E_{appl} - iR \quad (1.2)$$

The cell resistance R depends on the resistivity of the solution and the size of the electrode and it can be described by:

$$R = \rho (4r)^{-1} \propto r^{-1} \quad (1.3)$$

Where r is the radius of the electrode in cm and ρ is the specific resistivity of the solution in Ωcm . Equation (1.3) shows that the cell resistance increases as the size of the electrode decreases.

The current from the iR drop has two components: a Faradaic component, which is generated by the reaction of the electroactive species at the electrode surface, and a non-faradaic current or charging current usually generated by the double-layer

capacitance. Both currents are proportional to the electrode area because both are generated at the electrode surface. Consequently, the total cell current can be described as follows:

$$i_{\text{cell}} = (i_b + i_f) \propto A \propto r^2 \quad (1.4)$$

Where i_{cell} is the cell current in A, i_b is the background current, i_f is the faradaic current, A is the area of disk UME ($A = \pi r^2$) in cm^2 , and r the radius of the disk UME in cm. Equation 1.4 shows that the cell current increases with the square root of the electrode radius. By combining Equations (1.3) and (1.4), a relationship between iR drop and the electrode size can be obtained:

$$iR \propto r \quad (1.5)$$

Equation 1.5 shows that the iR drop can be reduced by decreasing the size of the electrode.

Cell time constant, which is the time required to charge the double-layer after a potential is applied, is another unwanted problem related to conventional size electrodes. The cell time constant can be expressed by the following equation:

$$\tau = C_d R \quad (1.6)$$

Where τ is the cell time constant in s, C_d is the double-layer capacitance, and R is the cell resistance in Ω . The double-layer capacitance is a function of the electrode area:

$$C_d = CA = C\pi r^2 \propto r^2 \quad (1.7)$$

Where C is the double layer capacitance per unit of area in Fcm^{-2} . By substituting Equations (1.3) and (1.7) in Equation (1.6) the following expression is obtained:

$$\tau = C_d R \propto r^2 r^{-1} \propto r \quad (1.8)$$

Equation 1.8 shows clearly that the cell time constant decreases when the electrode radius decreases.

Fast Scan Voltammetry (FSV)

Fast scan voltammetry can not be performed with conventional size electrodes because the cell time constant and the iR drop are too large to allow the use of this technique. A detailed discussion about the principles of FSV is presented in Chapter 2.

Fast scan voltammetry was first introduced by Miller's group [Miller et al., 1981] and improved by Kuhr and Wightman [Kuhr and Wightman, 1986]. Fast scan voltammetry offers many advantages over conventional electroanalytical techniques. One of the biggest advantages of FSV is its high temporal resolution which allows determinations in real-time [Kuhr and Wightman, 1986; Stamford et al., 1986]. Due to the high temporal resolution of FSV, signal averaging has been used to improve *signal-to-noise* ratio [Wiedemann, et al., 1991]. Hsueh and Brajter-Toth reported that the high frequency noise is rapidly reduced by signal averaging as the number of scans increases,

however the low frequency noise remains the same even after thousand of scans [Hsueh and Brajter-Toth, 1993].

The other advantage is that FSV can be used as a kinetics filter tool. For instance, Hsueh and co-workers reported the determination of 10^{-4} M dopamine in the presence of 10^{-2} M ascorbic acid. The electrochemical kinetics of ascorbic acid are very slow compared to the kinetics of dopamine. FSV exploits this situation so that the oxidation potential of ascorbic acid shifts away from the oxidation peak potential of dopamine as the scan rate increases [Hsueh et al , 1997].

Another major asset of FSV is the back scan, which can increase the stability of the UME. The back scan can force electrode reaction products to undergo reverse electrochemical reaction and be converted back to the original analyte before chemical reaction occurs in the solution [Baur, et al., 1988; Stamford, 1990]. The back scan can also be used to identify compounds. For example, many compounds have similar oxidation potentials however the reduction peaks are different [Stamford, 1990].

The limit of detection (LOD) and sensitivity of FSV can be a limitation. The LOD in cyclic voltammetry arises from interferences by currents different from the faradaic processes of interest. This background current has at least two components: the double-layer capacitance and the redox reaction of the surface-bound species [Hsueh and Brajter-Toth, 1996].

Carbon Fibers

Carbon materials in the form of graphite, glassy carbon, carbon fibers, etc. have been widely used in electrode development. Carbon materials are available in many different forms at a very low price. Carbon materials can also be used in wide potential

ranges, particularly in the positive direction. Besides, carbon materials are inert and have a rich surface chemistry which can be exploited to increase the selectivity and sensitivity in analytical determinations.

Carbon fiber materials (CF) are not new. In 1879, Thomas A. Edison patented the manufacture of carbon filaments to be used as electric lamps [Edison 1890; 1891]. However, it was in the early 1960s when the commercial production of CF started. Carbon fibers have many different commercial applications. They are used in the aerospace and space shuttle industry, automotive industries, and in the development of new recreational equipment. In the electrochemical field, CFEs were initially introduced in 1978 when Gonon and co-workers reported their use as working electrodes. These CFEs were made in pipettes, with a 8 to 12 μm diameter CF and a 0.5 mm length protruding from the end [Gonon, et al., 1978].

Origin and Structure of CFE

A large variety of fiber precursors are used to produce CFEs of different morphologies and different characteristics. The most prevalent precursors are polyacrylonitrile (PAN), viscose rayon, petroleum or coal tar pitch and certain phenolic fibers [Kinoshita, 1988; McCreery, 1991; McCreery and Cline, 1996].

Carbon fibers can be manufactured by controlled pyrolysis of organic precursors in fibrous form. This is a heat treatment process of the precursor that removes the oxygen, nitrogen and hydrogen to form carbon fibers. It is well known in CF literature [Kinoshita, 1988; McCreery, 1991; McCreery and Cline, 1996] that the mechanical properties of CF can be improved by increasing the crystallinity and orientation, and by reducing the defects in the fiber. The finished fiber has a cross section of “onion,”

“radial,” or “random” type, as illustrated in Figure 1.2.A. The fiber end generally has a high fraction of edge planes.

The surfaces of graphitic material such as CF are very complex [McCreery, 1991]. In general, graphitic carbon is formed of extensive sheets of fused aromatic rings, stacked in a planar fashion. The surface of an uninterrupted basal plane is hydrophobic, nonionic, has low polarity and is rich in π -electron density with little, if any, chemical functionality [Murray, 1984]. Consequently, the basal plane of the fiber is almost inert electrochemically in aqueous solution. This suggests that most of electron transfer occurs at the edges of the basal plane where there are a large number of functional groups such as phenol (a), carbonyl (b), carboxyl (c), quinone (d), and lactone (e) as illustrated in Figure 1.2.B.

There is no “standard carbon fiber” with well-known electrochemical properties. Untreated carbon fibers have only a very modest sensitivity and resolution in electrochemical applications [Stamford, 1989]. However, rich surface chemistry of CF allows chemical and physical modification of the surface, to enhance desirable properties which was accomplished during this work.

Electrode Activation

The four techniques that are commonly applied in order to activate carbon fiber electrodes (CFEs) are: (a) mechanical polishing, (b) electrochemical polishing, (c) chemical treatment, and (d) thermal treatment.

Mechanical Polishing

The initial polishing step is commonly performed with 600-grit emery paper, to remove gross surface defects and impurities. The electrodes are then polished with 5,

0.3, and 0.05 μm alumina using a polishing cloth and a polishing wheel to produce a mirror like surface. This total polishing process can take from 45 to 60 minutes [Howell and Wightman, 1984; Wightman and Wipf, 1985]. Once the electrode has been polished, the electrode is dipped in propanol [Cahill, et al., 1996] and sonicated in water to remove possible impurities from the polishing process. Different groups have been polishing the CFE with embedded diamond particles rather than alumina to avoid possible contamination of the surface with alumina [Kawagoe et al., 1993; Paras and Kennedy, 1995; Cahill, et al., 1996]. Usually, mechanical polishing is combined with other activation techniques such as electrochemical treatment to produce active CFE.

Electrochemical Pretreatment

Electrochemical pretreatment (ECP) has been found to be effective in improving electrode sensitivity and selectivity [McCreery, 1991]. Gonon and co-workers reported a remarkable improvement in sensitivity and selectivity for detection of dopamine *in vivo* by ECP [Gonon, et. al., 1981]. ECP procedures for CFEs were classified in two main groups: mild and strong by McCreery and Cline. This classification was based on the electrochemical conditions of the treatment. For example, ECP procedures with positive potential limits of 2.0 V or less were called “mild.” ECP procedures with positive potential limits bigger than 2.0 V were called “strong” [McCreery and Cline, 1996]. “Mild” conditions appear to form surface oxides and eventually graphite oxides. The oxide layer may increase the sensitivity for cations such as dopamine and repel anions such as ascorbic acid [Feng, et al., 1987; Michael and Justice, 1987]. “Strong” ECP on CF may produce an insulating oxide film over the surface of the CF. Cracks in this film

exhibit fast electron activity. However, the cell time constant of this CFE is big due to the high resistivity of the insulation oxide film [Kovach, et al., 1986].

There are some problems with the strong electrochemical treatment. For instance, at untreated CFE, dopamine oxidation is more reversible than that of dihydroxyphenylacetic acid. Thus dihydroxyphenylacetic acid does not interfere with detection of dopamine [Ewing, et al., 1983]. However, at treated CFE resolution is compromised by dihydroxyphenylacetic acid oxidation at +50 mV and dopamine at +85 mV [Gonon, et al., 1984].

Thermal Pretreatment

Few publications, of laser and vacuum heat activation of CFEs have only been reported [Strein and Ewing, 1991; Swain and Kuwana, 1992]. Wightman and co-workers reported an increase in the oxidation rate of AA by heat-treatment at 540 °C, 4.5 h, 1 torr and cool air [Wightman, et al., 1984]. Strein and Ewing used a small nitrogen laser to pretreat a 11 µm diameter disk UME. They reported improvements in voltammetric wave shapes and electron wave for several catecholamines [Strein and Ewing, 1991].

Chemical Pretreatment

Chemical activation of UMEs has also been reported. Gonon and co-workers showed that a very poorly resolved peak for AA and dopamine could be obtained by chemical oxidation of graphite fiber with HNO₃, H₂SO₄, H₂O₂ and acidic dichromate [Gonon, et al., 1981].

Modification of Carbon Fiber Electrodes

Because of the rich surface chemistry of the CFEs, improvements in sensitivity and selectivity can not only be achieved by electrode activation but also by attaching or

immobilizing a foreign molecule at the surface of the CFE. The term known as “chemically modified electrodes” (CME) was first introduced by Murray [Murray, 1980] in the mid-1970s to define the modification of the electrode surface by attaching foreign molecules. Since the foreign molecules are intentionally attached to the surface, many electroanalytical problems can be resolved by finding the right foreign molecule to accomplish a specific work such as the selectivity in *in vivo* determinations. Significant improvement in selectivity and sensitivity of CFE have been achieved by coating the electrode surface with permselective polymers which can block unwanted interferences from the surface and by using enzyme modified electrodes.

Polymer Modified Electrodes

Polymer modified electrodes (PMEs) have been extensively used to improve selectivity and sensitivity of analytical determinations [Cheng and Brajter-Toth, 1992; Gao and Ivaska, 1993; Palmisano et al., 1995]. In general, polymer films can be classified as conducting and non-conducting polymers [Emr and Yacynych, 1995]. Conducting polymer films are frequently used to enhance electron transfer properties [Saruceno, et al., 1986; Lyons, et al., 1991; Saunders et al., 1995]. Non-conducting polymer films are often used for their permselective properties [Gerhardt, et al., 1984; Whiteley and Martin, 1987; Witkowski and Brajter-Toth, 1992; Hsueh and Brajter-Toth, 1994]. Both types of polymers have been used to immobilize biocomponents such as enzymes and to avoid fouling problems [Gorton, et al., 1990; Sasso, et al., 1990; Bremle, et al., 1991; Geise, et al., 1991; Cooper and Hall, 1992; Reynolds and Yacynych, 1993].

Adsorption [Cosnier and Innocent, 1992; Rhode, et al., 1993], solvent casting [Hua, et al., 1992], spin coating [Wang, et al., 1991], and electropolymerization [Witkowski and Brajter-Toth, 1992; Cui, et al., 1993] are some of the methods used to modify conventional-size electrodes with polymers. However, the main technique to modify UMEs has been electropolymerization, which offers advantages over other methods. Since Faraday's law governs electropolymerization [Funt 1986], the amount of polymer generated at the surface of the electrode is directly proportional to the amount of charge transferred. Consequently, the thickness of the layer can be controlled by the total amount of charge applied to the system. Other advantages of electropolymerization are that the nature of the film and the polymerization rate can be controlled *via* the applied potential used during the electropolymerization process, therefore very small and/or irregularly shaped electrode surfaces can be coated. Electropolymerization can be performed using potential cycling methods, fixed potential techniques, pulsed potential approaches, and galvanostatic techniques.

Conducting Polymers

The idea of conducting polymers was a theoretical debate until 1977 when Shirakawa and co-workers discovered that poly(acetylene) (PA) can increase its conductivity by several orders of magnitude when exposed to halogen vapors [Shirakawa, et al., 1977]. A couple years after the discovery of conducting PA, the electrochemical synthesis of polypyrrole (PPy) was developed by Diaz and co-workers [Diaz, et al., 1979]. This discovery opened up a vast field in the conducting polymer modified conventional-size electrodes. On the other hand, only a few publications have been reported using conducting polymer CFEs and metal UMEs [John and Wallace,

1991a; 1991b; Sadik and Wallace, 1994; Hsueh and Brajter-Toth, 1994; Imides, et al., 1996; Wood and Iroh, 1996].

Polypyrrole has been extensively applied in analytical applications due to its excellent advantages in sensor fabrication such as its easy electropolymerization which produces homogeneous films strongly adhered to the electrode surface and its ability to be a suitable medium for the immobilization of biomolecules.

The mechanism of electropolymerization of heterocyclic monomers such as pyrrole has been extensively studied but it is still not completely clarified. The most accepted mechanism is presented in Figure 1.3. The first step is the oxidation of the monomer accompanied by the release of one electron to produce a radical cation [Raymond and Harrison, 1993; Tanaka, et al., 1988; Andrieux, et al., 1990; Andrieux, et al., 1991; John and Wallace, 1991]. Since electron transfer is much faster than the diffusion of the monomer to the bulk solution, a high concentration of the radical cation at the vicinity of the electrode surface is produced and radical coupling is favored to form a dimer. The second step is still under debate and continues to be a controversial part of the overall mechanism. The coupling can proceed either by (2a) the combination of two radicals to produce a dimeric pyrrole dication or (2b), electrophilic addition of pyrrole radical cation to pyrrole followed by oxidation to a dimeric pyrrole dication [Lowen and Van Dike, 1990; Scharifker, et al., 1991]. The dication obtained by coupling of two radical cations subsequently undergoes deprotonation to produce the dimer, as shown in step (3). The soluble dimer may preferentially undergo further oxidation accompanied by the release of one electron at the surface of the electrode since the dimer has a lower half-wave oxidation potential than the monomer. Finally, the dimer may couple with

another radical-cation and deprotonate to form a trimer. As this process continues, oligomers are formed which eventually precipitate onto the electrode surface when the solubility limit is exceeded. Consequently, this process can be described as an $E(CE)_n$ mechanism. This mechanism is interesting at microelectrodes because the products of the electrolysis reaction may diffuse away from a microelectrode very fast. John and Wallace found that the optimal conducting polymer deposition at platinum disk microelectrodes (10 μm diameter) requires experimental conditions that increase the rate of the coupling step. For example, high monomer concentration, high supporting electrolyte, and high current densities (or potentials) all increase the rate of chemical coupling and therefore improve the electropolymerization at microelectrodes. Additionally, they reported that the choice of the solvent is critical and the presence of water interferes with the radical-radical coupling step. It can slow down the effective rate of the chemical process [John and Wallace, 1991]. The nature of the counterion used during synthesis can also have a marked effect on the electrodeposition of the conducting polymer. For instance, the presence of a surfactant such as sodium dodecyl sulfate in the deposition of polypyrrole increases the deposition rate of the polymer at microelectrodes by three orders of magnitude compared to macroelectrodes [John, et al., 1992]. Also, Wood and Iroh reported that the amount of the coating formed increases with the increase of pyrrole concentration, supporting electrolyte, applied voltage and electropolymerization time for carbon fiber bundles electrodes [Wood and Iroh, 1996].

Permselective Polymers

One of the major possible problems with *in vivo* UA determination comes from electrochemical interferences such as ascorbic acid, (AA) (0.2 V vs SCE). Usually, this

kind of interference may be eliminated using a permselective film [Gerhardt, et al., 1984; Kristensen, et al., 1987; Whiteley and Martin, 1987; Marsden, et al., 1988; Rice and Nicholson, 1989; Capella, et al., 1990]. However, electrodes coated with permselective films such as Nafion or a thick film of overoxidized polypyrrole (OPPy) [Witkowski and Brajter-Toth, 1992] are not practical for selective determinations of UA in the presence of high concentrations of AA.

In previous work in our group, a new class of cation permselective films has been investigated [Freund, et al., 1991; Witkowski, et al., 1991; Witkowski and Brajter-Toth, 1992; Hsueh and Brajter-Toth, 1994]. It has been shown that overoxidized polypyrrole films can be made quite permeable, have ionic conductivity, even though the electrical conductivity of polypyrrole (PPy) is lost after oxidation of the polymer. During the overoxidation, carbonyl groups are introduced into the polymer backbone forming OPpy [Beck, et al., 1987]. The high electron density of the carbonyl groups can act as a barrier to anion diffusion in the film. Films (which have a thickness of 0.1 μm) have been shown to have an excellent cation selectivity. Since the OPpy mechanism of selectivity is based on neutral carbonyl groups instead of negative charge sites, electrostatic binding does not occur and OPpy has a faster response time and lower memory effects than Nafion.

Wightman's group reported that overoxidized polypyrrole-coated CFE are more sensitive to dopamine than Nafion-coated electrodes when FSV at 300 Vs^{-1} was used. The OPpy modified CF was stable for several hours in *in vivo* determinations when the electrode was scanned to relatively high potentials [Pihel, et al., 1996].

Zhang and co-workers, reported the development of a CFE modified with OPPy film and equipped with a micro Ag/AgCl reference electrode to detect dopamine in the presence of AA in extremely small volumes (10 nL) [Zhang, et al., 1996].

Inorganic Polymers

Electroactive films can also be prepared on electrodes from inorganic lattice-forming compounds such as metalocyanates, tungsten oxides and oxometallates. Faulkner and co-workers found that electroreduction of a solution containing a tungsten oxide suspension and chloroplatine produces an electroactive tungsten oxide-Pt microparticle film with excellent electrocatalytic properties, specially for hydrogen evolution [Kulesza, et al., 1988a, 1988b, 1989a, 1989b]. Nadjo and co-workers entrapped oxometallates such as $[\text{SiW}_{12}\text{O}_{40}]^{4+}$ in polymeric ion-exchange films and reported a high stability for these electroactive films [Keita, et al., 1989, 1988, Keita and Nadjo, 1988].

Uric Acid

Biological Significance of Uric Acid

Uric acid (UA) [7,9-dihydro-1H-purine-2,6,8(3H)-trione] is the principal end product of purine metabolism. All mammals except the primates are uricolytic organisms. These organisms have the ability to convert UA to allantoin, a more water soluble compound. This reaction is catalyzed by the enzyme uricase. This enzyme is missing in primates, insects, birds, and reptiles [Wimsatt 1999]. As a result, UA is the major product of purine catabolism of these species.

In humans, UA circulates in plasma as sodium urate and is excreted by the kidneys. It is derived from the breakdown of nucleic acids that are ingested or from the

destruction of tissues cells and it is also synthesized in the body from simple compounds. The formation of UA in humans is illustrated in Figure 1.4 [Kaplan et al., 1995].

Because of its low solubility in water (6.5 mg/ 100mL) and plasma (7×10^{-2} mg mL⁻¹) [Wyngaarden and Kelly, 1976] UA can be easily precipitated when a local rise of hydrogen ions occurs in tissues [Kaplan, et al., 1995]. The normal UA serum levels range from 4.1 to 8.8 mg dl⁻¹ and urinary excretion is typically 250-750 mg day⁻¹ [Lawrence, et al., 1987]. The determination of the concentration of UA has been used as a marker for the detection of several disorders associate with purine metabolism, such as gout and Lesch-Nyhan syndrome [Kaplan, et al., 1995; Start 1995; Winsatt,1999].

Gout, which is called the “king of diseases” and the “disease of kings,” occurs when sodium urate crystals are deposited in the joints, soft tissue, bursae and tendons due to the overproduction of UA and/or the decrease of fractional UA excretion by the kidneys. Lesch-Nyhan syndrome is an X-linked chromosome disorder that results in the absence of the enzyme hypoxanthine-guanosine phosphoribosyl transferase (HGPRT). This disorder is characterized by striking growth and mental retardation, compulsive self-mutilation, and excessive UA production. Hyperuricemia, or elevated concentration of UA, may indicate other medical conditions such as kidney injury, leukemia, and pneumonia. Diagnosis is confirmed by monitoring serum or urinary UA levels.

New hypothesis about the role of UA in biological systems such as brain and heart open new frontiers for the determination of UA in these systems. For example, Ames and co-workers demonstrated the very effective action of UA as an antioxidant scavenger of free radicals generated during normal metabolism within the cell [Frei, et al., 1989]. They hypothesized that UA might protect against widespread cellular damage

produced by free radicals generated through oxidative reactions [Ames, et al., 1981]. Kanemitsu and co-workers reported elevated concentration of UA in the brain after ischemia/reperfusion [Kanemitsu, et al., 1988]. Tayag and coworkers reported that cerebral UA increased following experimental traumatic brain injury in rats [Tayag, et al., 1996].

Layton and co-workers studied electrolytes in concentration of UA before and after ischemia/reperfusion in rat liver to verify that tissue damage is mediated by oxidative stress [Layton, et al., 1996].

The adenosine hypothesis (which was introduced in 1963) suggests that adenosine serves as the metabolic link between myocardial oxygen demand and myocardial oxygen supply [Berne, 1963]. Consequently, adenosine may be used as a marker to predict heart attacks since during a heart attack the ratio of oxygen demand to oxygen supply decreases [Deussen, et al., 1986; 1989]. Unfortunately, the adenosine oxidation potential which is greater than one volt at typical electrodes makes electrochemistry based sensing difficult. Uric acid is the final product of adenosine metabolism and it has a lower oxidation potential (0.3 V vs SCE) than adenosine; thus changes in UA concentrations could be also used to predict heart attacks.

Previous Strategies for Detection of UA

Several different analytical approaches have been used for UA determinations. These methods can be classified in two main groups: (a) spectroscopic and (b) electrochemical methods. However, separation methods are also used to enhance the selectivity of UA detection in perfused heart samples and microdialysis samples.

Spectroscopic methods

They are based on the oxidative degradation of UA and they can be subclassified in two groups: redox-colorimetry and enzymatic methods. Redox-colorimetric methods are based on the reduction of sodium tungstate by UA. Changes in the absorbance between 660 and 720 nm are proportional to the UA concentration. These methods are the most popular methods used in clinical UA determinations even though they present several problems such as a no linear dependence between the developed color and concentration of UA, and interferences from other reducing agents in biological samples like AA, caffeine, etc [Benedict, 1930; Jung and Parekh, 1970; Tietz, 1974; Wyngaarden and Kelley, 1976].

Uric acid has a characteristic ultraviolet absorption with a maximum peak at 292 nm at pH 9.4. In the presence of uricase, UA is converted to allantoin which has no ultraviolet absorption at this wavelength. Uricase methods monitor the decrease in absorbance (292 nm) which results from the oxidative destruction of UA. The enzymatic reaction is very specific however, the presence of several purines such as xanthine may produce poor reproducibility [Dilena, et al., 1986; Haeckel 1978].

Chromatographic Methods

Many of the spectroscopic and electrochemical methods are susceptible to interferences. Consequently, separation methods have been used to increase the selectivity of the system such as serum [Senfleber, et al., 1976], microdialysis brain samples [Tayag, et al., 1996], and perfused heart samples [Van Wylen, et al., 1992].

Ultraviolet detection has frequently been used for UA (280-292 nm). Serum and urine were the matrix targets in the earliest separation and determinations of UA by UV

detection. Senftleber and co-workers separated several metabolites and other compounds in uremic patients by using a gradient elution [Senftleber, et al., 1976]. Hartwick and co-workers resolved 84 compounds in plasma from normal and neoplasma patients [Hartwick, et al., 1979]. Wung and Howell reported a method capable of simultaneously measuring 5-fluorouracil, uridine, hypoxanthine, allopurinol, oxypurinol, and uric acid in plasma [Wun and Howell, 1980].

Van Wylen and co-workers used cardiac microdialysis in the isolated perfused heart to detect the interstitial purine metabolites such as adenosine, inosine, xanthine, and UA during ischemia. Dialysate solutions were separated using a reverse-phase column with a gradient elution KH_2PO_4 / methanol. All peaks were detected by absorbance at 254 nm, and unknown samples were identified and quantified by comparing retention times and peak heights to known standards. The dialysate concentrations in the samples taken 60-80 minutes after implantation were 0.34 μM adenosine, 0.53 μM inosine, 0.20 μM hypoxanthine, 0.32 μM xanthine and 1.8 μM UA [Van Wylen, et al., 1992].

Becker and Gerlach reported that UA (which is the major catabolite of cardiac adenine nucleotides and adenosine) originates in the coronary endothelium. Samples were separated by reverse phase HPLC in conjunction with a variable wavelength detector [Becker and Gerlach, 1987]. Mei and co-workers reported the simultaneous determination of adenosine, inosine, hypoxanthine, xanthine, and UA in heart microdialysis samples using microbore column with a diode array detector. They reported a base interstitial UA concentration of 4 μM and then UA concentration increased to 12 μM after 20 minutes of myocardial ischemia/reperfusion [Mei, et al., 1996].

The first determination of UA by HPLC with amperometric detection was developed by Kissinger and co-workers [Kissinger, 1974]. Diluted urine samples containing UA and AA were injected directly onto an anion-exchange column. Iwamoto and co-workers described a reverse phase HPLC method for UA in rat serum using a thin layer glassy carbon electrode ($E_{\text{applied}} = +0.8 \text{ V vs. Ag/AgCl}$) [Iwamoto, 1984]. Tayag and co-workers reported the determination of cerebral UA by using microdialysis. Dialysate solutions were analyzed by HPLC with amperometric detection [Tayag, et al., 1996]

Electrochemical Properties of UA

The mechanism for the electrochemical oxidation of uric acid is shown in Figure 1.5. This process involves a $2e^- 2H^+$ electrooxidation of UA to a diimine (II). This step is followed by a double hydration to form a 4,5-diol (IV) [Owens et al., 1978]. The electrooxidation of UA was investigated by Dryhurst [Dryhurst 1972a], and the major products of the oxidation depended on solution pH [Dryhurst 1972b]. In acidic solution (pH 1-3), alloxan and urea were the major products whereas at higher pH the major product was allantoin.

At neutral pH, UA exists in its monoanionic form ($pK_a=5.75$) which is oxidized to a labile diimine anion (II). The peak oxidation potential is pH-dependent at pyrolytic graphite electrode in 0.5 M phosphate buffer according to the following equation [Brajter-Toth et al., 1981]:

$$E_p (\text{pH } 0-11.5) = (0.685 - 0.055 \text{ pH}) \text{ vs. SCE at } 25^\circ\text{C} \quad (1.9)$$

Species I and II are a quasi-reversible couple, and the cathodic peak can be observed with a rough pyrolytic graphite electrode at scan rates greater than 200 mV s^{-1} , the peak can be also observed at smooth or more highly polished electrodes by applying higher scan rates, $> 20 \text{ Vs}^{-1}$ [Wrona, et al., 1979]. The very unstable dimine anion (II) is hydrated in two steps. The first step is very fast and is characterized by a pseudo first order rate constant of 32.5 s^{-1} at pH 8 (phosphate buffer, 0.5 M ionic strength). This value corresponds to a half-life for species II of 21 ms [Owens, et al., 1978]. At lower or higher pH values, the rate of the reaction is increased. Species II can also undergo a $2e^- 2H^+$ reduction of nonhydrated double bond to produce a dihydro derivate [Brajter-Toth, et al., 1981]. The peak reduction potential for species II is pH dependent according to the following equation:

$$E_p (\text{pH } 2.8\text{-}10.0) = (-0.5 - 0.066 \text{ pH}) \text{ vs. SCE at } 25^\circ\text{C} \quad (1.10)$$

The second hydration reaction from species III to IV is slower with a half-life of 3 minutes for species III. Finally, UA diol (IV) decomposes *via* of an isocyanate to allantoin (V) and carbon dioxide in neutral and weakly alkaline solutions [Owens et al., 1978]. Based on these results, Marsh and Dryhurst [Marsh and Dryhurst, 1979] and Brajter-Toth and co-workers [Brajter-Toth, et al., 1981] demonstrated that both electrochemical and enzymatic oxidation of UA proceed by an identical method.

Electrochemical Methods

Electrochemical methods for the determination of UA can also be classified in two main categories: direct and enzymatic. Direct methods are rapid and have a minimum of sample preparation. Cyclic voltammetry is the most common electroanalytical technique

for direct determinations of UA. Mueller and co-workers used a carbon paste microelectrode for *in vivo* voltammetry to detect UA production by rat brain [Mueller, et al., 1985].

As was mentioned before, enzymatic methods are based on the oxidation of UA to allantoin in the presence of uricase. This is best illustrated in the following equation:



Several amperometric methods of detection are based on the determination of H_2O_2 produced during the reaction. These procedures use the anodic electroactivity of peroxide but its oxidation can require relatively high applied potentials (>0.4 V) and the system is susceptible to interferences from readily oxidizable interferents such as ascorbic acid. Different approaches have been used to eliminate the interferences [Kulys, et al., 1983; Watanabe and Tatsuma, 1991] but the complexity of the procedure and the lack of selectivity still need to be overcome.

New methods based on surface-modified electrodes have been used [Gilmartin, et al., 1992; Gilmartin and Hart, 1994a; 1994b; Miland, et al., 1996]. One method uses a cobalt phthalocyanine base tailored for the electrocatalytic oxidation of H_2O_2 in combination with a cellulose acetate-uricase bilayer.

Purpose of Work

The purpose of this work was to develop novel surfaces for enhancement of selectivity and sensitivity in determinations at CFEs using fast scan voltammetry. Since fast scan voltammetry technique relies on a background current subtraction, the initial

focus was on the development of a stable and reproducible background current at CFE. A stable and reproducible background current at CFE was achieved using a combination of mechanical and electrochemical pretreatment. This treatment produces a nanostructured CFE surface, which increases the sensitivity in analytical determinations. Next, electrochemical parameters such as capacitance, roughness factor, area of the electrode, kinetics of different probes were used to follow and validate structural changes at the CFE surface before and after electrochemical pretreatment.

A possibility of using the nanostructured CFE surface as a template for the electropolymerization of an ultrathin OPPy film was finally investigated. High sensitivity of the nanostructured CFE (NCFE) was maintained while the background current was decreased by the presence of the OPPy film.

Bare NCFE and OPPy NCFE were used to detect low concentrations of UA in the presence of high concentrations of ascorbic acid which can be the main electrochemical interference in UA determination in biological fluids and perfused heart samples. Preliminary UA determinations in biological systems such as urine and heart perfused samples were performed at NCFE using fast scan voltammetry. Also, the possible effects of pH in UA determinations were evaluated. Finally, the possibility to enhance UA sensitivity using an inorganic polymer was evaluated. The phosphotungstic acid modified electrode enhances UA response due to catalysis of UA oxidation reaction.

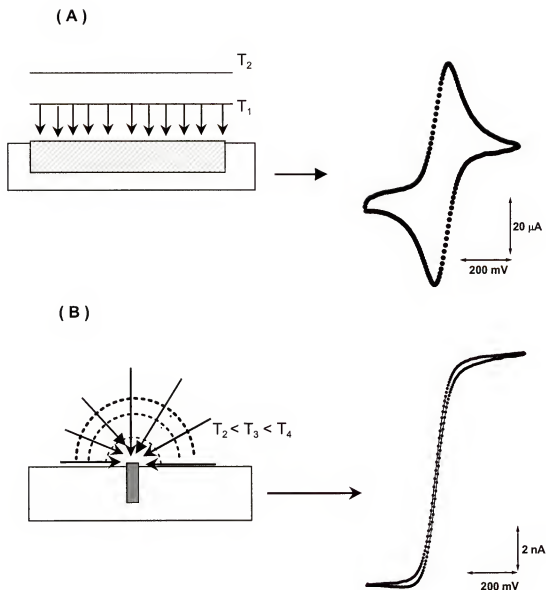


Figure 1.1. Diffusion layer profiles and representative cyclic voltammograms (CV) for (A) planar diffusion and CV from a conventional size electrode (ca. 0.1 cm^2 area); (B) radial diffusion and CV from a disk carbon fiber electrode ($7 \mu\text{m}$ diameter). Solution: $10 \text{ mM Fe(CN)}_6^{3-}$ in 0.5 M KCl (pH 6.0). Scan rate 50 mV s^{-1} .

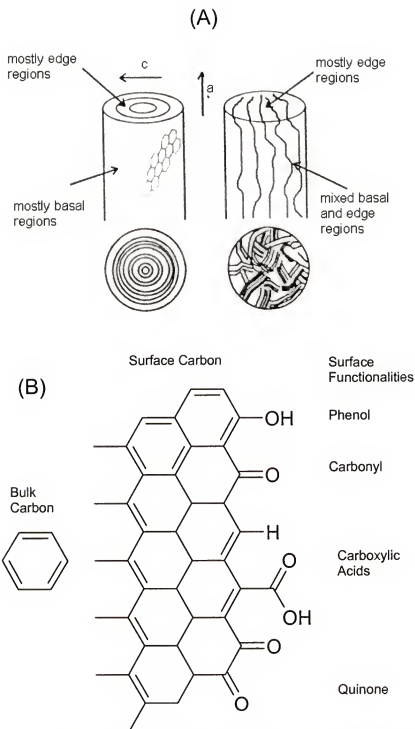


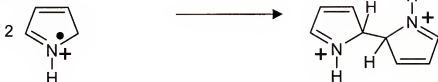
Figure 1.2. (A) Illustration of carbon fibers, side and end view: (left) ordered “onion”; (right) disordered “random” fiber. (B) Graphite oxide surface structure found in carbon materials.

1. Monomer oxidation

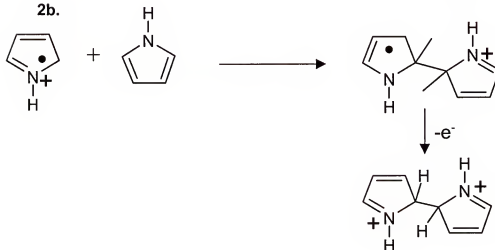


2. Radical-radical coupling

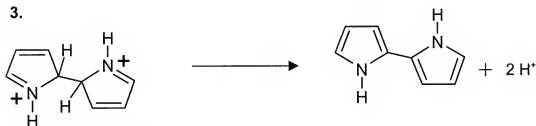
2a.



2b.



3.



4. Chain propagation

Repeat oxidative coupling
Process with monomer and
with oligomers

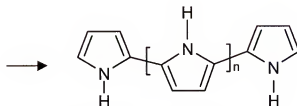


Figure 1.3. General mechanism for the oxidative polymerization of pyrrole

ANABOLISM

Ingestion:

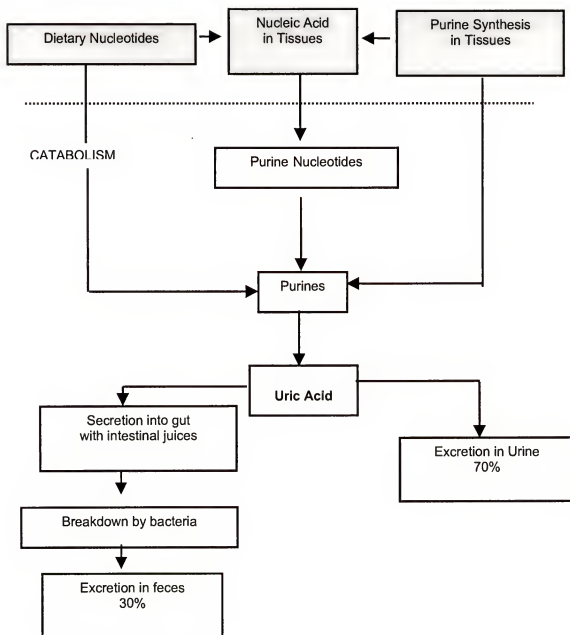


Figure 1.4. Schematic representation of uric acid formation and excretion [Kaplan et al., 1995].

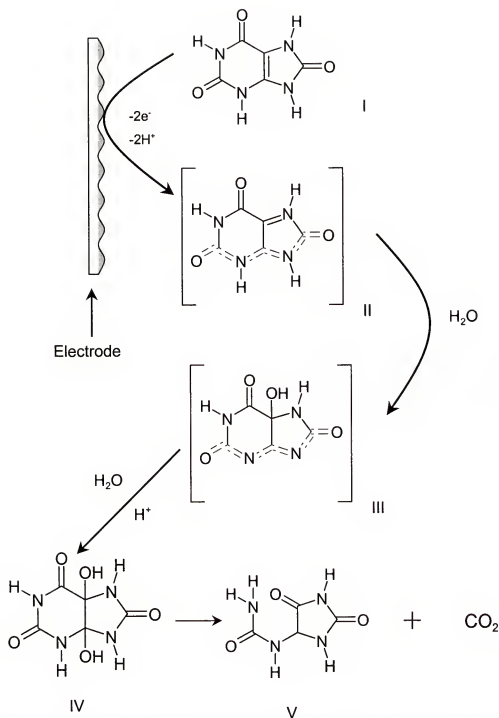


Figure 1.5. Mechanism for the electrochemical oxidation of uric acid [Dryhurst, 1972a; 1972b].

CHAPTER 2 EXPERIMENTAL SECTION

Reagents and Solutions

Acetonitrile (MeCN) HPLC grade, ACS certified methanol (MeOH), tetrabutyl ammonium perchlorate (TBAP), potassium chloride (KCl), sodium phosphate mono-basic (NaH_2PO_4) and di-basic (Na_2HPO_4), ethylenediaminetetraacetic acid (EDTA), sodium chloride (NaCl), magnesium chloride, potassium hexacyanoferrate (III) ($\text{K}_3(\text{Fe}(\text{CN})_6)$) were obtained from Fisher (Pittsburgh, PA). N-2-hydroxyethylpiperazine-N'-2-ethanesulfonic acid (HEPES), glucose, tris(hydroxymethylaminomethane-HCl) (tris-HCl), uric acid, dopamine, ascorbic acid, Pyrrole (PY) were obtained from Sigma Chemical Co. (St. Louis, MO). Phosphotungstic acid and pyruvic acid were obtained from Aldrich Chem. Co. (St. Louis, MO). $\text{Ru}(\text{NH}_3)_6\text{Cl}_3$ was obtained from Johnson Matthey (Alfa Products, Ward Hill, MA). Py was purified by passing it through a series of Pasteur pipettes, usually three, filled with neutral 80-200 mesh (Fisher, Pittsburgh, PA) alumina until the color becomes stable. All solutions were freshly prepared and aqueous solutions were prepared with doubly distilled water, non-degassed. Other chemicals were at least of analytical reagent grade and were used as received. All determinations were performed at room temperature.

The composition of the electrolytes and buffers for electrolytic treatment and for the determinations was, in mM: 100 KCl; 12.5 Tris-HCl (tris(hydroxymethyl)aminomethane hydrochloride $K_a=8.08$); Krebs-Henseleit: 117.9

NaCl, 4.8 KCl, 2.5 $\text{CaCl}_2 \cdot 2\text{H}_2\text{O}$, 1.18 $\text{MgSO}_4 \cdot 7\text{H}_2\text{O}$, 1.2 KH_2PO_4 , 0.5 $\text{Na}_2\text{EDTA} \cdot 2\text{H}_2\text{O}$, 0.14 ascorbic acid, 5.5 glucose, 25.0 NaHCO_3 , 2.0 pyruvic acid; 70 $\text{NaH}_2\text{PO}_4/\text{Na}_2\text{HPO}_4$; Krebs:126.0 NaCl, 2.5 KCl, 2.4 $\text{CaCl}_2 \cdot 2\text{H}_2\text{O}$, 20.0 HEPES, 1.2 NaH_2PO_4 , 0.5 $\text{Na}_2\text{EDTA} \cdot 2\text{H}_2\text{O}$, 0.14 ascorbic acid, 5.5 glucose, 25.0 NaHCO_3 ; 70 and 300 phosphate buffer. Unless otherwise specified, the pH was 7.4. The pH was adjusted with HCl or NaOH and the determinations were performed at room temperature.

Electrodes.

Reference and Auxiliary Electrodes

A saturated calomel electrode (SCE) (Fisher, Pittsburgh, PA) was used as a reference electrode. When MeCN was used as the solvent, a quasi-reference electrode (a 5 cm long and 0.5 mm diameter silver wire (Goodfellow, Berwyn, PA)) was used as a reference to avoid water contamination of the organic solvent and to prevent liquid-liquid junction potentials [Sawyer et al., 1995]. When a rough pyrolytic electrode was used as working electrode, a conventional three-electrode electrochemical cell was used. Platinum foil electrode (area ca.1 cm^2) was used as the auxiliary electrode.

Working Electrodes

Rough pyrolytic graphite electrodes (RPG) were constructed from rectangular rods of RPG obtained from The Electrosynthesis Co. Inc., (Lancaster, NY). The RPG rod was cut into 0.5 cm in length and ca. 0.3 cm in width pieces. Each piece was sealed, cut side facing out, into the end of a glass rod using Epoxy-Patch (Dexter Corporation, Seabrook, NH). After drying overnight, the excess epoxy was sanded off using 600-grit silicon carbide (SiC) paper (Mark V Laboratory, East Granby, CT) on a polishing wheel (Ecomet I, Buchler Laboratory, Evanston, IL) until the surface of RPG was exposed.

Electrical contact was made to the unpolished side of the electrode using mercury and a piece of copper wire. Finally, the open end of the electrode was sealed with Teflon tape. Before any determination, the RPG electrodes were polished on 600-grit SiC paper for 1 min, using a polishing wheel, and sonicated in doubly distilled water for at least three minutes. The electrodes were rinsed with doubly distilled water and dried before any determination. Electrode areas were determined using chronocoulometry by stepping the potential from 0.4 to -0.2 V *versus* SCE with 5×10^{-3} M $\text{K}_3\text{Fe}(\text{CN})_6$, $D_0 = 7.63 \times 10^{-6}$ $\text{cm}^2 \text{ s}^{-1}$ [Stackelberg et al., 1953], in 0.5M KCl (pH 6.0). Typical RPG areas were $(0.033 \pm 0.005) \text{ cm}^2$.

Carbon fiber of ca. 7 μm diameter (Textron Specialty Materials, Lowell, MA) was used as the working electrode. A single carbon fiber was connected to a copper wire with silver epoxy (EPO-TEK 410E, Epoxy Technology, Billerica, MA). After the epoxy dried (ca. 24 hrs at room temperature), the fiber was sealed in a micropipet tip with Shell Epoxy (Shell Epon 828, Miller-Stephenson Chemical, Danbury, CT), with methylenediamine (Miller-Stephenson Chemical, Danbury, CT) as hardener (12% by weight). The epoxy was dried overnight at room temperature, and was cured in an oven for 1h at 150°C . After curing, the excess epoxy was removed from the fiber disk surface by polishing on 600-grit SiC paper (Mark V Laboratory, East Granby, CT) for 1 min, using a polishing wheel (Ecomet I, Buehler Laboratory, Evanston, IL). The response of the polished electrodes was tested by voltammetry in 5×10^{-3} M $\text{K}_3\text{Fe}(\text{CN})_6$ in 0.5 M KCl at 50 mV s^{-1} (pH 6.0). Electrodes that did not respond were repolished; electrodes that did not respond after repolishing were discarded.

The electrodes were next polished with $\gamma\text{-Al}_2\text{O}_3$ suspension of 0.1 μm particle size (Gamal, Fisher Scientific, Pittsburgh, PA) for a determinate time, usually 10 s, on a polishing cloth (Mark V Laboratory, East Granby, CT), using a polishing wheel (Ecomet I, Beuhler Laboratory, Evanston IL). The electrodes were rinsed with water, dipped in 2-propanol for 10-15 min [Cahill, et al., 1996], and were finally sonicated in doubly distilled water for 5 minutes. Electrodes were electrochemically treated (ECP), by potential cycling from -1.0 to 1.5 V vs. SCE, except in HCl and Krebs, -1.0 to 1.2V, for 30 min at 10 V s^{-1} . The electrode area of the CFE was determined before and after ECP. Discussion about the area determinations is presented in Chapter 4.

Instrumentation

Instrumental Setup for Determinations at Low Scan Rate

A Bionalytical Systems Electrochemical Analyzer (BAS-100, West Lafayette, IN) was used for all the chronocoulometric and voltammetric determinations at scan rates lower than 1 Vs^{-1} . The electrochemical data was downloaded to an IBM PS/2 model 50 computer and analyzed using Origin 5.0 (Microcal Software, Inc., Northampton, MA). When a carbon fiber electrode (CFE) was used as working electrode, a homemade current amplifier based on Faulkner's design [Huang et al., 1986] was connected to the BAS and properly grounded [Hsueh and Brajter-Toth, 1996] as illustrated in Figure 2.1. Briefly, the home-made preamplifier is formed by an input operational amplifier (AD515A, Analog Devices), various resistors and capacitors and a second operational amplifier (OP27) as illustrated in Figure 2.2.

The input amplifier AD515A of the current transducer was a monolithic precision, low power, FET-input operational amplifier. The AD515A functioned as a

current-to-voltage converter which, amplified and converted the input currents to voltages. Various resistors (1, 10 and 100 M Ω) and capacitors (1, 10, 100 pF) in the feedback loop controlled the gains (100, 1,000, and 10,000) and RC time constants (1, 10, and 100 μ s). Because the current-to-voltage converter (AD515A) inverted the signal phases, a second operational amplifier (OP27) with a unit gain was used as an inverter to invert the signal phase back to normal. The capacitors and resistor on OP27 function as a first order filter to minimize noise in the circuit.

The minimum current measurable by the BAS was 0.1 μ A, but the gain of the current amplifier ranged from 100 to 10,000 so the BAS with the preamplifier could measure currents as low as 0.1 nanoamperes. The time constant should be as large as possible if the experimental conditions allow it. For cyclic voltammetry a suitable time constant for a potentiostat is decided by the following equation [Howell et al., 1986; Wipf et al., 1988].

$$RCn\nu \leq 4mV \quad (2.1)$$

Where R is the resistance in Ω of the first order filter, C is the capacitance in F, n is the number of electrons of the redox reaction and ν is the scan rate in Vs^{-1} . At low scan rates (less than 40 Vs^{-1}), the time constant of the system was set at 100 μ s which allows use of scan rates up to 40 Vs^{-1} for one electron (or 20 Vs^{-1} for two electron reactions) with negligible distortion in the ΔE_p .

Instrumental Setup for Determinations at High Scan Rate

A fast scan voltammetry (FSV) system is illustrated in Figure 2.3. Basically, a high-frequency triangular potential waveform was applied to the SCE reference electrode using a function generator (Universal Programmer, Model 175, EG&G Princeton, NJ, USA) in a two-electrode configuration system. The applied triangular wave was simultaneously monitored using the Channel 1 of the oscilloscope (LeCroy Model 9310, Chestnut Ridge, NY). Current at the CFE was transduced to voltage by the current transducer of the preamplifier and amplified by OP AD515A. The output of OP AD515A bypassed the OP27 as illustrated in Figure 2.1 and was directly connected to the oscilloscope by using Channel 2 which measured the output voltage. The ratio of the transduced current to the input current of the CFE was determined by the feedback resistance of OP AD515A. Conversion factors for the potentiostat were 10^6 , 10^7 and 10^8 $V A^{-1}$ when the resistors in the amplifier were 1, 10, 100 $M\Omega$ respectively. The RC time constant of the current transducer (1, 10, and 100 μs) was controlled by the feedback resistance and the capacitance on OP AD515A to minimize noise. Equation 2.1 can be used as a guide for setting the time constant of the potentiostat. A 1 μs time constant (which allows a scan rate of 2,000 Vs^{-1} for uric acid with a negligible distortion in the voltammogram) was used for typical UA determination a scan rates of 500 and 1,000 Vs^{-1} .

Because the large background current can obscure the Faradaic current at high scan rates, voltammograms were background subtracted. Since the high temporal resolution of the technique allows the use of signal averaging, 250 cycles were usually used for each determination. The background voltammograms were obtained in a buffer

solution, averaged and stored in the memory (M_1) of the oscilloscope. A buffer solution with the analyte was then added and the voltammogram was acquired. The averaged background response was subtracted from the averaged analyte response using the oscilloscope. The background subtracted response of the analyte was transferred to an IBM PS/2 model 50 computer via a simple BASIC program for plotting cyclic voltammograms using Origin 5.0. The phase of the potential at the CFE was reversed relative to the waveform potential at the reference electrode by the potentiostat [Hsueh, 1995]. Therefore, the phase of the potential waveform measured at the oscilloscope had to be inverted. Also, the phase of the current at the CFE was inverted by the inverting input of AD515A. The current from the background subtracted analyte response was inverted and amplified (depending on the gain used) to obtain the final cyclic voltammogram using Origin 5.0.

A copper mesh Faraday cage was used in FSV to minimize the environmental noise. The buffer and the analyte were injected with a syringe into the electrochemical cell (which has a volume of 80 μL) which allowed the solutions to be pumped into the cell, and this in turn allowed a permanent contact to be maintained between the solution and the electrode.

Fundamentals of Electrochemical Methods

Cyclic Voltammetry

Cyclic voltammetry (CV) has been used extensively as an analytical tool [Kashyap and Gratzl, 1998, Wen et al., 1998; Cavalheiro and Brajter-Toth, 1999]. CV is an extension of the linear sweep voltammetry where a triangular waveform is applied to an electrode immersed in an unstirred solution under controlled-diffusion of the analyte

and the resulting current is measured. In CV experiments, the potential of a stationary working electrode is changed linearly from an initial potential, where no faradaic reaction of the analyte occurs, to a final potential where reduction or oxidation of the analyte occurs and a current maximum is obtained. After traversing the potential region, peak potential (E_p), in which one or more electrode reactions take place and a maximum current has been reached (i_p), the direction of the linear sweep is reversed and the electrode reactions of intermediates and products, formed during forward scan, can be detected. The rate of potential change is the scan rate, v ($V\ s^{-1}$), and the potential range between the initial and the final potential is called the potential window which depends on the electrochemical properties of the analyte, electrode, and electrolyte. In a cyclic voltammogram, the current from the redox reaction of the analyte gradually rises after the potential is swept past the potential peak where the redox reaction takes places. After reaching this point, the current decays as the analyte diffusion controls the response of the electrode. The potential difference between the reduction, E_{pc} , and the oxidation, E_{pa} , is expressed as a

$$\Delta E_p = E_{pc} - E_{pa} \quad (2.2)$$

The theoretical peak current, i_p (A), for a diffusion controlled, reversible reaction is given by the Randles-Sevcik equation [Bard and Faulkner, 1980]:

$$i_p = (2.69 \times 10^{-5}) n^{1/2} A D_o^{1/2} v^{1/2} C_o^* \quad (2.3)$$

and for an irreversible reaction:

$$i_p = (2.99 \times 10^5) n (\alpha n_a)^{1/2} A D_o^{1/2} \nu^{1/2} C_o^* \quad (2.4)$$

where n is the number of electrons transferred per mole. A is the electrode area in cm^2 , D_o is the diffusion coefficient in $\text{cm}^2 \text{s}^{-1}$, ν is the scan rate in V s^{-1} , C_o^* is the concentration of the analyte in mol cm^{-3} , α is the transfer coefficient, and n_a is the number of electrons in the rate determining step. For adsorption controlled reactions, the peak current for a reversible reaction is given by:

$$i_p = (n^2 F^2 A \nu \Gamma_o) (4RT)^{-1} \quad (2.5)$$

and for an irreversible reaction:

$$i_p = (n \alpha n_a F^2 A \nu \Gamma_o) (2.718 RT)^{-1} \quad (2.6)$$

where Γ_o is the surface excess of the analyte in mol cm^{-2} , R is the gas constant in $\text{J mol}^{-1} \text{K}^{-1}$, T is the temperature in K , F is the Farady's constant in C , and the remaining variables are the same as for diffusion controlled process. Voltammograms at conventional size electrodes are peak-shaped and the peak current depends on scan rate as illustrated in Figure 2.4.A.

The area under current peaks corresponds to the charge associated with the oxidation or reduction of absorbed layer. The surface coverage can be obtained by the following equation [Bard and Faulkner, 1980].

$$\Gamma = Q (nF)^{-1} \quad (2.7)$$

where n number of electrons and F is the Faraday's constant.

As mentioned in Chapter 1, the voltammograms at UMEs are sigmoidal in shape as illustrated in Figure 2.4.B and the limiting current is independent of the scan rate up to ca. 1 Vs^{-1} which results from the edge effect which was previously discussed. For a disk UME the limiting current at steady state is expressed by:

$$i = 4nFD r C \quad (2.8)$$

Where n is the number of electrons, F is the Faraday's constant ($9.648531 \times 10^4 \text{ C mol}^{-1}$), r is the electrode radius in cm, D is the diffusion coefficient of the electroactive specie in $\text{cm}^2 \text{ s}^{-1}$, t is experimental time in s, and C is the concentration of the electroactive specie in the bulk solution in mole cm^{-3} . At scan rates bigger than 1 Vs^{-1} , voltammograms at UMEs are peak-shaped and the peak current depends on the scan rate.

The steady-state limiting current of Fe(CN)_6^{3-} , $7.7 \times 10^{-6} \text{ cm}^2 \text{ s}^{-1}$ [Stackelberg et al., 1953], was used to evaluate the apparent geometric area of the UME assuming a disk area of the electrode before and after electrochemical pretreatment. The obtained values from these determinations are well discussed in Chapter 4.

$$A_{\text{disk}} = \pi r^2 \quad (2.9)$$

Where r is the radius of the electrode which was calculated from the steady state limiting current.

Reversibility or Nernstian behavior of the redox reaction can be tested in several ways. For example, the value of ΔE_p (see Equation 2.2) can be used as an indicator of the reversibility of the electrode reaction. A one-electron reaction at 25 °C is considered reversible if ΔE_p is ca. 59.1 mV; quasi-reversible if ΔE_p is between 60 to 212 mV and irreversible if ΔE_p is greater than or equal to 212 mV [Bard and Faulkner, 1980]. This criterion is very effective and easy when a peak-shape voltammogram (conventional size electrodes or fast scan voltammetry) is obtained for the analysis. But low scan rate voltammograms at UME have a steady-state response, so a different criterion should be applied in these cases.

A couple of definitions about the voltammetric response of disk UMEs are required as review before discussing the applied criteria for the reversibility analysis. Limiting current in voltammetry is the maximum current which is reached during the redox reaction and is characterized by having a plateau sector on the voltammogram as illustrated in Figure 2.4.B. The steepest region of the voltammogram (E_r) is the sector in which the current changes linearly as a function of the applied potential.

One fast way to determine the reversibility of the system is using Thomeš criterion which is expressed in the following equation [Oldham and Myland, 1994]:

$$\Delta E_T = E_{3/4} - E_{1/4} \quad (2.10)$$

Where $E_{3/4}$ is the potential in mV when the response current is equal to three-quarters of the limiting current, and $E_{1/4}$ is the potential in mV when the response current is equal to one-quarter of the limiting current. A one-electron reaction is considered reversible if ΔE_T is equal to 56 mV; quasi-reversible if ΔE_T has a value from 57 to 113 mV; and irreversible if ΔE_T is equal or bigger than 113 mV.

Another way to determine the reversibility of the system is using the log-plot analysis. This criterion was used in this work to determine the reversibility of the system when a steady-state voltammogram was obtained. Consider the reaction $O + ne^- \rightarrow R$, the applied potential of the system can be given by [Bard and Faulkner, 1980]:

$$E = E^0 + 2.3 (RT/nF) \log (D_R^{1/2} / D_O^{1/2}) + 2.3 (RT/nF) \log ((i_l - i_a) / i_a) \quad (2.11)$$

Where E^0 is the standard potential of the redox reaction in mV; n is the number of electrons of the reaction; R is the gas constant in $J \text{ mol}^{-1} \text{ K}^{-1}$, T is the temperature in K, D_R is the diffusion coefficient of the oxidizable species in $\text{cm}^2 \text{ s}^{-1}$; D_O is the diffusion coefficient of the reducible species in $\text{cm}^2 \text{ s}^{-1}$; i_l is the limiting current in A; and i_a is the current at a specific potential point.

When $i_a = i_l / 2$, the current ratio becomes unity so that the third term vanishes. The potential for which this is so is $E_{1/2}$, the half-wave potential:

$$E_{1/2} = E^{0'} + 2.3 (RT/nF) \log (D_R^{1/2} / D_O^{1/2}) \quad (2.12)$$

and Equation 2.8 is often written as:

$$E = E_{1/2} + 2.3 (RT/nF) \log ((i_l - i_a) / i_a) \quad (2.13)$$

Equation 2.10 predicts a wave that rises from the baseline to the diffusion-controlled limit over a narrow potential region centered on $E_{1/2}$. Because the ratio of the diffusion coefficient ($D_R^{1/2} / D_O^{1/2}$) is nearly unity in almost any case, $E_{1/2}$ can be used as a good approximation for E^0 for a reversible couple.

A plot of E versus $\log ((i_l - i_a) / i_a)$ for a voltammetric wave should be linear with a slope of $2.3 (RT/nF)$ mV at 25 °C. A one-electron reaction is considered reversible if the slope is equal to 59.1 mV; quasi-reversible if the slope has a value from 60 to 119 mV; and irreversible if the slope is equal or bigger than 120 mV. The i_a values used for the determination of the slope were taken from the steepest region of the voltammograms.

Determination of the Electrode Capacitance

The apparent electrode capacitance, C_{obs} (F cm⁻²) was determined from the voltammetric background current measured at 10 V s⁻¹ at 0.75V *versus* SCE. The background was recorded in the experimental potential window in the absence of analyte in solution. It was assumed that at 0.75 V, the current due to surface faradaic reactions is low, and the voltammetric background current results from double layer charging. The apparent capacitance was normalized by the microdisk electrode area, using the radius determined from voltammetry using $\text{Fe}(\text{CN})_6^{3-}$. The Equation 2.14 was used to calculate the capacitance from the experimental background current [Anjo et al., 1989]

$$C_{obs} = \Delta I / 2 \nu A \quad (2.14)$$

Where ΔI is the background current, at 0.75 V, from the separation between the anodic and the cathodic sections of the voltammogram in A, and ν is the scan rate in $V s^{-1}$.

The ratio of the microscopic surface area to the projected electrode area is usually designated the roughness factor, and can vary from 1 to 5 for typical solid electrodes, or much higher for porous electrodes. The roughness factor can be indirectly used to determine the porosity of the surface and can be estimated from the following equation [McCreery and Cline 1996]:

$$\delta = C_{obs} [C_{flat}]^{-1} \quad (2.15)$$

where δ is the roughness factor, C_{obs} is the apparent capacitance in $F cm^{-2}$, and C_{flat} is the capacitance for a perfectly flat electrode in $F cm^{-2}$.

Fast scan voltammetry (FSV)

FSV is a modification of CV. In FSV a high-frequency triangular potential wave is applied to the cell instead of the low-frequency triangular potential wave which is applied to the cell in CV [Armstrong-James, et al., 1980]. Typical high-frequencies used in this work are usually 100 Hz and 200 Hz. Thus, a 100 Hz waveform scanning from –1.0 V to 1.5 V (which is the usual potential window in this work) gives a scan rate of 500 Vs^{-1} and the time for each scan is 10 ms.

Initially the voltage goes from –1.0 V to 1.5 V, and then back to –1.0 V. This pattern of positive and negative voltage sweeps generates a pattern of currents through

the working electrode, even in a simple supporting electrolyte solution without electroactive analyte. As previously mentioned, this background current is a result of double-layer charging and is produced by the complex impedance of the electrode/electrolyte interface.

When an electroactive analyte such as UA is added to the supporting electrolyte solution an extra current flow is generated through the electrode at certain specific regions on the waveform. Consequently, the signal is formed by the currents coming from the faradaic process and non-faradaic process as illustrated in Equation (1.4)

By using the capabilities of the oscilloscope, the background current which is recorded and stored in the memory of the oscilloscope can be subtracted from the total analyte signal to produce a background subtracted voltammogram, as illustrated in Figure 2.5.

The theoretical peak currents, i_p (A) (for diffusion controlled, reversible and irreversible, reactions and for adsorption controlled, reversible and irreversible, reactions) are calculated by using the same equations applied in cyclic voltammetry.

Chronocoulometry

Chronocoulometry (CC) is a potential step method in which the potential is changed almost instantaneously between a potential E_1 (where no faradaic reaction occurs) and a potential E_2 (where the redox process takes place) and the resulting charge is recorded as a function of time.

During a potential step experiment with electroactive species in solution, the faradaic process that occurs at a potential E_2 decreases the concentration of the reactive species at the electrode surface to zero. This situation produces a concentration gradient

that yields a mass transport from the bulk solution to the electrode surface that is controlled by diffusion.

The total charge, Q_{total} , in CC that is measured as a result of the potential step experiment has three different sources [Anson and Osteryoung, 1983]: (A) double-layer charging, Q_{dl} , (B) electrolysis of adsorbed species, Q_{ads} , and (C) electrolysis of the diffusing species in solution, Q_{diff} .

$$Q_{total} = Q_{diff} + Q_{ads} + Q_{dl} \quad (2.16)$$

The charge-time diffusion controlled, Q_{diff} behavior can be obtained from the integrated Cottrell equation, and Equation 2.7 can be expressed as follows:

$$Q_{total} = 2 n F A C_o * D_o^{1/2} t^{1/2} \pi^{-1/2} + Q_{ads} + Q_{dl} \quad (2.17)$$

Where n is the number of electrons associated with the redox reactions; F the Faraday constant, 9.6485309×10^4 C; A area of electrode in cm^2 ; D_o diffusion coefficient in $\text{cm}^2 \text{s}^{-1}$; C concentration in mol cm^{-3} ; t is time in s.

The second term of Equation 2.16 is the charge associated with surface-attached species at the electrode. Since the absorbed species should be on the electrode surface, it should be electrolyzed instantly when the potential is applied. Consequently, this term is not time dependent. The charge required to move the cell potential from E_1 to E_2 or double layer charge, Q_{dl} , is also a time independent term. A plot of Q_{total} vs. $t^{1/2}$ should be a straight line with a slope of $2 n F A C_o D_o^{1/2} \pi^{-1/2}$ and the intercept should be equal to

$Q_{\text{ads}} + Q_{\text{dl}}$. In a separate experiment, Q_{dl} was determined by using supporting electrolyte without the electroactive species. This procedure assumes Q_{dl} to be identical in the presence or absence of electroactive species.

The value of the slope was used to determine electrode area (A) for conventional size electrodes and diffusion coefficients (D_o) of analytes under diffusion-controlled reactions. In the experiments with polypyrrole films, background subtracted chronocoulograms were used to determine the amount of polypyrrole polymerized on the surface of the CFE.

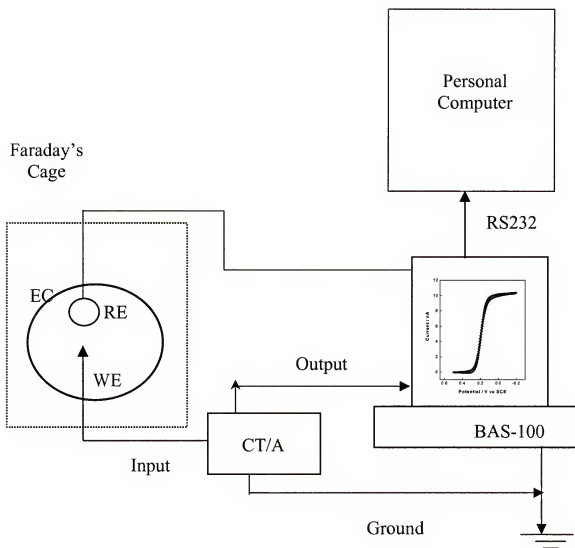


Figure 2.1. Schematic instrumental setup for ultramicroelectrodes at low scan rate; BAS-100: potentiostat, CT/A: Current transducer /amplifier, WE: working electrode, RE: reference electrode which also works as counter electrode, EC: electrochemical cell, RS232: connection port between potentiostat and computer.

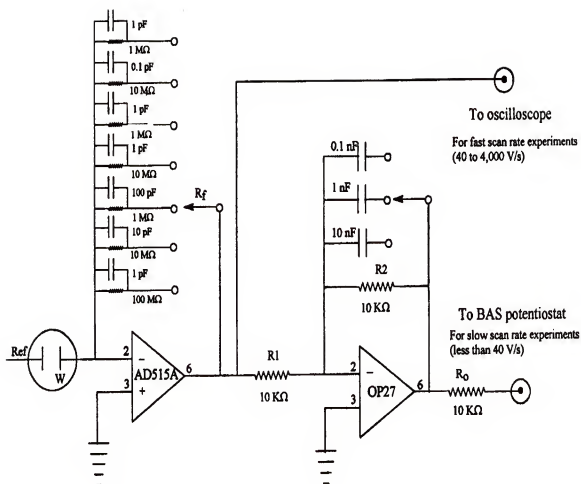


Figure 2.2. Schematic diagram of the current transducer [Hsueh and Brajter-Toth, 1996].

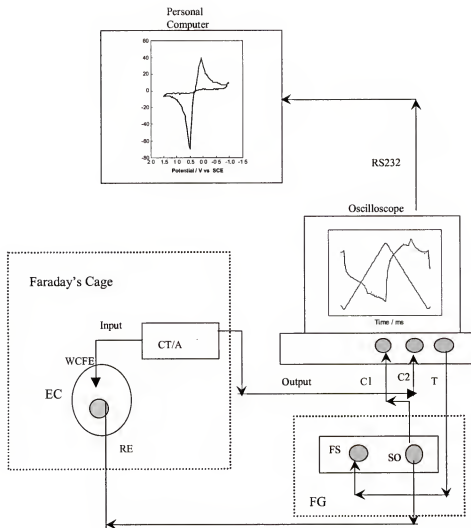


Figure2.3. Schematic instrumental setup for ultramicroelectrodes at fast scan rate; oscilloscope: C1: channel 1 to monitor applied waveform, C2: channel 2 to monitor response of electrode, T: trigger of oscilloscope to trigger the FG; FG: function generator: FS: frame synchronizer of FG, SO: signal output of FG; CT/A: Current transducer /amplifier, WCEF: working carbon fiber electrode, RE: reference electrode (SCE) which also works as counter electrode, EC: electrochemical cell (80 μ l volume), RS232: connection port between oscilloscope and computer.

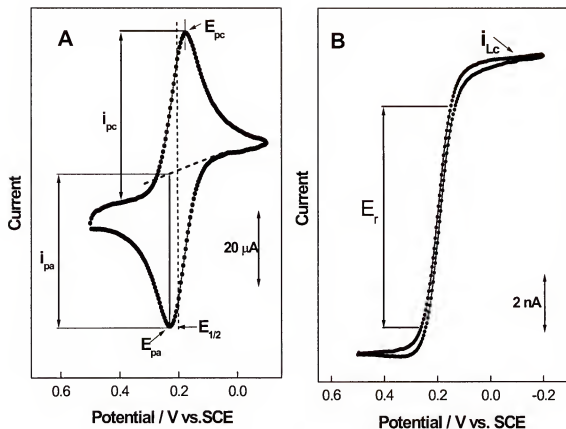


Figure 2.4. Cyclic voltammetry: (A) conventional size electrode (rough pyrolytic electrode) area 2 mm²; E_{pc} : cathodic peak potential, E_{pa} : anodic peak potential, $E_{1/2}$: half-wave potential, i_{pc} : cathodic peak current, i_{pa} : anodic peak current; (B) ultramicroelectrode (carbon fiber electrode) 7 μm diameter; i_{Lc} : limiting current, E_r : steepest region; 10 mM $\text{Fe}(\text{CN})_6^{3-}$ in 0.5 M KCl (pH 6.0). Scan rate 50 mVs⁻¹.

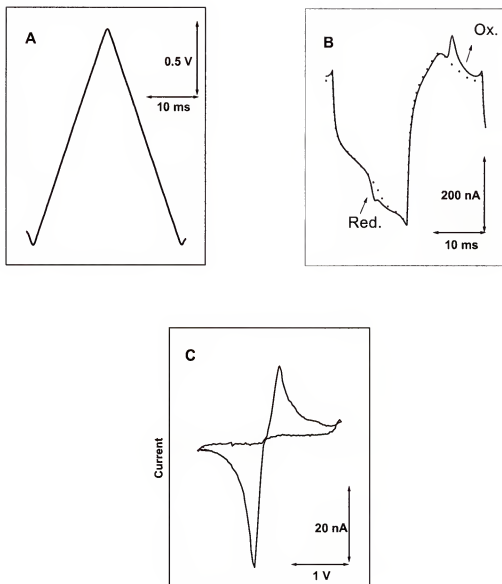


Figure 2.5. Schematic illustration of fast cyclic voltammetry and background subtraction at carbon fiber electrode ($7 \mu\text{m}$ diameter): (A) applied potential waveform as a function of time; (B) current as a function of time; dashed line is the background current of 70 mM phosphate buffer and solid line is the current in the presence of 1×10^{-4} M uric acid at 500 Vs^{-1} ; (C) A background subtracted voltamogram of 1×10^{-4} M uric acid at 500 Vs^{-1} .

CHAPTER 3

A HIGHLY ACTIVE CARBON FIBER ELECTRODE SURFACE FOR THE DETERMINATION OF URIC ACID IN PHYSIOLOGICAL BUFFERS

Background

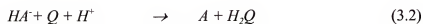
Electrodes with high sensitivity in bioanalysis can be produced by treating the electrode surface in various ways [Marino and Brajter-Toth, 1993; Cheng and. Brajter-Toth, 1995; Hsueh, et al., 1997]. In addition, loss of electrode activity during analysis creates a demand for surface regeneration [Bobalbhahi and Brajter-Toth, 1990; Marino and Brajter-Toth, 1993]. Electrochemical treatment is an attractive method of surface regeneration/activation since it can be performed in solution under conditions compatible with analysis [Feng, et al., 1987; Bobalbhahi and Brajter-Toth, 1990; Chen, et al., 1994].

The first electrochemical pretreatment (ECP) performed by Lord and Rogers demonstrated that anodization can produce a significant improvement in the voltammetric response for the reduction of Fe(III) in 0.1 M KCl at graphite electrodes [Lord and Rogers, 1954].

The reasons for the activation have been rationalized as: (a) an increase in the electrode area due to surface roughening [Freund, et al., 1991]; (b) generation of surface nano-cracks which expose carbon defects and edges, and which may generate new sites for electron transfer [Kovach, et al 1986; Hathcock, et al., 1995]; (c) removal of debris from the surface [Zak and Kuwana, 1982; Engstrom and Strasser, 1984]; and, (d) the ability to produce an oxide layer, rich in groups such as carbonyl, carboxyl, phenol, and

quinone [Evan and Kuwana, 1977; Cabannis, et al, 1985; Kamau, et al, 1985; McCreery and Cline, 1996].

Groups such as quinone (Q) can enhance the rates of proton-coupled electron transfer reactions [Kamau, et al, 1985] as illustrated below in Equations 3.1, 3.2, and 3.3 for the oxidation of ascorbic acid [Kamau, et al, 1985; Gomathi and Rao, 1985]:



However, high density of surface oxygen groups may decrease the response of some analytes, which may be prevented from approaching the electrode surface [McCreery and Cline, 1996]. The same surface groups may help preconcentrate other analytes through surface interactions. Such effects may explain the high sensitivity of *in vivo* determinations of cationic dopamine (DA) in the presence of ascorbate (anion) [Adams 1976; Wightman, et al., 1985; Feng, et al, 1987]

The enhancement of the response of the electrode depends on the nature of the pretreatment. The potential window, the composition of the electrolyte and, the length of time used for the pretreatment can be considered the main variables of the ECP. [Beilby, et al., 1995].

Alternating (ac) [Wang, et al., 1987] and direct current (dc) ECP [Chen, et al., 1994], and a combination of both [Gonon and Buda, 1985; Kovach, et al., 1986] has been used to activate carbon fiber electrodes (CFE). In one of the first examples of CFE pretreatment, Gonon and co-workers applied a 70 Hz triangular wave to a fiber electrode. The potential was cycled for 20 s between 0 V (vs Ag/AgCl) and an anodic potential that was varied with a target analyte and the matrix from 2.45 to 3.0 V. For monitoring DA release *in vivo* in the presence of 3,4-dihydroxyphenylacetic acid (DOPAC) anion, an anodic potential limit, required for ECP, was smaller than that used to monitor DA in the absence of DOPAC [Gonon1988].

Chen and co-workers found that the electrodes are not activated unless an anodic potential higher than + 1.8 V *versus* sodium-saturated calomel electrode (SSCE) and a cathodic potential more negatives than 0.5 V *versus* SSCE are used for the voltammetric determination of adenosine. Additionally, they suggested that even though the total amount of current can improve the effectiveness of the ECP, the treatment at cathodic and anodic potentials appears to be the principal key for the activation [Chen, et al., 1994]. However, Gonon and co-workers have suggested that the total amount of current passing through the electrode during ECP could be an important factor for the electrode.

Many studies have been done on the effects of the ECP by different electrolyte solutions such as strongly acid solution [Kozłowski, et al., 1985; Cabannis, et al., 1985; Rojo, et al., 1986], buffered solutions [Ewing, et al., 1981; Wang and Tuzhi, 1986; Zhang and Wang, 1995], salt solutions [Cheng and Falat, 1982; Wang, et al., 1987], and strongly basic solutions [Beilby and Carlsson, 1988; Chen, et al., 1994]. Kuhr and co-workers reported that the anodic pretreatment at neutral or basic pH increased the

adsorption of $\text{NADH} / \text{NAD}^+$ and the same anodic pretreatment in acid solution produced a more reproducible, diffusion-controlled profile for the oxidation of NADH at 100 Vs^{-1} [Kuhr, et al., 1993]. Wang and co-workers reported that ECP in sodium chloride (NaCl) solution results in larger residual current, and may result in different degrees of activation. For instance, fibers treated in NaCl solution produce a sharper and larger steady-state voltammetric response for acetaminophen, uric acid, and hydroquinone at 50 mVs^{-1} compared to surfaces undergoing a similar treatment in phosphate buffer pH 5.6. They attributed this effect to surface roughening that may induce an adsorption process [Wang, et al., 1987]. On the other hand, Falat and co-workers reported a significant amount of chlorine confined to the epoxy-graphite surface after vigorous pretreatment of the graphite electrode for 5 minutes in NaCl solution at $\pm 6.0\text{V}$ *versus* saturated calomel electrode (SCE) with 35 Hz square wave. It was followed by repetitive cycling over the working range in phosphate buffer pH 7.4 for a few minutes. The chloride can be incorporated as certain chlorinated organic structures that could produce a catalytic effect in the charge transfer reaction. Anjo and co-workers studied the response of dopamine *versus* pH from acidic to basic ECP treatments and found that the optimum pH was at or above 14 for the ECP in dopamine determination [Anjo, et al., 1989].

The time at which the electrode is held at a fixed potential (dc pretreatment) or how rapidly the electrode can be switched between the anodic and cathodic potential (ac) is another variable in the ECP. Anjo and co-workers reported that the periodic activation should be long enough to ensure complete activation of the surface in contact with the solution, but should not be so long that the surface could be damaged [Anjo, et al., 1989]. However, Chen and co-workers did not find any relationship between the period of

activation and the response of the electrode in the voltammetric determination of adenosine [Chen, et al., 1994].

As a result of ECP, stable background currents can be produced at electrodes used for analysis [Hsueh et al., 1997]. When the potential of the electrode is scanned (as in voltammetry when a qualitative identification of an analyte is needed) the background current can be large. When the background current is large, sensitive analysis is possible only when the current is stable and can be subtracted [Bravo, et al., 1998]. ECP can also increase the background current, and can contribute to an increase in adsorption [Kovach, et al., 1986; Feng, et al., 1987] which may in turn passivate electrodes.

We have previously reported that ECP can increase the sensitivity and the selectivity of carbon fiber electrodes in the determination of uric acid by FSV [Hsueh, et al., 1997; Bravo, et al., 1998]. In this work we have investigated the effect of the ECP parameters such as the potential window, the time needed for treatment, and the electrolyte, on the activity of carbon fiber electrodes for the determination of uric acid under physiological conditions. As a result of these investigations an optimized approach for CFE treatment, which combines polishing and ECP, is presented.

Results and Discussion

Effect of Mechanical Polishing

The goal of this work was to develop a reproducible method of fabrication of a sturdy and sensitive CFE for the determination of uric acid in biological samples. Because of the fabrication method of CFE used (Experimental), it was necessary to first polish the electrode surface to remove the excess of epoxy that was present at the surface

after the electrode was sealed in a pipet tip. The effect of polishing on the activity of CFE was, therefore, investigated first.

Although not extensively studied, conventional methods of polishing of carbon fiber are similar to those used for polishing of glassy carbon (GC) electrodes [McCreery, 1996]. Michael and Justice found that polished carbon fiber electrodes responded poorly to dopamine unless the electrodes were also electrochemically pretreated [Michael and Justice, 1987]. It has been shown previously [Engstrom and Strasser, 1984; Cabannis, et al., 1985; Hu et al. 1985] that at GC the k^0 of $\text{Fe}(\text{CN})_6^{3-/4-}$ varies from 10^{-4} to 0.14 cm s^{-1} depending on the method of polishing. Changes in the sensitivity of GC have been attributed to the polishing history. Typically, GC is polished with fine grade alumina or a diamond paste to obtain a mirror-like surface [Hu, et al., 1993; Kuhr, et al., 1993]. At these highly polished surfaces the residual current is low and the response is reproducible [McCreery and Cline, 1996]. However, surface analysis has shown that polishing debris such as alumina and carbon micro-particles may be embedded in the surface [Kamau et al., 1985]. In other reports it has been shown that the use of a polishing cloth decreased the rate of $\text{Fe}(\text{CN})_6^{3-/4-}$ reaction at GC [Engstrom and Strasser, 1984].

The effect of polishing with $\gamma\text{-Al}_2\text{O}_3$ was investigated here by controlling the polishing time. Table 3.1 summarizes the results. The results show that as the polishing time increases the capacitance of the electrode decreases. This is especially apparent at longer polishing times (Table 3.1). Lower capacitance and roughness factor after polishing leads to lower capacitance and roughness factor after the ECP. Apparently, the polishing time is associated with the kinetics at the electrode since the separation of the cathodic and anodic peaks of uric acid is the smallest when the polishing time is short

(Table 3.1). Presumably, after a long polishing time the surface becomes less active and the reaction of uric acid becomes slow.

The $\gamma\text{-Al}_2\text{O}_3$ polished electrodes were dipped in 2-propanol [Cahill et al., 1996] and were sonicated in doubly distilled water for 5 min [Zak and Kuwana, 1982] to remove surface impurities. These cleaning steps, and the electrochemical pretreatment/activation that followed, were most effective when the time of polishing was short as indicated by the smallest separation of the anodic and cathodic peak of uric acid (Table 3.1).

Short polishing may contribute to surface roughness, associated with a high background capacitance, and may also contribute to a complex background current. However, a stable background current can be subtracted quite effectively facilitating determinations by FSV [Hsueh and Brajter-Toth, 1996; Bravo et al., 1998].

Activation Potential

Effect of Positive Potential Limit.

The potential limits used in ECP were 1.0, 1.2, 1.5 and -0.8 and -1.0 V. The potential limits were selected to allow identification of uric acid by FSV which requires a display of a complete voltammogram. The limits were also selected to optimize surface pretreatment and background subtraction [Hsueh and Brajter-Toth, 1996; Bravo et al., 1998]. After the ECP, the electrode capacitance, roughness factor, the stability of the background current, the separation of the cathodic and the anodic peaks of uric acid in FSV and, the sensitivity and the limit of detection (LOD) of uric acid in FSV were determined.

Cyclic voltammograms (CV) obtained at 10 V s^{-1} at a CFE before (dashed line) and after the ECP (solid line) are shown in Figure 3.1 at different positive potentials. A significant change in the overall background current can be seen after 30 min of continuous treatment of the electrode by potential cycling. In addition, after the treatment, a well-defined anodic and cathodic peak is observed at 0 and -0.1 V, respectively.

As shown in the voltammograms, the background current obtained after the ECP is reasonably stable at potentials around 0.75 V. Assuming that the current is due to double-layer charging, the electrode capacitance can be determined from the current using Equation 2.14. The capacitance of $2091 \mu\text{F cm}^{-2}$ (Table 3.2) was determined for the treated CFE from Figure 3.1.C. This capacitance is an order of magnitude higher than the capacitance of $167 \mu\text{F cm}^{-2}$ reported by Feng and co-workers [Feng et al., 1987] for a fresh cut 30-40 μm diameter CFE which was not pretreated or polished. Adams and co-workers determined the capacitance at 0.3 V (vs Ag/AgCl) from cyclic voltammograms recorded in a pH 7.5 phosphate-buffered saline solution (11.5 g of Na_2HPO_4 , 2.47 g of NaH_2PO_4 and 9 g of NaCl per liter) in a potential window of -0.2 to 0.6 V. Tschuncky and Heintze reported that a normalized capacitive current increased with a decrease in electrode radius [Tschuncky and Heintze, 1995]. The ca. 7 μm diameter of the CFE used here is only five times smaller than the radius of the electrode used by Adams's group [Feng et al., 1987].

The large capacitance obtained here could be due to the construction method of the CFE, since factors such as the imperfections of the seal between the carbon fiber and the epoxy have been reported to play an important role [Fox et al., 1980; Wehmeyer and

Wightman, 1995]. A significant source of the capacitive current may also arise from the dielectric properties of the insulator body and from the silver epoxy used to establish the electrical contact. An excess of silver epoxy may coat the interior walls at the electrode tip and thus may contribute to a large capacitance [Tschuncky and Heintze, 1995].

Table 3.2 summarizes the capacitance values that were determined for different carbon fiber electrodes constructed by the same method. Before ECP, the capacitance and roughness factor were similar at all electrodes, and were high as expected for electrodes polished on 600-grit SiC paper. After the ECP the capacitance and roughness factor increased [Anjo et al., 1989; Beilby and Carlsson, 1988] especially when the positive potential limit of the pretreatment increased (Table 3.2, Figure 3.1). Thus, the ECP contributes to the large electrode capacitance that was determined.

The capacitance of the electrode is a measure of the electrode area [Gagnon and Austin, 1973] and may reflect contributions from surface faradaic reactions, and from adsorption. The effect of surface faradaic reactions was minimized here by measuring the background current at 0.75 V, where the contribution of such reactions to the background current, and thus to the capacitance, is small (Figure 3.1.C). Adsorption was minimized by using a low ionic strength buffer as electrolyte. Thus, the high capacitance after the ECP, which increased with an increase in the positive potential limit of the pretreatment, must reflect an increase in the electrode area from treatment.

Nano-cracking can occur at the surface of the electrode during ECP [Hathcock et al., 1995; Zhang and Wang, 1995]. Therefore, the high area of the fiber disk electrodes, after polishing and after the ECP at positive potentials, likely results from processes which nanostructure the surface of the electrode.

Small peaks in the voltammograms in Figure 3.1 at ca. - 0.1 and 0 V are usually associated with the reduction/oxidation of quinone/hydroquinone surface groups [McCreery, 1996]. Voltammograms in Figure 3.1 obtained before the ECP (dashed line) show only a small peak at these potentials. However, after the ECP (solid line, Fig. 3.1) a surface redox process is evident at ca. 0 V. As the potential limit of the ECP becomes more positive, the peak current at 0 V associated with the redox couple increases. In the potential window of -1.0 to 1.0, 1.2 and 1.5 V the cathodic current at -0.1 V is 0.44, 0.81 and 1.64 nA at 10 Vs, respectively. The faradaic current was measured by extrapolating the baseline at the foothill of the peak to avoid contributions of charging current to the measured current.

Effect of Negative Potential Limit

When the negative potential limit of the ECP was increased from -0.8 to - 1.0 V, the charging current increased over entire potential range, especially when the positive potential limit of the ECP was 1.5 V. The increase was accompanied by an increase in the current at 0 V produced by the surface redox couple quinone/ hydroquinone [Evans and Kuwana, 1977; Kamau et al., 1985].

It has been postulated that in aqueous solutions, electrogeneration of hydroxide results from the following processes [O'Brien et al., 1998]:



At potentials from -0.4 to -0.8 V generation of hydroxide is regulated by the reduction of oxygen (Equation 3.4). At potentials more negative than -0.8 V, hydroxide forms predominantly via reduction of water (Equation 3.5).

The concentration of oxygen dissolved in solution is finite but the amount of water is virtually unlimited. Thus, generation of hydrogen and hydroxide via processes in Equation 3.5 may be the principal factor responsible for the increase in the background current (and capacitance) when the negative potential limit of the ECP is extended to -1.0 V (Table 3.2). The increase in the negative potential limit also improves electrode kinetics as indicated from the peak separation for uric acid, and this is most apparent at electrodes pretreated at the most positive potential of 1.5 V (Table 3.2). This may be due in part to the ability of hydroxide and hydrogen to react with an oxide-layer that may be produced during anodization. Additionally, hydrogen evolution may contribute to nanocracking at the surface of the CFE [O'Brien et al., 1998] yielding a rougher surface.

Effect of Electrolyte

Kuhr and co-workers have applied a cyclic waveform from -0.2 to 2.0 V vs Ag/AgCl at 50 Hz for 3 s to pretreat carbon fiber electrodes for the determination of NADH. The pretreatment was performed in phosphate buffer at pH 7.4 and 12, and in 1.0 M HCl. The treatment in acid yielded the most reproducible response. It was postulated that the treatment in acid produced a CFE surface that was rich in oxide-containing groups such as the quinone/hydroquinone. It was argued that during treatment at high pH, surface oxidation was much less extensive and may have reduced the density of hydroxyl and carbonyl groups while increasing the density of carboxylates.

Since the detection of uric acid is of interest under physiological conditions

[Bravo et al., 1998], the activity and the stability of the carbon fiber electrodes was tested following the ECP in different physiological buffers (pH 7.4). The buffers tested included sodium phosphate, Krebs, Krebs-Henseleit, trisHCl and KCl.

The results obtained show that the capacitance (at 0.75 V) is essentially independent of the buffer used in the ECP (Table 3.3). Since the background current is a measure of the electrode area this indicates that the area of the electrode is independent of the buffer used in treatment. Similar capacitance values confirm the absence of specific adsorption and indicate that a similar surface is produced after the ECP in different buffers, leading to a response which is essentially independent of the buffer.

Before ECP, typically, a higher capacitance was determined at 0.75 V in buffers with high concentration of chloride. It is possible that this effect is due to the ability of chloride ions or chlorine, which can evolve at positive potentials, to penetrate the electrode [Wang and Tuzhi, 1986]. However, the capacitance at 0.75 V vs. SCE was not higher in chloride after the ECP.

The high capacitance that resulted from the ECP is responsible for the high background current (Table 3. 3). After the ECP, the principal factor which controls the sensitivity in the determinations of uric acid by FSV is the high background current [Hsueh and Brajter-Toth, 1996]. Although the capacitance of CFE is similar at 0.75 V in different physiological buffers that were tested, the background current of the CFE varies from buffer to buffer at the potentials where uric acid is detected. For example, for a typical detection potential of 0.5 V, the background current in K-H buffer was 20 nA (at 10 V s^{-1}), and was higher than the background current in phosphate buffer (10 nA). The higher background in K-H likely results from the presence of electroactive materials in

the buffer which can contribute to the current at the detection potential of 0.5 V. Additionally, background currents of electrodes (which were ECP treated in solutions with high concentration of chloride) present a very high background tail at 1.5 V *versus* SCE. This high background tail was associated with the oxidation of the carbon surface [Kinoshita, 1988].

A high current was observed at positive potentials in HEPES, and in other buffers which contained tertiary amines which are electroactive at 1.4 V, [Pihel et al., 1994]. In such buffers, uric acid was determined after the ECP in the potential window from 1.2 to -1.0 V, which resulted in lower background currents.

Stability of Background Current

A stable background current facilitates background subtraction that is necessary in fast scan voltammetry. We have established that a stable steady-state background current can be obtained at CFE after 30 minutes (or 3600 cycles) of continuous cycling the electrode in the potential in the potential window from -1.0 to 1.5 V vs. SCE in 7×10^{-2} M potassium phosphate buffer (pH 7.4) at scan rate of 10 Vs^{-1} [Bravo et al., 1998; Bravo and Brajter-Toth, 1999].

A comparison of the voltammograms before ECP (1) and after ECP (2) in Figure 3.2 shows a significant change in the overall background current after first 30 min of continuous cycling in the potential window from -1.0 to 1.5 V vs SCE. The charging current increases in the entire potential window. The absence of significant changes in the overall background current after additional 30 and 60 minutes of continuous cycling (curves 3 and 4 in Figure 3.2) indicates that a reasonably stable background can be reached after 30 minutes of continuous cycling in this potential window.

Stability of the Electrode After ECP

In previous work [Hsueh et al., 1997] we have reported that the amount of surface oxygen, as well as the roughness of the electrode surface, can change during a voltammetric determination when the potential of the electrode is scanned. This can in turn produce a significant change in the background current. We also observed that the background current was unstable after the ECP from -0.8 to 1.2 V, after the treated electrode was removed from the electrochemical cell. To avoid problems with stability of the electrode, a syringe was used to inject the analyte into the electrochemical cell, which allowed the solution to be pumped into the cell without removing the CFE.

In order to evaluate the electrode stability after the ECP from -1.0 to 1.5 V, the background current was measured after the treated electrode was removed from the cell for different periods of time. To examine the stability of the treated electrodes, the background current was recorded right after the ECP, and the electrode was then removed from the cell for 5, 10 or 15 min before the background current was recorded again. Additionally, the electrode background current was measured at the treated electrodes before and after a calibration curve was obtained for uric acid by FSV in a concentration range from 5 to 20 μM . With four measurements at each concentration and 250 cycles for each measurement this amounted to around 4,000 cycles in the analytical potential window.

Figure 3.3 shows that unlike the background current of the CFE treated in the potential window of -0.8 to 1.2 V, the current of the electrodes treated from -1.0 to 1.5 V is stable after the treated electrode is removed from the cell. The same results were

obtained for electrodes removed from the cell for 5, 10 and 15 min [Bravo and Brajter-Toth, 1999; Bravo et al., 1999].

A response analogous to that shown in Figure 3.4 was obtained before and after a calibration curve was obtained for uric acid by FSV at 500 V s^{-1} . Even though close to 4,000 cycles were recorded in the potential window of -1.0 to 1.5 V to obtain the calibration curve, the background current remained essentially constant.

Determination of Uric Acid

Figure 3.4 shows typical voltammograms of uric acid obtained by FSV at 500 V s^{-1} at electrodes treated in different potential windows. The results are summarized in Table 3.2. The best sensitivity and limit of detection (LOD) were obtained for uric acid after the ECP in the potential window from -1.0 to 1.5 V (Fig. 3.5.C, Table 3.2). The high sensitivity is accompanied by high electrode capacitance, and by a high activity of the electrode as verified by the kinetics of uric acid (from ΔE_p , Table 3. 2).

We postulate that the ECP in the potential window from -1.0 to 1.5 V produces a surface structure, which facilitates the reaction of uric acid [Zak and Kuwana, 1982; Hatcock et al., 1995]. ECP in other potential windows, which leads to significantly lower sensitivity of uric acid, may favor formation of inert surface oxides [Evans and Kuwana, 1977; McCreery, 1996]

Proposed Model of Electrode Activation

Figure 3.5 shows a scheme of the proposed model. Initially, a non-uniform rough surface can be produce by mechanical polishing of the disk CFE surface. Figure 3.5.A is the schematic micro cross section of the CFE prior to electrochemical pretreatment. The four horizontal lines represent individual graphite crystallites. Previous studies

demonstrated that carbon surfaces have active site defects, which are marked D in figure 3.5.A. Mechanical polishing can also contribute to the formation of these defects. Positive scans such as 1.5 V vs. SCE produce more defects, moderate oxidation, and possible intercalation of solvent, electrolyte and analyte. The most positive potential can produce the surface richest in defects as illustrated in Figure 3.6.B.

Sweeping to negative potential can yield the evolution of species such as hydroxyl and hydrogen. Assuming that water and supporting electrolyte were able to diffuse through surface defects, the production of these species inside the carbon layer is controlled by the negative applied potential as illustrated in Figure 3. 6.C. Equations 3.4 (at -0.8 V) and 3.5 (at -1.0 V) may govern the evolution of species inside of porous carbon surface. The proposed surface may have a homogenous roughness which is characterized by the presence of blisters and channels between them. The evolution of gas inside the carbon structure has been proposed as the primary driving force for blister growth.

The repeating negative and positive sweeping creates a surface of uniform roughness that is characterized by a stable and steady-state background current after 30 minutes of continuous cycling in the experimental potential window.

Conclusions

The results of this work reaffirm the value of surface pretreatment for achieving a stable background current and high sensitivity of carbon fiber electrodes. The active and stable electrodes were produced here by a combination of polishing and electrochemical treatment. Polishing produced a rough, active surface. After the electrochemical pretreatment surface homogeneity appeared to improve. The ECP also appeared to clean

the surface and affirm its chemical stability. An additional effect that was observed was a correlation of the effectiveness of the treatment with surface area and background current.

Based on the results, it can be postulated that the effective ECP that was developed results in the formation of surface nanocracks and edge nanostructures. In the potential window that was used for effective pretreatment this restructuring is more likely than the formation of surface oxides which can interfere with the response of uric acid. In addition, through the treatment, a background current which is stable at open cell potential is achieved presumably because of a stable surface composition.

The effect of the buffer composition on the outcome of the ECP was also examined. The surface conditions are independent of the buffer used for the ECP of the CFE. However, the amplitude and the shape of the background current at 0.5 V, a potential used in uric acid determinations by FSV, which is linked to surface faradaic processes, is a function of the composition of the buffer.

Table 3.1. Effect of polishing time on electrode parameters

Time ^a s	Capacitance ^{b,c} $\mu\text{F cm}^{-2}$		Roughness Factor ^d		ΔE_p^e mV
	Before ECP	After ECP	Before ECP	After ECP	
10	772 \pm 120	2091 \pm 200	286 \pm 44	774 \pm 75	307 \pm 35
30	454 \pm 100	1890 \pm 200	168 \pm 37	700 \pm 74	442 \pm 27
90	336 \pm 110	1075 \pm 230	124 \pm 41	398 \pm 85	502 \pm 25

- Time of polishing with alumina (0.1 μm particle size).
- Assuming disk area ($A = \pi r^2$), $r = 3.8 \pm 0.3 \mu\text{m}$, determined from voltammetry. Results for at least three electrodes ($n = 12$).
- ECP and capacitance measured in 70 mM phosphate buffer, pH 7.4. ECP from -1.0 to 1.5 V vs SCE. Capacitance calculated from background current obtained at 0.75 V at 10 V s^{-1} .
- Roughness factor is the ratio between the capacitance observed to the capacitance of a flat electrode ($(\delta) = C_{\text{obs}} [C_{\text{flat}}]^{-1}$), $C_{\text{flat}} = 2.7 \mu\text{F cm}^{-2}$ for a carbon fiber electrode 7 μm diameter [Frysz et al., 1997].
- 20 μM uric acid, 70 mM pH 7.4 phosphate, scan rate 500 V s^{-1} . Values obtained after ECP as in c, performed after polishing for different periods of time.

Table 3.2. Effect of the potential window of electrochemical pretreatment on electrode parameters.

Potential Window ^a V	Capacitance ^b $\mu\text{F cm}^{-2}$		Roughness ^c Factor		ΔE_p ^d mV	UA ^e Sensitivity $\text{nA } \mu\text{M}^{-1}$	LOD ^e μM
	Before ECP	After ECP	Before ECP	After ECP			
1.0 to -1.0	376	467	139	173	581 ± 23	0.02_6^f	60^f
1.2 to -1.0	443	720	164	266	367 ± 39	0.080 ± 0.004	10
1.5 to -1.0	772	2091	286	774	307 ± 35	0.44 ± 0.02	5
1.5 to -0.8	745	1303	276	483	448 ± 31	0.30 ± 0.02	5
1.2 to -0.8	352	905	130	335	518 ± 15	0.02_0^f	70^f

- versus* saturated calomel electrode (SCE). Three electrodes were used for each determination ($n = 12$).
- At 0.75 V vs SCE, 70 mM phosphate buffer, pH 7.4, scan rate 10 V s^{-1} , 50 cycles. Electrode area assuming a disk area from radius determined from voltammetry, $r = 3.8 \pm 0.3 \mu\text{m}$.
- Roughness factor is the ratio between the capacitance observed to the capacitance of a flat electrode ($(\delta) = C_{\text{obs}} [C_{\text{flat}}]^{-1}$), $C_{\text{flat}} = 2.7 \mu\text{F cm}^{-2}$ for a carbon fiber electrode $7 \mu\text{m}$ diameter [Frysz et al., 1997].
- $50 \mu\text{M UA}$, 70 mM phosphate buffer, pH 7.4, 500 V s^{-1} , 250 cycles averaged
- Sensitivity from the slope of the calibration curve
- Sensitivity based on one calibration point.
- LOD when $S/N = 3$. Noise = peak-to-peak rather than N_{rms}

Table 3.3. Effect of the supporting electrolyte in the electrochemical treatment on electrode parameters.^a

Supporting Electrolyte ^b	Capacitance ^c $\mu\text{F cm}^{-2}$		I_b ^d nA	ΔE_p mV	UA ^e Sensitivity $\text{pA } \mu\text{M}^{-1}$	LOD ^f μM
	Before ECP	After ECP				
KCl	1304	1797	25	258 ± 32	78 ± 5	25
Tris-HCL	550	1975	25	628 ± 16	38 ± 2	20
Krebs- Henseleit	1412	2227	18	583 ± 21	346 ± 2	10
70 mM Sodium Phosphate	772	2091	10	307 ± 35	440 ± 2	5
300 mM Sodium Phosphate	559	1700	10	450 ± 35	340 ± 5	5
Krebs ^g	N/A	N/A	N/A	680 ± 45	57 ± 9	15

- ECP by continuous potential cycling for 30 minutes at 10 V s^{-1} in the experimental potential window from -1.0 to 1.5 V except in Tris-HCl and Krebs, -1.0 V to 1.2 V.
- Composition of pH 7.4 supporting electrolytes (mM): 100 KCl; 12.5 Tris-HCl (tris(hydroxymethyl)aminomethane hydrochloride, $\text{pK}_a = 8.08$); Krebs-Henseleit 117.9 NaCl, 4.8 KCl, 2.5 $\text{CaCl}_2 \cdot 2\text{H}_2\text{O}$, $1.18\text{MgSO}_4 \cdot 7\text{H}_2\text{O}$, 1.2KHPO_4 , 0.5 $\text{Na}_2\text{EDTA} \cdot 2\text{H}_2\text{O}$, 0.14 ascorbic acid, 5.5 glucose, 25.0 NaHCO_3 , 2.0 pyruvic acid; 70 sodium phosphate; Krebs 126.0 NaCl, 2.5 KCl, $2.4 \text{CaCl}_2 \cdot 2\text{H}_2\text{O}$, 20.0 HEPES, 1.2 NaH_2PO_4 , 0.5 $\text{Na}_2\text{EDTA} \cdot 2\text{H}_2\text{O}$, 0.14 ascorbic acid, 5.5 glucose, 25.0 NaHCO_3 .
- Capacitance determined at 0.75 V from voltammetry at 10 V s^{-1} in the potential window from -1.0 to 1.5 V except in Tris-HCl and Krebs, 50 cycles.
- Background current at 0.25 V, 10 V s^{-1} , 50 cycles, after ECP as in a.
- From the slope of the calibration curve. At least 5 points for each calibration curve and 4 determinations for each point were taken for three different electrodes.
- LOD when $\text{S/N} = 3$. Noise = peak-to-peak rather than N_{rms}
- Not available

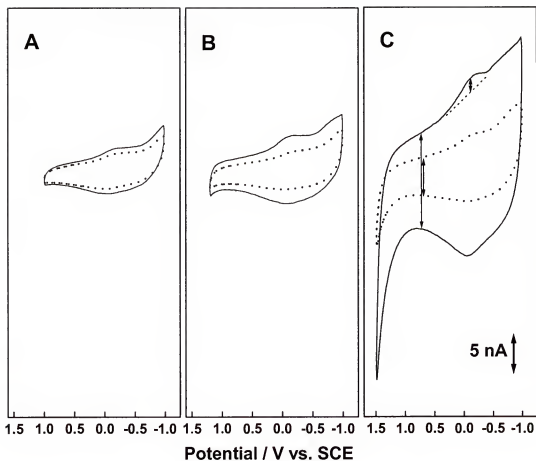


Figure 3.1. Background current at ca. $7\mu\text{m}$ diameter carbon fiber electrode, before (dashed line) and after (solid line) electrochemical treatment by continuous 30 min cycling in 7×10^{-2} M phosphate buffer pH 7.4 in the potential window (*versus* SCE) from -1.0 to different positive potential limits. Scan rate 10 V s^{-1} . The voltammograms were signal averaged 50 times. Potential windows of treatment shown in the voltammograms.

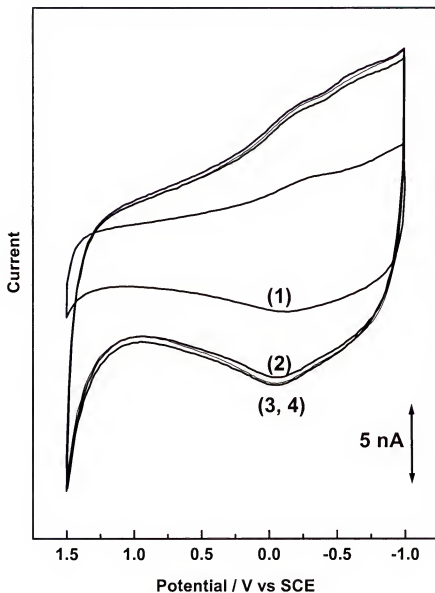


Figure 3.2. Background current at 10 V s^{-1} after continuous cycling in $7 \times 10^{-2} \text{ M}$ potassium phosphate buffer (pH 7.4) in the potential window from -1.0 to 1.5 V versus SCE. Cyclic voltammograms obtained (1) with a fresh polished carbon fiber (approximately $7 \mu\text{m}$ diameter), (2) after 30 minutes of continuous cycling at a scan rate of 10 V s^{-1} , (3 and 4) after additional 30 and 60 min of continuous cycling, respectively. The background currents at carbon fiber electrodes were signal averaged 50 times.

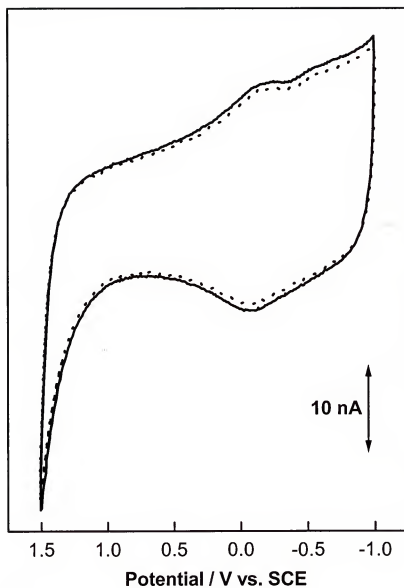


Figure 3.3. Stability of the electrochemically pretreated CFE. Background current: before (dashed line) and after (solid line) a calibration curve of uric acid was obtained or when the electrode was exposed to air for 15 minutes. Other conditions as in Fig. 3.3.

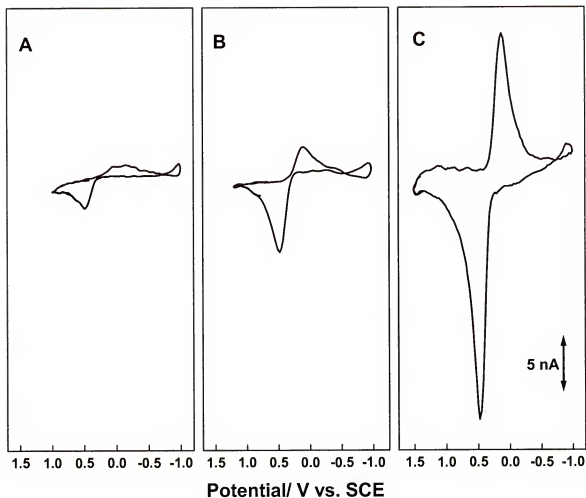


Figure 3.4. Fast scan voltammetry of 9×10^{-5} M uric acid in 70 mM phosphate buffer pH 7.4 at 500 V s^{-1} . Effect of the positive potential limit of the electrochemical pretreatment, 30 minutes continuous cycling at 10 V s^{-1} . CFE was pretreated in the potential window shown in voltammogram. The cyclic voltammograms were background subtracted after 250 cycles for the background and UA were recorded at 500 V s^{-1} in the potential window shown in the voltammograms.

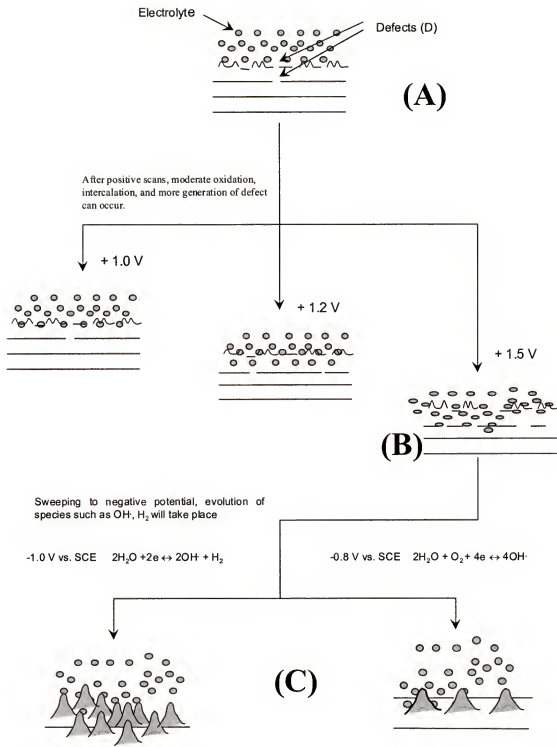


Figure 3.5. Schematic illustration of possible effects of the pretreatment at the carbon fiber electrode surface.

CHAPTER 4 ELECTROCHEMICAL CHARACTERIZATION OF CARBON FIBER SURFACES

Background

Carbon has the exceptional ability of forming materials with a very high surface area (up to $3000 \text{ m}^2 \text{ g}^{-1}$), low densities (below 0.1 g cm^{-3}), and a high concentration of nanometer size pores. Examples of porous carbon are activated carbon fibers (ACF) which have very high surface area and carbon aerogels, which have a very low mass densities [Dresselhaus and Dresselhaus, 1997]. One attraction of the activated carbon fiber over other porous carbon materials is the relatively small pores ($< 2 \text{ nm}$) and the relatively narrow size distribution of the nano-pores.

Since highly ordered pyrolytic graphite (HOPG) electrodes are structurally well defined [Goss et al., 1993; McCreery, 1991], they have been used as a model for the characterization of treated carbon surfaces. Combinations of surface techniques such as atomic force microscopy (AFM), X-ray microprobe, Raman spectroscopy and Auger surface analysis have been used to characterize the surface of HOPG, during and after, electrochemical pretreatment [McCreery, 1991]. Dresselhaus and co-workers reviewed and analyzed the characterization techniques for activated carbon fiber surfaces. Parameters and techniques such as X-ray, Raman spectra, transport properties, photoconductivity, and electron spin resonance were used to characterize the activated carbon fiber surfaces [Dresselhaus et al., 1998]. The reported results reveal a significant

agreement with the results reported in this Chapter using electrochemical characterization of CFE.

In Chapter 3, we reported the development of a novel carbon fiber surface, which was obtained by using mechanical and electrochemical activation [Bravo et al., 1998; Bravo and Brajter-Toth, 1999]. This surface was developed to optimize the determination of biological purines such as uric acid and adenosine, which are much less active than previously studied biological analytes such as dopamine [Pihel et al., 1995]. In this Chapter, conventional electrochemical approaches were used to characterize the activated carbon fiber. First, a method for the determination of the geometric area of the disk carbon fiber was developed at different pH (3.0 and 7.4 physiological pH). Next, structurally different electrochemical probes $\text{Fe}(\text{CN})_6^{-3/-4}$, $\text{Ru}(\text{NH}_3)_6^{+3/+2}$, ascorbate, uric acid, and dopamine were used to characterize the surface of the ACF electrodes. Additionally, the surface was characterized through the determinations of capacitance and the roughness factor, which can be used to validate the porosity of the surface.

The principal goal of this Chapter is to monitor the electrochemical treatment of CFE by using a combination of diagnostic electrochemical measurements. The results show that highly ACF electrodes can be fabricated for the targeted analytes by a method that combines polishing and electrochemical pretreatment [Bravo and Brajter-Toth, 1999, Bravo et al., 1998]. This method minimizes irreversible oxidation of the surface [Goss et al., 1993], and produces nanostructured electrodes. The surface groups that are formed appear to intercalate analytes [Besenhard and Fritz, 1983] and to engage in efficient proton transfer [Thorp, 1992; Snider et al., 1997].

Results and Discussion

Determination of the Apparent Geometric Areas

The area of the CFEs were calculated from voltammetric measurement of limiting current of $\text{Fe}(\text{CN})_6^{3-}$ at 50 mV s^{-1} , assuming a disk geometry. As previously mentioned, the limiting current of CFE is proportional to the concentration of analyte as shown in Equation 2.8. A plot of current (i) *versus* concentration (C) was a straight line with slope of $4nFD_0r$ as illustrated in Figure 4.1.

Since the literature reported diffusion coefficient value for $\text{Fe}(\text{CN})_6^{3-}$, $7.7 \times 10^{-6} \text{ cm}^2 \text{ s}^{-1}$, at pH 3 [Stackelberg et al.,1953], the initial determinations of the area of CFE were obtained at the same pH. Thus, solutions of five different concentration of $\text{Fe}(\text{CN})_6^{3-}$ (from 2×10^{-3} to $1 \times 10^{-2} \text{ M}$) in 0.5 M KCl were prepared at pH 3.0 (adjusted with HCl) and used to determine the area of the CFE before and after ECP. The typical areas of the CFE before and after ECP are summarized in Table 4.1.

Because electrochemical phenomena are surface processes and pH can alter them, determinations of electrode area at pH 7.4 were also evaluated. As shown in Table 4.1, appreciable differences between area determinations at pH 3.0 and 7.4 were not observed. The linearity of the plot of limiting current (i_L which was determined at -100 mV *versus* SCE) *versus* concentration (C) suggests that is possible to estimate the area of the electrode using one point calibration.

Based on these results, one determination point of limiting current for ferricyanide has been used as an initial parameter to screen which electrode is “good” and can be used for electrochemical pretreatment. A “good” electrode should give a limiting current of $5.0 \pm 0.5 \text{ nA}$ (at -100 mV *versus* SCE) and E° of $135 \pm 10 \text{ mV}$ for 5

$\times 10^{-3}$ M $\text{Fe}(\text{CN})_6^{-3}$ in 0.5 M KCl (pH 6.0) at 50 mV s^{-1} . After ECP, a “good” electrode should give a limiting current of $4.0 \pm 0.5 \text{ nA}$ (at -200 mV *versus* SCE) and E^0 of $165 \pm 10 \text{ mV}$ for 5×10^{-3} M $\text{Fe}(\text{CN})_6^{-3}$ in 0.5 M KCl (pH 6.0) at 50 mV s^{-1} .

The proposed model of mechanical and electrochemical activation in Chapter 3 predicts that the activated CFE surface (after ECP) may be characterized by its high degree of roughness. At low scan rates, changes in the microscopic surface domain of the electrode are impossible to be detected due to large thickness of the diffusion layer. For instance, ferricyanide determinations were obtained at 50 mVs^{-1} in the potential window from 500 to -200 mV and the required time for one cycle was 28 s. The estimated thickness of the diffusion layer (using Equation 1.1, $D_0 = 7.7 \times 10^{-6} \text{ cm}^2 \text{ s}^{-1}$) was $2.6 \times 10^{-1} \text{ cm}$ (260 μm). Consequently, changes on the order of 1 to 2 μm of the surface roughness can not be detected at these low scan rates [McCreery and Cline, 1996].

The required time in FSV for one cycle at 500 Vs^{-1} in a potential window from 800 to -200 mV is $2.8 \times 10^{-3} \text{ s}$ and this time produces a thickness of the diffusion layer of 2.6 μm . For the experiments such as FSV at 500 Vs^{-1} the diffusion layer can track changes in roughness on the μm scale or less.

Figure 4.2 shows the determination of the microscopic area of the CFE after electrochemical treatment using fast scan voltammetry at 500 Vs^{-1} with ferricyanide in 0.5 M KCl (pH 6.0) as a probe. The limiting current of CFE is proportional to the concentration of analyte as shown in Equation 2.4 in FSV. A plot of current (i_{lc}) *versus* concentration (C) was a straight line with slope of $(2.99 \times 10^{-5} n(\alpha n_a)^{1/2} \text{ A } D_0^{1/2} \text{ v}^{1/2})$. Figure 4.2 shows the background-subtracted voltammograms of different concentrations

of ferricyanide at 500 Vs^{-1} . The microscopic area of the CFE was determined (1.7 ± 0.1) $\times 10^{-6} \text{ cm}^2$ from the slope of the calibration curve.

Oxidation/reduction Voltammetry of Carbon Fiber Electrode Surfaces

The primary goal of this work was to produce stable and active carbon fiber electrodes for the determination of physiological purines, under physiological conditions. Electrochemical activation of carbon fiber electrodes in physiological buffers, at pH 7.4, was therefore evaluated as a method of electrode treatment/activation, to avoid a need for reequilibration of electrodes during voltammetric determinations, in physiological media, at pH 7.4 [Bravo and Brajter-Toth, 1999].

Electrochemically treated carbon fiber electrodes showed a response independent of buffer composition of buffers that were used in electrode treatment; this was discussed in Chapter 3. AFM analysis has shown that surface features of electrochemically treated graphite in phosphate buffer (pH 7) are similar to surface features of graphite treated in KNO_3 [Freund et al., 1991]. Generally, anodic behavior of carbon depends on electrolyte composition, if it contains chloride or oxygen groups, and depends on concentration and pH of the electrolyte [Beck et al., 1981; Kinoshita, 1988; Besenhard and Fritz, 1983].

Conditions, which minimize irreversible side reactions during electrolytic activation of carbon fiber electrodes in different electrolytes, can not be easily predicted because of differences in structure of graphite, and in composition of electrolytes. Irreversible side reactions, which occur during electrolytic activation of carbon, contribute to irreversible behavior of carbon electrodes. These reactions lead to the formation of nonconductive surface oxides and carbon dioxide and oxygen, the latter during electrolysis of water [Besenhard and Fritz, 1983; Goss et al., 1993].

To minimize irreversible side reactions that can occur during electrolytic treatment of carbon, and to integrate electrolytic treatment and reactivation of electrode surface with acquisition of analytical signals, carbon fiber electrodes were treated by continuous cycling of electrode potential, at a rate of 10V/s, in a potential window of 1.5 to -1.0V versus SCE. The treatment involved oxidation of the electrode surface, followed by a reduction, until a steady-state response was achieved as mentioned in Chapter 3 [Hsueh, et al., 1997].

Average background currents, before and after electrolytic treatment of carbon fiber electrodes, are shown in Figure 4.3. Several features can be identified in the background response obtained by voltammetry after electrolytic treatment of the carbon fiber surface. First, as indicated by an increase in background current at ca.1.5V, the carbon fiber electrode surface becomes oxidized after electrolytic treatment by continuous potential cycling at a rate of 10Vs⁻¹ in a potential window of 1.5 to -1.0V (small dash) [Besenhard and Fritz, 1983; Goss et al., 1993]. Secondly, mostly amorphous character of electrochemically treated carbon fiber surface is indicated from the featureless shape of the background current at positive potentials, which lacks peaks that are typically associated with oxidation of crystalline graphite [Besenhard and Fritz, 1983; Goss et al., 1993]. This is consistent with the method of fabrication of carbon fiber electrodes, which are first polished on 600-grit SiC paper to remove an excess of epoxy from the microdisk surface of the fiber, after the fiber is sealed with epoxy [Bravo and Brajter-Toth, 1999]; this roughens and may oxidize the surface, contributing to amorphous surface character.

Although oxidation of carbon fiber electrode surface after electrolytic treatment is apparent from the increase in background current at ca. 1.5 V, as shown in Figure 4.3, the relatively small oxidation current (25 ± 5 nA) at positive potentials (1.5 V) indicates a lack of extensive oxidation of the surface [Besenhard and Fritz, 1983; Goss et al., 1993] as a result of treatment by potential cycling at a rate of 10V/s in a potential window of 1.5 to -1.0V, which involves relatively fast surface oxidation and reduction.

An increase in background current after electrolytic treatment in the entire window of potential cycling, of 1.5 to -1.0 V, indicates an increase in the total electrode capacitance. Determinations of the voltammetric background current of 70 mM phosphate buffer (pH 7.4) at 0.75 V *versus* SCE, 10 Vs⁻¹, before (5 ± 1 nA) and after (10 ± 1 nA) electrochemical treatment were used as a diagnostic tool of the quality of the CFE prior to any electrochemical determination. Only, CFEs (which have these background current values) were used in analytical determinations.

Average (250 cycles) background currents at 500 Vs⁻¹ (before, solid line, and after, dashed line, electrolytic treatment of carbon fiber electrodes) are shown in Figure 4.4. The background voltammogram after ECP is characterized by an enormous current over the experimental potential window. This enormous background current should be subtracted from the analyte current to produce a background-subtracted voltammogram. This background current (which is one of the main limitations of FSV and consumes the resolution of the oscilloscope) was also used in this work as a diagnostic tool of the quality of the CFEs. Only, CFEs that have background currents lower than 200 ± 20 nA at 0.5 V *versus* SCE were used for analytical determinations since the oxidation potential of UA at 500 Vs⁻¹ is 0.5 V *versus* SCE.

Determination of the Roughness Factor

An increase in the electrode capacitance after electrolytic treatment, compared to the capacitance of a polished carbon fiber surface before the treatment, was detected as a result of surface oxidation/reduction during treatment. This increase in capacitance has been associated to the increase in surface roughness of the CFE. The roughness of the surface can be estimated from the capacitance of the double-layer.

The double-layer capacitance increases with the increase in surface roughness such that the apparent capacitance (C_{obs}) is larger than the value for a perfectly flat electrode as shown in Equation 2.14. The roughness factors (δ) or the ratio of the microscopic surface areas to the projected electrode areas were estimated from the capacitance values. Typical roughness factor values of 286 ± 44 and 774 ± 75 were found for untreated and treated CFE, respectively. A value of $2.7 \mu\text{F cm}^{-2}$ was used as the capacitance of a flat CFE [Frysz et al., 1997]. The δ value can vary from 1 to 5 for solid electrodes, or much higher for porous electrodes [McCreery and Cline, 1996]. Therefore, δ may be used to verify the porosity of the CFE.

Based on δ values before and after ECP two conclusions can be obtained. First, a very non-uniform rough CFE surface was obtained using mechanical polishing without ECP. Second, the electrolytic treatment can increase the roughness of the electrode from 286 ± 44 to 774 ± 74 , a factor 3, yielding a very active and stable surface.

Electrochemically treated carbon fiber electrode surfaces can also incorporate a significant amount of solvent and electrolyte due to its high porosity. After a prolonged (ca. 24 h) exposure of electrochemically treated carbon fiber electrodes to phosphate

buffer, at open circuit potentials, a considerable increase in background current was observed.

$\text{Fe(CN)}_6^{3-/4-}$ and $\text{Ru(NH}_3)_6^{3+/2+}$ as Electrochemical Probes of Activity and Structure of Carbon Fiber Surface

Figure 4.5. shows voltammetric curves of $\text{Fe(CN)}_6^{3-/4-}$ that were obtained at a carbon fiber electrode before (solid line) and after (small dash) electrochemical treatment of the electrode surface. Several features of the steady-state voltammograms of ferricyanide in Figure 4.5 are of interest. First, there is a visible change in shape of voltammetric curve of ferricyanide after the electrolytic treatment of the carbon fiber electrode surface. A gradual rise in current, and a poorly defined plateau, observed before treatment (solid line), are replaced by a steep current increase and a flat well-defined plateau (small dash). The changes in shape of the i - E curve of ferricyanide in the rising part and in the plateau region reflect changes at the carbon fiber electrode surface, from an initially rough surface [Zoski, et al., 1990], formed by polishing to a more uniform and more active surface, formed by electrochemical treatment.

Higher activity of carbon fiber electrodes after electrochemical treatment, in electrode reaction of ferricyanide is confirmed from analysis of the i - E curves, illustrated in Figure 4.5. Results of the analysis of i - E curves are summarized in Table 4.2 and show that the slope of E versus $\log ((i_1 - i_a) / i_a)$ plots of i - E curves obtained for ferricyanide at pH 6 decreases from 100 ± 2 to 66 ± 5 mV after electrochemical treatment of the carbon fiber electrode surface. A slope value of 60 mV is expected for a fast electrode reaction of ferricyanide and this slope value has been obtained at active carbon electrodes [McCreery, 1991].

In addition, after electrolytic treatment of carbon fiber electrode surfaces, separation between forward and reverse current traces in i-E curves of ferricyanide increases. This can be clearly seen in the plateau region and at the foothill of the i-E curve in Figure 4.5 where double layer charging controls the current. Increased separation of the forward and reverse current traces after electrolytic treatment indicates that electrode capacitance of the electrochemically treated electrode increases [Green, et al., 1997]. This increase in capacitance after electrochemical treatment shown by slow scan voltammetry results in Figure 4.5 is in agreement with the results in Figure 4.3 where a significant increase in background current throughout an entire window of potential cycling was shown in background i-E curves obtained by fast scan voltammetry.

Electrochemical treatment of carbon fiber electrodes, by continuous cycling of electrode potential under experimental conditions used here must lead to formation of surface defects as a result of oxidation and reduction of the surface during the treatment. High capacitance of defects can account [Besenhard and Fritz, 1983] for the observed increase in electrode capacitance.

In addition, defects formed by surface treatment can contribute to improved electrode kinetics of ferricyanide, which are apparent from lower slope values of semilogarithmic plots of i-E curves of ferricyanide obtained after electrolytic treatment (Table 4.2). The small change in magnitude of the limiting current of ferricyanide, measured before and after electrolytic treatment at the plateau of i-E curves in Figure 4. 5 at -0.2V, verifies that the active area (~radius) of carbon fiber disk electrodes, seen by the negatively charged ferricyanide, does not significantly decrease after electrolytic

treatment of the carbon fiber surface [Cheng and Brajter-Toth, 1992; Cheng and Brajter-Toth, 1995; Cheng and Brajter-Toth, 1996]. Thus, formation of surface defects during electrolytic treatment, under the conditions used here, is not accompanied by formation of a significant density of negatively charged [Besenhard and Fritz, 1983], nonconducting surface oxides which can cause a decrease in the limiting current of ferricyanide anion [Cheng and Brajter-Toth, 1992; Cheng and Brajter-Toth, 1995; Cheng and Brajter-Toth, 1996]. The low density of non-conducting oxides at the electrode surface is also supported by a relatively small background current in Figure 4.3, at a treated electrode at positive potentials around 1.5 V, which confirms limited oxidation of the electrode surface after treatment, and thus a limited formation of surface oxides.

Effect of Solution pH on Electrode Response

Results, which show an effect of solution pH on electrode kinetics of ferricyanide are summarized in Table 4.2. These results provide additional insights into surface structure of carbon fiber electrodes. Before electrolytic treatment, electrode kinetics of ferricyanide at carbon fiber electrodes depends on solution pH and are slow at high pH as indicated by a 100 mV slope of E versus $\log ((i_l - i_a) / i_a)$ plot of i - E curves at pH 6. Electrode kinetics of ferricyanide become faster at untreated carbon fiber electrodes as the solution pH decreases, as shown by a decrease in slope of E versus $\log ((i_l - i_a) / i_a)$ plot from 100 to 60 mV at pH 1 (Table 4.2). This observation is consistent with an inner-sphere electrode reaction of ferricyanide [McCreery, 1991].

Faster kinetics of ferricyanide at untreated electrodes at low pH point to or indicate the presence of surface functional groups at an untreated carbon fiber electrode surface which can be protonated at low solution pH. Protonation of surface functional

groups can create additional surface sites for electrode reaction of negatively charged ferricyanide and can thus improve electrode kinetics of ferricyanide [McCreery, 1991; Cheng and Brajter-Toth, 1992; Cheng and Brajter-Toth, 1995; Cheng and Brajter-Toth, 1996].

After electrolytic treatment of the electrode surface of carbon fiber, electrode kinetics of ferricyanide become fast at high solution pH as indicated by a 60 mV slope of E versus $\log ((i_l - i_a) / i_a)$ plot of i - E curves at pH 6 (Table 4.2). An additional important observation is that electrode kinetics of ferricyanide become independent of solution pH after electrolytic treatment of the carbon fiber electrode surface.

These results, obtained after electrochemical treatment of the carbon fiber electrode surface, point to the formation of new surface sites at the electrode surface as a result of the treatment, which can facilitate electrode reaction of ferricyanide at the treated electrodes at high as well as low solution pH. This conclusion is consistent with a formation and a reported stoichiometry of oxide defects ($C_{10}O_{1.4}K_{0.66}$) which have been identified at moderately oxidized carbon [Goss, et al., 1993]. These defects differ from nonconducting surface oxides which are present at heavily oxidized graphite surfaces and may be present at an untreated carbon fiber electrode surface [Besenhard and Fritz, 1983]; such groups can slow down electrode reactions of anions at high solution pH [McCreery, 1991; Hsueh, et al., 1997].

Results of analysis of $Ru(NH_3)_6^{3+/2+}$ voltammetric curves obtained at carbon fiber electrodes before and after electrolytic treatment are also summarized in Table 4.2. These results support the results obtained for ferricyanide.

Electrode kinetics of $\text{Ru}(\text{NH}_3)_6^{3+/2+}$ are faster at untreated carbon fiber electrodes at high pH than the electrode kinetics of ferricyanide. Electrode kinetics of $\text{Ru}(\text{NH}_3)_6^{3+/2+}$ cation at untreated carbon fiber electrodes become a little slower at low solution pH as indicated by a small increase in slope of log plot of i-E curves of $\text{Ru}(\text{NH}_3)_6^{3+/2+}$ in Table 4.2. This is expected if surface functional groups present at the surface of untreated carbon fiber electrode become protonated at low solution pH. Protonated surface groups can interfere with the electrode reaction of $\text{Ru}(\text{NH}_3)_6^{3+/2+}$ cation [McCreery, 1991; Cheng and Brajter-Toth, 1992; Cheng and Brajter-Toth, 1995; Cheng and Brajter-Toth, 1996]. At untreated carbon fiber electrodes sensitivity of $\text{Ru}(\text{NH}_3)_6^{3+/2+}$ is lower than the sensitivity of ferricyanide to surface changes with change in solution pH, as indicated by a smaller change in slope of semilogarithmic plots of i-E curves of $\text{Ru}(\text{NH}_3)_6^{3+/2+}$ in Table 4.2 with change in solution pH. This difference in behavior of $\text{Ru}(\text{NH}_3)_6^{3+/2+}$ and ferricyanide is consistent with faster electrode kinetics of outer-sphere $\text{Ru}(\text{NH}_3)_6^{3+/2+}$ [McCreery, 1991].

After electrochemical treatment of carbon fiber electrodes, electrode kinetics of ferricyanide and $\text{Ru}(\text{NH}_3)_6^{3+/2+}$ become independent of solution pH. However, electrode kinetics of $\text{Ru}(\text{NH}_3)_6^{3+/2+}$ are a little slower at electrochemically treated carbon fiber electrodes than at untreated electrodes at high pH. Somewhat slower and pH-independent electrode kinetics of $\text{Ru}(\text{NH}_3)_6^{3+/2+}$ at electrochemical treated electrodes indicate that, as a result of electrolytic treatment, surface groups must form at the electrode surface which are cation-exchanged at high as well as at low solution pH slowing down electrode reaction of $\text{Ru}(\text{NH}_3)_6^{3+/2+}$ cation at high as well as at low solution pH [Cheng and Brajter-Toth, 1992; Cheng and Brajter-Toth, 1995; Cheng and Brajter-

Toth, 1996]. This is in agreement with the stoichiometry of oxide defects ($C_{10}O_{1.4}K_{0.66}$) [Goss, et al., 1993] that form at moderately oxidized carbon and is supported by an already discussed increase in background current at carbon fiber electrode surfaces after electrochemical treatment which is associated with electrooxidation and formation of some surface oxides.

Relatively fast apparent kinetics of both probes at carbon fiber electrodes after electrochemical treatment are consistent with a fraction of carbon fiber electrode area covered by oxide defects, of less than 1 [Amatore, et al., 1983; Freund and Brajter-Toth, 1991].

Ascorbic Acid, Uric Acid and Dopamine as Electrochemical Probes of Activity and Structure of Carbon Fiber Surface

Voltammetry of Ascorbic Acid (AA), Uric Acid (UA), and Dopamine (DA) at Low Scan Rates

Voltammograms of ascorbic acid at physiological pH 7.4 are illustrated in Figure 4.6.A. After ECP, the half-wave potential for the oxidation of AA is shifted from 195 ± 19 mV to 48 ± 3 mV *versus* SCE. The position of the oxidation wave after ECP is close to that observed by Vavrin [Vavrin, 1950], $E_p = -80$ mV *versus* SCE, in a polarographic determination of AA at pH 7.4 at 25 °C. In order to verify changes in the kinetics of AA before and after ECP, plots of the E *versus* $\log ((i_1 - I_a)/I_a)$ were obtained. The slope of the plot before and after ECP was 183 ± 9 mV and ECP 139 ± 8 mV, respectively. Even though, AA kinetics are faster after the ECP, both plots are indicative of an irreversible wave for a two-electron process. The wave height after ECP is lower than before ECP and implies lower sensitivity for AA at the electrochemically treated CFE [McCreery and Cline, 1996].

Figure 4.6.B illustrates slow scan voltammetry of uric acid before (solid line) and after (small dash) electrochemical treatment of carbon fiber electrode surface by potential cycling at a rate of 10Vs^{-1} in a potential window of 1.5 to -1.0V. After ECP, the half-wave oxidation potential for UA is shifted from $366 \pm 19\text{ mV}$ to $211 \pm 7\text{ mV}$ *versus* SCE. The position of the oxidation wave before ECP is close to that observed by Wightman's group [Kelly and Wightman, 1986], $E_{1/2} = 330\text{ mV}$ *versus* sodium chloride-saturated calomel electrode, at polished graphite electrodes. Plots of the potential *versus* $\log((i_l - i_a) / i_a)$ were used to identify the kinetics of UA before and after ECP. The plot before ECP gave a slope of $66 \pm 2\text{ mV}$ indicative of an irreversible wave for two-electron process. The slope of the plot after ECP was $42 \pm 3\text{ mV}$ indicating a quasi-reversible wave for two-electron process.

After electrochemical treatment of the electrode surface an *i*-E curve of uric acid (Figure 4.6.B) has a steep rising part and a well-developed plateau, in contrast to a response obtained for uric acid before electrolytic treatment of the electrode surface (solid line). Steep rising part of the *i*-E curve of uric acid and a well-developed plateau both point to fast electrode kinetics of uric acid at an electrochemically treated carbon fiber electrode surface [Bravo, et al., 1998]. Similar behavior is observed for ferricyanide at electrochemically treated carbon fiber electrodes (Figure 4.6. B).

Voltammograms of DA at physiological pH are illustrated in Figure 4.6.C. After ECP, the half-wave oxidation potential for DA is shifted from 268 ± 48 to $79 \pm 4\text{ mV}$ *versus* SCE. Plots of the potential *versus* $\log((i_l - i_a) / i_a)$ were used to identify changes in the kinetics of DA. The plot before ECP gave a slope of $112 \pm 38\text{ mV}$ indicative of an

irreversible wave for two-electron process. The slope of the plot after ECP was 26 ± 4 mV indicating of a reversibility of the two-electron process.

Small peaks are observed on top of steady state voltammograms of UA and DA in Fig.4.6.B and C after electrochemical treatment of carbon fiber electrode. The DA peak obtained is larger and better defined than the UA peak. These peaks indicate some accumulation of these probes at the electrochemically treated CFE surface. Accumulation of the probes at the electrochemically treated carbon fiber electrode surface must result in part from large surface area of the treated electrode, which is apparent from a large electrode capacitance. Large electrode capacitance is indicated by large current at the foothill of uric acid and dopamine wave in i-E curves in Figures 4.6.B and C.

High sensitivity of DA and UA at electrochemically treated carbon fiber electrodes is shown in Table 4.3 at $1,000 \text{ Vs}^{-1}$. These high values of sensitivity may also be due to an apparent efficient accumulation of these probes at electrochemically treated electrode surface of CFE, which is facilitated by a large surface area of the treated electrodes apparent from large electrode capacitance. Large surface areas are due to defects resulting from electrolytic treatment of the electrode surface. Diffusion can be quite rapid in defect rich graphite [Besenhard and Fritz, 1983; Goss, et al., 1993]. At electrochemically treated CFE voltammetric current of dopamine is influenced by slightly adsorption process and UA is a diffusion-controlled process [Hsueh, et al., 1997; Bravo, et al., 1998].

Determination of the Sensitivity Enhancement Factor

Determinations of 3×10^{-4} M of UA, DA, AA, and ferricyanide in phosphate buffer pH 7.4 at 50 mV s^{-1} were used to calculate the accumulation factor which can also be called sensitivity enhancement factor.

Since ferricyanide is considered an inner-sphere probe with a well-documented redox characteristics and non-adsorptive behavior at CFEs, this probe was used to normalize the experimental currents of the other probes. Therefore, the sensitivity enhancement factor was determined from the peak current ratio of experimental current of the probe (UA, AA, DA) to experimental current of ferricyanide. Table 4.4 summarizes the results for the three different probes and shows that AA has the lowest sensitivity before and after ECP. Factors for UA and AA show that both probes have approximately the same sensitivities at electrochemically treated CFE.

Even though the treated CFE presents an improvement in kinetics for all probes compared to untreated electrodes, the sensitivity enhancement factor before ECP is larger than the f_s after ECP. These contradictory results may be produced by the difficulty to evaluate the current before ECP due to lack of a well-defined plateau of the steady-state i-E curves. The limiting current was evaluated at 800 mV *versus* SCE for all three probes before ECP. Additionally, fast techniques were used to evaluate the sensitivity enhancement factor. The results of these experiments are well presented in Chapter 6.

Conclusions

The voltammetric properties of CFE are drastically altered by electrochemical treatment. The apparent electron-transfer rates for several compounds $\text{Fe}(\text{CN})_6^{3-}$, $\text{Ru}(\text{NH}_3)_6^{3+}$, DA, UA, and AA are accelerated. The differential capacitance after the ECP

treated CFE is indicative of the drastic changes in surface properties that result from this treatment. ECP treatment increased the capacitance twofold.

Although the capacitance data suggest that the total microscopic area of the electrode is increased, diffusion-controlled electrochemistry at low scan rate of ferricyanide demonstrated that a smaller area was available for interfacial electron transfer of ferricyanide. However, a tenfold increase in the microscopic area of electrochemically treated CFE was obtained using FSV with the same probe. This can be a clear example that fast techniques are able to track the nanostructured area of the electrochemically treated CFE [McCreery and Cline, 1996]. Additionally, The capacitance can also be used to estimate the roughness of the CFE surface, which was increased by a factor of 3 after ECP yielding a nanoporous CFE.

Nanostructuring of carbon fiber electrode surfaces that were developed using electrochemical treatment may be characterized by the final formation of surface defects and formation of some cation-exchanged defect oxides. These characteristics are verified by several pieces of evidence, including a significant threefold increase in electrode capacitance after electrochemical treatment of carbon fiber electrode surface. For moderately oxidized carbon fiber electrodes defects have been associated with high electrode capacitance and with facilitated electron transfer. This is observed here for the electrode reactions of all investigated probes which were structurally quite different [McCreery, 1991]. Cation-exchanged oxide defects have been shown to promote an electrode response which is independent of solution pH, as is observed here in electrode reactions of ferricyanide and $\text{Ru}(\text{NH}_3)_6^{3+/2+}$ [Thorp, 1992; Snider, et al, 1997]. Only a

small surface coverage by oxide-containing groups is evident at nanostructured carbon fiber electrodes that were prepared here.

Additionally, high stability of moderately oxidized carbon fiber electrodes after electrolytic treatment appears to result from the reduction of surface oxides which form during initial oxidation of electrode surface during electrochemical treatment at positive potentials [Cavalheiro and Brajter-Toth, 1998]. Reduction of surface oxides at graphite is a slow process [Besenhard and Fritz, 1983] and formation of oxides is known to contribute to instability of carbon fiber electrode [Cavalheiro and Brajter-Toth, 1998].

Surfaces of carbon fiber disk electrodes that have been fabricated here which have a large density of surface defects, have a large area and can selectively and rapidly preconcentrate selected analytes [Cavalheiro and Brajter-Toth, 1998]. Accumulation of analytes at surface defects, together with high electrode activity of analytes such as dopamine and uric acid at surface defects that are formed result in high sensitivity in analytical determinations.

Table 4.1. Determination of the projected geometric area of carbon fiber electrode (CFE)^a.

pH ^b	Untreated CFE		Treated CFE	
	Area ^c x 10 ⁷ cm ²	R	Area ^c x 10 ⁷ cm ²	R
3.0	3.4 ± 0.4	0.997 ± 0.003	1.5 ± 0.2	0.999 ± 0.001
7.4	3.0 ± 0.4	0.998 ± 0.001	1.7 ± 0.2	0.999 ± 0.001

- Solutions: 2, 4, 6, 8, and 10 mM of $\text{Fe}(\text{CN})_6^{3-}$ in 0.5 M KCl were used for the calibrations plot. Scan rate 50 mVs⁻¹.
- pH 3 was adjusted with HCl, pH 7.4 was adjusted with NaOH.
- Assuming disk area ($A = \pi r^2$), limiting current for ferricyanide solutions was determined at -100 mV *versus* SCE
- Four electrode, five solutions and four determinations for each solution were used for calculations, n = 80.

Table 4.2. $\text{Ru}(\text{NH}_3)_6^{3+}$ and $\text{Fe}(\text{CN})_6^{3-}$ at carbon fiber electrode (CFE).

pH	Analyte ^{a, b}	Untreated CFE		Treated CFE	
		$E^{o'}$ mV	Slope ^c E vs $\text{Log}(i_l - i_a)/i_a$	$E^{o'}$ mV	Slope ^c E vs $\text{Log}(i_l - i_a)/i_a$
1.11	$\text{Fe}(\text{CN})_6^{3-}$	289 ± 1	69 ± 5	290 ± 3	68 ± 5
3.11	$\text{Fe}(\text{CN})_6^{3-}$	160 ± 5	79 ± 3	171 ± 3	66 ± 2
6.08	$\text{Fe}(\text{CN})_6^{3-}$	137 ± 8	100 ± 2	166 ± 4	66 ± 5
2.87	$\text{Ru}(\text{NH}_3)_6^{3+}$	-246 ± 1	69 ± 1	-244 ± 3	71 ± 2
5.59	$\text{Ru}(\text{NH}_3)_6^{3+}$	-242 ± 1	64 ± 1	-251 ± 1	72 ± 1

- 1.97 mM $\text{Ru}(\text{NH}_3)_6^{3+}$, in 0.5 M KCl, pH adjusted with HCl, 50 mVs^{-1} .
- 1.675 mM $\text{Fe}(\text{CN})_6^{3-}$, in 0.5 M KCl, pH adjusted with HCl, 50 mVs^{-1} .
- Three electrodes and four determinations for each electrode were used for calculations ($n=12$); limiting current for $\text{Fe}(\text{CN})_6^{3-}$ and $\text{Ru}(\text{NH}_3)_6^{3+}$ solutions were determined at 100 and -375 mV *versus* SCE, respectively.

Table 4.3. Relative sensitivity of uric acid (UA) (-1) and dopamine (DA) (+1) at 1,000 Vs^{-1} (pH 7.4) at treated carbon fiber electrodes.

Analyte ^a	Sensitivity ^b nA μM^{-1}	LOD ^c μM
Uric acid	0.48 ± 0.01	5
Dopamine	0.97 ± 0.01	1

- Analytes were prepared in 70 mM phosphate buffer, pH 7.4, 250 cycles. At least three electrodes, five different concentrations and four readings for each concentration were used for the calibration plot, $n = 80$.
- Sensitivity from the slope of the calibration plot; limiting current for UA and DA solutions were determined at 500 ± 25 and 550 ± 25 mV *versus* SCE, respectively.
- LOD when $S/N = 3$. Noise = peak-to-peak noise rather than N_{rms}

Table 4.4. Determination of the sensitivity enhancement factor for carbon fiber electrodes (CFE).

Sensitivity ^a Enhancement Factor	Untreated CFE ^b	Treated CFE ^b
Uric acid	3.1 ± 0.8	1.7 ± 0.2
Dopamine	2.7 ± 0.8	0.6 ± 0.2
Ascorbic acid	1.1 ± 0.3	1.6 ± 0.3

- a. Sensitivity enhancement factor was defined as the ratio of the experimental signal of analyte (UA and DA) to the experimental signal of ferricyanide. Concentration used for UA, DA and ferricyanide was 0.3 mM. Solutions were prepared in 0.5 M phosphate buffer pH 7.4. Scan rate 50 mVs⁻¹. Limiting current for UA, DA, AA, and ferricyanide solutions before ECP were determined at 800, 800, 800 and -100 mV *versus* SCE, respectively. Limiting current for UA, DA, AA, and ferricyanide solutions After ECP were determined at 400, 400, 400 and 0 mV *versus* SCE, respectively.
- b. Four electrodes and four determinations for each electrode were used for calculations (n= 16)

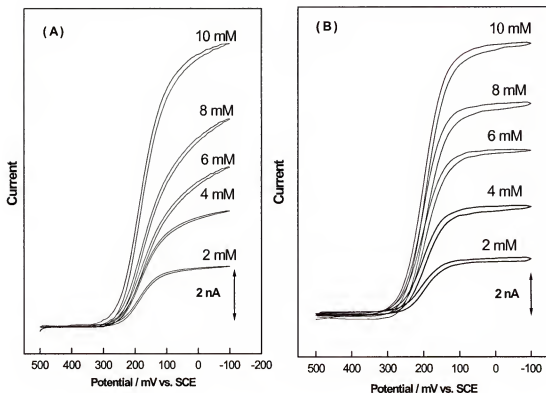


Figure 4.1. Cyclic voltammetry of Fe(CN)_6^{3-} in 0.5 M KCl pH 3.0 at (A) untreated and (B) treated carbon fiber electrode. Experimental electrode radius of $3.3 \pm 0.2 \mu\text{m}$ for untreated and $2.2 \pm 0.2 \mu\text{m}$ for treated carbon fiber electrodes were obtained assuming a disk geometric area.

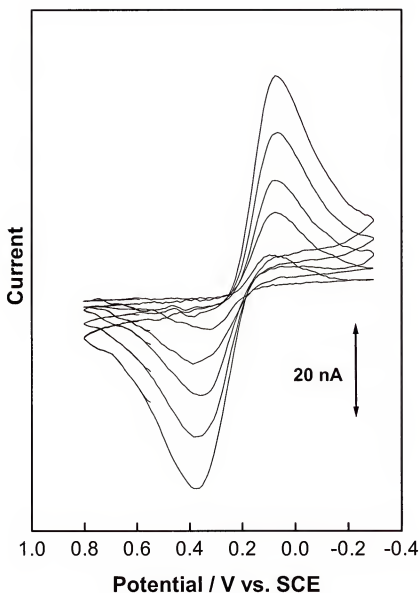


Figure 4.2. Fast scan voltammetry at 500 V s^{-1} of 0.42, 1.1, 1.5, 2.1, and 2.9 mM Fe(CN)_6^{3-} in 0.5 M KCl (pH 6.0) at treated carbon fiber electrode ($7 \mu\text{m}$ diameter). The cyclic voltammograms are background subtracted, 250 cycles for the background (0.5 M KCl (pH 6.0)) and 250 cycles for ferricyanide were used for data processing.

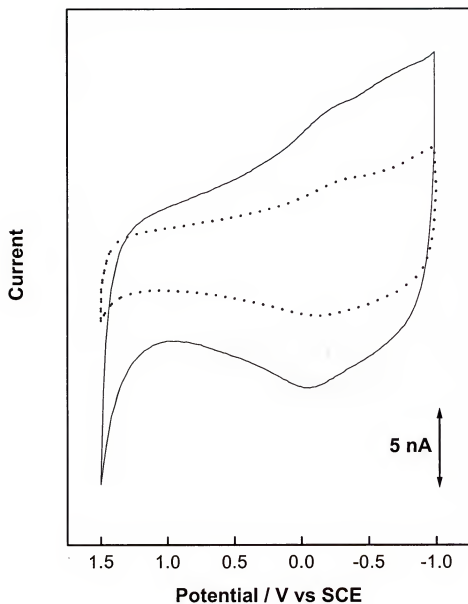


Figure 4.3. Background current at carbon fiber electrode at untreated (small dash) and treated carbon fiber electrode. Ca. 7 μm electrode diameter, scan rate 10 Vs^{-1} , 50 cycles, 70 mM pH 7.4 phosphate buffer.

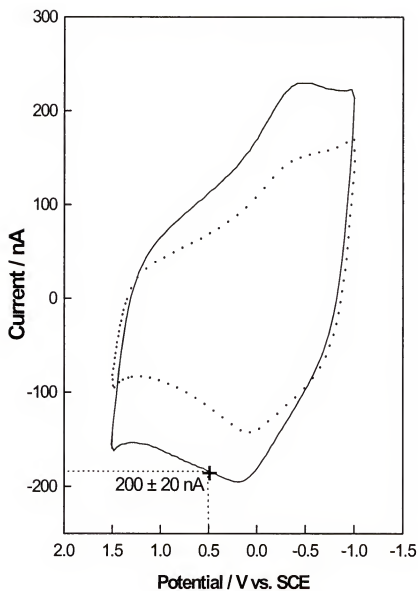


Figure 4.4. Background current at carbon fiber electrode at untreated (small dash) and treated carbon fiber electrode. Ca. 7 μm electrode diameter, scan rate 500 Vs^{-1} , 250 cycles, 70 mM (pH 7.4) phosphate buffer.

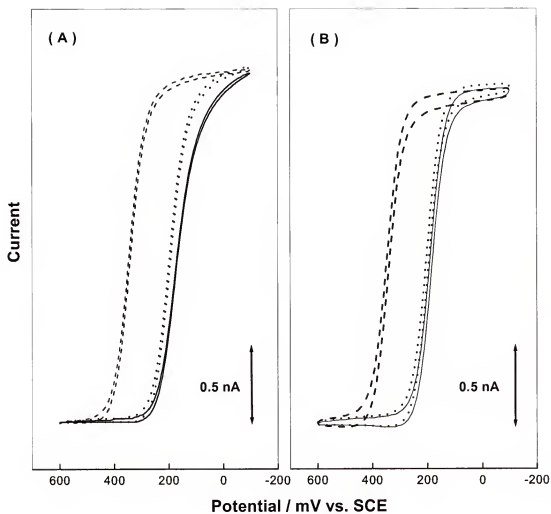


Figure 4.5. Cyclic voltammetry of 2.2 mM $\text{Fe}(\text{CN})_6^{3-}$ in 0.5 M KCl pH 6.0 (solid line), pH 3.0 (small dash), and 1.1 (dash) at (A) Untreated and (B) treated carbon fiber electrode. Scan rate 50 mVs^{-1} . Electrode radius $r = 3.2 \pm 0.2 \text{ } \mu\text{m}$.

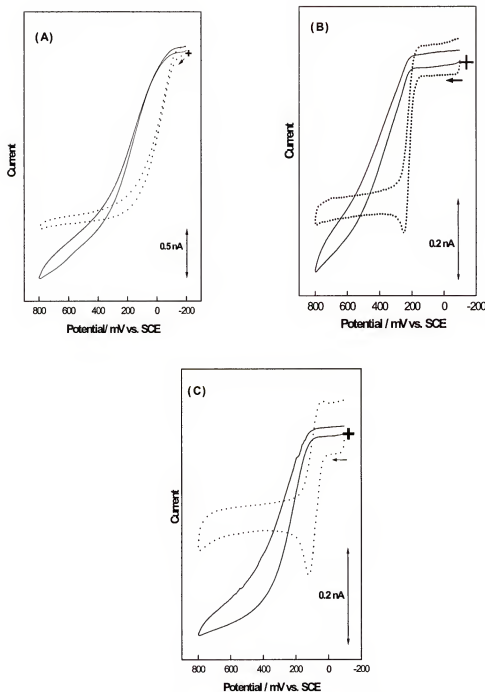


Figure 4.6. Voltammetric response of 3.0 mM ascorbic acid (A), 0.3 mM uric acid (B), and 0.3 mM dopamine in 0.5 M phosphate buffer (pH 7.4) at untreated (solid line) and treated (small dash) carbon fiber electrode. Scan rate 50 mV s^{-1} . Electrode radius $r = 3.3 \pm 0.3 \text{ }\mu\text{m}$.

CHAPTER 5

ELECTROCHEMICAL POLYMERIZATION AND CHARACTERIZATION OF AN ULTRATHIN OVEROXIDIZED POLYPYRROLE FILM

Background

Polymer modified electrodes (PMEs) have become popular in the last decade due to their high selective electrochemical detection of species in solution [Witkowski, et al., 1991; Freund, et al., 1991; Hsueh and Brajter-Toth, 1994; Cheng and Brajter-Toth, 1995]. This selectivity can be achieved by mechanisms such as size exclusion, ion exchange, and hydrophobic interactions. Nafion, which is the most widely used modifier, acts as a cation exchanger. However, the use of Nafion presents disadvantages such as slow response time due to the diffusional barrier of the membrane, and memory effects due to strong binding between cationic analytes and Nafion [Guadalupe and Abruña, 1985; Wang and Tuzhi, 1986; Whiteley and Martin, 1988].

The electrochemical polymerization of pyrrole (Py) has been extensively used to produce PMEs because of its excellent analytical advantages such as the incorporation of redox mediator [Velazquez-Rosenthal, M. et al., 1985; Eavez, et al., 1986; Ikeda and Yoneyama, 1989] and enzymes [Koopal, et al., 1991; Matsue, et al., 1991] into polypyrrole (PPy) matrices. Overoxidized polypyrrole (OPPy) has shown remarkable properties such as permselectivity, which can be exploited in sensor design.

PMEs obtained from the electropolymerization of pyrrole have been investigated in our laboratory [Witkowski, et al., 1991; Witkowski and Brajter-Toth, 1992; Hsueh

and Brajter-Toth, 1994]. Our previous work showed that overoxidized polypyrrole (OPPy) films can be permeable and have ionic conductivity even though the electrical conductivity of polypyrrole (PPy) is lost after overoxidation. Morphological differences between OPPy grown on rough pyrolytic graphite (RPG) and glassy carbon electrodes (GCE) were found. Overoxidized polypyrrole films grown on RPG were found to have greater porosity and relatively low charge density due to a greater spacing between the electron-rich groups, carbonyl groups, that were introduced by the overoxidation process [Witkowski, et al., 1991; Witkowski and Brajter-Toth, 1992]. The choice of RPG or GC substrate can determine whether the film has a more compact or porous morphology, which may affect interactions with anions such as uric acid. Consequently, the morphology of the OPPy film depends on the surface used as a film substrate.

In Chapter 3, a new method of treatment of carbon fiber electrodes was developed through a combination of mechanical and electrochemical pretreatment (ECP), which produces stable and sensitive CFE surfaces. The high sensitivity of the treated carbon fiber electrodes was associated with the surface nanostructure, which was produced during electrochemical treatment. The treatment also led to large background currents that were background subtracted in analytical determinations [Bravo, et al., 1998; Bravo and Brajter-Toth, 1999].

In this Chapter, we explore the possibility to use the activated CFE as a template for the electrochemical polymerization of an ultrathin OPPy film. The main goal here is to keep the high sensitivity, which was achieved with ECP, while the background is decreased by the presence of the film. To achieve this goal, a well-designed and reproducible polymerization process should be used. This process is discussed in detail

in this Chapter.

Other research groups have used the combination of electrochemical activation with a formation of polymer at the surface of the electrode to yield a more selective and sensitive sensor for analytical determinations. For instance, Zen and co-workers found that a combination of a pre-anodization pretreatment, to increase sensitivity, and Nafion film modification, to increase the selectivity of glassy carbon electrode (GCE), can be used for uric acid ($pK_a = 5.8$) detection in the presence of ascorbic acid ($pK_a = 4.1$) at pH 5.0. The GCE first was manually polished and then a uniform Nafion coating was deposited by spin coating technique at 3000 rpm. The Nafion GCE was preanodized at + 2.0 V for 20 s in citrate buffer. They argued that the functional groups generated on the GCE surface during the ECP undergo chemical interaction with UA, probably through hydrogen bonds, which facilitates adsorption [Zen, et al., 1998].

Zang and co-workers used a combination of direct and alternating current ECP method to produce an activated glassy carbon electrode (AGCE). Prior to ECP, the GCE was polished by diamond paper followed by 0.5 μm alumina slurry, then sonicated in water. The GCE was treated in 0.05 M phosphate buffer, pH 7, by applying a positive potential of + 2.0 V vs saturated calomel electrode (SCE) for 60 s, followed by a cathodization of the electrode at -1.1 V for 30 s. Next, the GC electrode was continuously scanned between - 1.1 to 0.9 V at 200 mVs^{-1} for 10 minutes. They reported that the cyclic voltammetric response for electro-oxidation of phenol was highly dependent on the nature of the electrode surface. They claimed that very low sensitivity for H_2O_2 is achieved when a non-electrochemically activated GC was used to immobilize horseradish peroxidase (HP). However, a very sensitive response to H_2O_2

was obtained by employing an AGCE instead of a non-AGCE to immobilize HP [Zhang, et al., 1996].

Netchiporouk and co-workers investigated electrochemical properties of electrochemically pretreated carbon fiber microelectrode in the construction of an amperometric biosensor for glucose, using oxidase enzyme and Nafion membrane. They found that successive cycling from 0 V up to + 2.8 V, 2.4 V, 1.8 V, 15 s for each step, produced the most dramatic topographic effects on the surface of the CFE. Topographic effects were verified using scanning electron microscope. They also used ECP before any deposition of the enzyme to enhance sensitivity and to produce a reproducible carbon surface for hydrogen peroxide oxidation and ferricyanide as a soluble mediator [Netchiporouk, et al., 1995]. It appears that the polymer-modified electrode can maintain high sensitivity and selectivity that is achieved with ECP.

This chapter discusses the methodology used in the polymerization process developed to enhance the detection of UA. Additionally, electrochemical characterization of the film is discussed.

Results and Discussion

Preparation of Ultrathin OPpy Film Electrodes

Before modification of the electrodes, CFEs were tested with a solution of 5 mM $\text{Fe}(\text{CN})_6^{(-3/-4)}$ in 0.5 M KCl pH 7.4. Only electrodes producing a desired response were used as discussed in Chapter 4. CFEs were electrochemically treated in phosphate buffer as previously mentioned in Chapter 4. Preparation of OPpy films was based on a procedure described by Huesh and Brajter-Toth. [Hsueh and Brajter-Toth, 1994]. Background chronocoulometric (CC) response of 0.1M TBAP in MeCN was determined

and used for background subtraction. Next, 25 mL of a solution of 0.02M pyrrole, $d=0.98 \text{ g mL}^{-1}$, and 0.1M TBAP in MeCN was prepared with a precision microliter pipet. The pyrrole solution was polymerized on the CFE using CC with a potential step from 0.650 to 0.950 V *versus* Ag wire for 10 ms. The CFEs were held in solution at open circuit potential for 30 to 120 s to allow equilibration with the solution before the background charge and polymerization charge were recorded by CC.

The polypyrrole modified (PPY-modified) UME was rinsed with deionized water, then transferred to 0.5 M sodium phosphate buffer solution and overoxidized at 0.950 V vs. SCE using bulk electrolysis. The current was monitored during the overoxidation. Initially, a large current, ca. 8 nA, was observed, which rapidly decreased as the overoxidation progressed. The current eventually leveled off and began to fluctuate around a small value, lower than 1 nA, which indicated the end of the overoxidation of PPy. The PPy overoxidation process usually takes two minutes. The electrode was tested with a solution of $\text{Fe}(\text{CN})_6^{(-3/-4)}$ in 0.5 M KCl to verify the successful deposition of the film as illustrated in Figure 5.1.

Effect of Polishing on the Formation of OPPy Films

One strategy to improve the *signal-to-noise* ratio in FSV is to decrease the high background current which can consume the resolution of the digital oscilloscope at high scan rates and is produced during the electrochemical treatment. Polishing with $\gamma\text{-Al}_2\text{O}_3$ (0.1 μm size) can decrease the electrode capacitance due to the formation of relatively flat surface. Consequently, CFEs were initially polished with $\gamma\text{-Al}_2\text{O}_3$ at different periods of time. Next, the electrochemical treatment was performed and the OPPy modification was finally performed.

Table 5. 1 shows the dependence between the polishing time with $\gamma\text{-Al}_2\text{O}_3$ (0.1 μm size) and the geometric areas of the electrochemically treated electrodes, which were determined at 50 mVs^{-1} with ferricyanide in 0.5 m KCl, pH 6.0. The determination of the area at low scan rates was previously described in Chapter 4. When the polishing time was increased, the projected area became smaller due to the formation of a flat and less rough surface.

Additionally, Table 5. 1 shows the dependence between the extent of surface coverage by OPPy and the polishing time. As the polishing time is increased, the extent of surface coverage, as a result of the polymerization, is increased as shown by the greater percent decrease in the $\text{Fe}(\text{CN})_6^{3-}$ signal. Several possible explanations can be presented for this behavior. First, an increase in the polishing time yields a decrease of the projected area. Consequently, the amount of polymer per unit area deposited using the same amount of charge becomes higher for the smooth surface than for the rough surface. Second, the rough surface provides more active places, defects available for polymerization, which results in a more porous ultrathin film. The high porosity of the electrodes was estimated from the roughness factor, which is defined as the ratio of the microscopic surface area to the projected electrode area. Values of roughness factor before and after ECP are summarized in Table 5. 1. Finally, the double layer capacitance increases with the increase in surface roughness. Therefore, the initial current required to charge the double-layer of a smooth surface is smaller than the initial current required to charge the double-layer of a rough surface.

The effect of the polymerization coverage of the electrode by the OPPy film and/or the effect of polishing with $\gamma\text{-Al}_2\text{O}_3$ in the roughness of the electrode could be

evaluated from kinetics of UA response at OPPy film electrodes, at 500 V s^{-1} . The biggest ΔE , $547 \pm 48 \text{ mV}$, corresponds to the electrode with the longest polishing time, 60 s. On the other hand, for the shortest polishing time, UA shows the best kinetics response, $394 \pm 20 \text{ mV}$. It may mean that rough electrodes have a more active surface than smooth electrodes or the most polished electrode yield more oxides at the surface which may increase the resistance of the electrode. Based on this result, we can conclude that the polishing time with $\gamma\text{-Al}_2\text{O}_3$ can be one of the main parameters to alter UA kinetics at OPPy coated electrodes. The other possibility is that the extent of surface coverage for the smooth electrodes, which is bigger than the extent of the coverage for the rough electrodes, produces films which alter UA kinetics. However, by comparing the ΔE of the bare electrode, 307 ± 35 , and the ΔE of the OPPy modified electrode, 394 ± 20 , we can conclude that the kinetics of UA at OPPy modified CFE may be slightly altered by the presence of the film. Determinations of ΔE could be slightly distorted due to lack of iR compensation in the fast scan experiment

The results shown in Table 5.1 indicate that a high degree of coverage can decrease sensitivity of UA. Several observations about UA sensitivity can be formulated. Looking at the normalized UA sensitivities per area of the bare electrode (S/A), we can observe that the polishing time (10, 30, and 60 s) does not make any difference in the normalized sensitivity of UA at bare electrodes, because the S/A of bare electrodes are the same for the three cases. On the other hand, the S/A of UA at OPPy modified electrodes after polishing, 60s of polishing, is 60 % lower than the sensitivity for OPPy modified electrodes with 10 and 30 s polishing time. Consequently, polishing for 10 s or 30 s may produce a similar active area after OPPy modification.

Finally, comparing the S/A for a bare electrode *versus* OPPy modified electrode polished for shorter times, 10s and 30s, respectively, shows the biggest advantage at OPPy modified electrodes. For these cases, the improvement of the UA normalized sensitivity at OPPy coated electrodes is almost 60%. This issue is fully discussed in Chapter 6.

Characterization of OPPy Film Using Ferricyanide

Previous work demonstrated cation permselectivity of ultrathin OPPy films and the possible use of the $\text{Fe}(\text{CN})_6^{(3-/4-)}$ response as a direct measure of the extent of coverage of the electrode by the OPPy polymer [Witkowski, et al., 1991; Hsueh and Brajter-Toth, 1994]. The response of $\text{Fe}(\text{CN})_6^{3-}$ anion at an OPPy coated glassy carbon electrodes gradually decreases after each coating and almost disappears after six coatings. Compared to the bare electrode, the response of $\text{Fe}(\text{CN})_6^{(3-/4-)}$ decreases 95% after six coatings. Consequently, the $\text{Fe}(\text{CN})_6^{(3-/4-)}$ response, before and after polymerization, can be used as a direct determination of the extent of surface coverage by OPPy.

A comparison of $\text{Fe}(\text{CN})_6^{(3-/4-)}$ signals before and after modification of the electrode with OPPy was used to evaluate the extent of surface coverage by the film. Figure 5. 1 presents the cyclic voltammogram of 1×10^{-2} M $\text{Fe}(\text{CN})_6^{(3-/4-)}$ in 0.5 M KCl (pH 6.0) at bare electrochemically treated carbon fiber electrode, solid line, and at OPPY-modified electrochemically treated carbon fiber, dotted line, which was polished for 10 s. The signal for $\text{Fe}(\text{CN})_6^{3-}$ after OPPY modification, with 10 ms deposition time, was suppressed 36 ± 10 % compared to the signal before modification.

Determination of Surface Coverage by OPPy Polymer

Polymerization of pyrrole was performed using chronocoulometry (CC) and the total applied charge was used to calculate the coverage by OPPy. The total charge, Q_{total} , in CC measured as result of a potential step experiment has three different sources: (A) double layer charging, Q_{dl} , (B) electrolysis of adsorbed species, Q_{ads} , and (C) electrolysis of species diffusing in solution, Q_{diff} , as illustrated in Equation 2.15. The last term, Q_{diff} , is time dependent and is given by the integrated Cottrell equation as illustrated in Equation 2.17. As mentioned in Chapter 2, the Q_{dl} and Q_{ads} are not time dependent functions. Consequently, a plot of Q_{total} versus $t^{1/2}$ should be a straight line with a slope of $2 nFACoD_o^{1/2}\pi^{1/2}$ and intercept equal to $(Q_{\text{dl}} + Q_{\text{ads}})$.

Initial adsorption can be considered in terms of equilibrium [Anson, 1975] as illustrated in Figure 5.2, where the absorbing species, A, loses some or all of its solvent molecules and displaces oriented solvent molecules from the electrode surface so that contact between the electrode and adsorbate (A) is achieved.

The principal driving forces for the process in Figure 5.2 are: (A) the affinity between A and solvent; (B) possible interactions such as π - π interactions between the electrode and A; and (C) other binding between A and the surface of electrode.

We made the following considerations for our system: high solubility of pyrrole in acetonitrile decreases the probability of adsorption of Py at carbon fiber surface because a high amount of energy is required to expel the pyrrole from acetonitrile (MeCN). Lack of strong interactions between pyrrole in solution and the CFEs surface and the hydrophilic character of the electrochemically treated CFE can decrease the possibility of initial adsorption of pyrrole. Carbon fiber electrodes were held in 0.02 M

pyrrole solution at open circuit potential for 30 to 120 s to allow equilibration with MeCN solution after ECP in phosphate buffer. The possibility of adsorption of pyrrole is minimized by the short period of contact between pyrrole and the surface of CFEs. Based on the previous discussion we assumed that during the polymerization process $Q_{ads} \ll Q_{dl} + Q_{diff}$, thus Equation 2.17 can be approximated to:

$$Q_{total} = 2nFACD_o^{1/2} t^{1/2} / \pi^{1/2} + Q_{dl} \quad (5.1)$$

Where n is the number of electrons associated to the redox reactions; F the Faraday constant, 9.6485309×10^4 C; A area of electrode in cm^2 ; D_o diffusion coefficient in cm^2s^{-1} ; C concentration in $mol\ cm^{-3}$; t is time in s.

A plot of Q_{total} vs. $t^{1/2}$ should be a straight line with a slope of $2nFACD_o^{1/2}\pi^{1/2}$ and the intercept should be equal to Q_{dl} . Figure 5.3 shows a plot of Q_{total} vs. $t^{1/2}$ for OPPy formation and is an average obtained from eight CFEs, solid line. The double layer capacitance, Q_{dl} , was determined in a separate experiment by using supporting electrolyte (TBAP/MeCN) without pyrrole as illustrated in Figure 5.3, dashed lined. This procedure assumes Q_{dl} to be identical in the presence of pyrrole. Figure 5.4. shows the average of eight CFEs double step chronocoulometric responses of TBAP/MeCN or background charge (A) and of 0.02 M pyrrole in TBAP/MeCN (B). Figure 5.4.C illustrates the background subtracted chronocoulometry response of pyrrole which is obtained from the subtraction of voltammogram (A) from the voltammogram (B).

Characterization of Electrochemical System

Chronocoulometry (CC) was used to establish the time window over which electrochemical polymerization exhibits characteristics of planar diffusion. The Cottrell equation assumes semi-infinite linear diffusion to an electrode, instantaneous potential change from E_1 to E_2 , and that mass transfer of electroactive species to the electrode is solely by diffusion.

According with the Cottrell equation, a plot of $Q/t^{1/2}$ versus t should be linear with a zero slope as illustrated in Figure 5.5 [Heineman, 1986]. During polymerization of OPPy at CFE a positive deviation at the beginning of the pulse is observed. This positive deviation may be produced by a very high flux of analyte to the surface, at the beginning of the experiment, due to the highly active nanostructured surface of the electrochemically treated CFEs. Another explanation is the inability of the potentiostat to instantaneously change potential from E_1 to E_2 . The resolution of the potentiostat (BAS-100) is equal to 1 ms and the manufacturer suggests that eighty percent of the data points (toward the end of the pulse) should be analyzed for short experimental times.

We can observe from Figure 5.5 that the polymerization process occurs under a diffusion-controlled process. Consequently, we can assume that Q_{diff} is equal to Q_{pol} .

$$Q_{diff} = Q_{total} - Q_{dl} = Q_{pol} \quad (5.2)$$

The charge associated with the polymerization process was used to calculate the surface coverage using Faraday's law.

$$Q_{pol} = nFA\Gamma_e \quad (5.3)$$

Where n is the most common literature value of number of electrons associated with the polymerization (2.25) of polypyrrole [Diaz and Castillo, 1980]; F is the Faraday's constant, 96,485 in C; A is the geometric projected area of the electrode, cm^2 ; and Γ_e is the experimental coverage, mol cm^{-3} . Assuming a typical monolayer coverage of $\Gamma_0 = 1.5 \times 10^{-10} \text{ mol cm}^{-2}$ [Bard and Faulkner, 1980], we found that the amount of monolayer produced during the CC (10 ms) experiments is about 2.2 ± 0.6 .

Morphology of OPPy at Electrochemically Pretreated Carbon Fiber Electrode

Previous work in our group has shown that the morphology of the OPPy film can be controlled by selecting the electrode substrate used for PPy deposition. Glassy carbon (GC) and rough pyrolytic graphite (RPG) have greatly different surface activities, with nucleation and growth occurring much more rapidly at RPG [Witkowski, et al., 1991; Witkowski and Brajter-Toth, 1992]. High surface activity of RPG compared to GC was associated with the larger edge-plane character of RPG vs. GC. Noll and co-workers used pit defects (high edge-plane character) on highly ordered pyrolytic graphite (HOPG) as a template for the formation of PPy nanostructures with diameters $\leq 10 \text{ nm}$ [Noll, et al., 1998].

In the present work, we used an electrochemically treated carbon fiber electrode as a substrate for the polymerization of pyrrole. The mechanisms of polymerization and overoxidation of polypyrrole have been extensively studied but they are still not completely clarified. We adopted the most literature-accepted mechanism [Tanaka, et al., 1988; Andrieux, 1990; Andrieux, 1991; John and Wallace, 1991; Raymond and

Harrison, 1993] which was discussed in Chapter 1, to propose the polymerization process at electrochemically pretreated carbon fiber electrode.

As previously indicated, the Fe(CN)_6^{3-} signal may be used to estimate the extent of coverage of the electrode by OPPy. Assuming that the polymerization of OPPy produces an uniform monolayer of one unit of overoxidized pyrrole (full coverage of the surface), the Fe(CN)_6^{3-} signal after deposition of overoxidized pyrrole should decrease by 100%. However, experimental results show that only $36 \pm 10\%$ of the total surface was modified with OPPY because the experimental Fe(CN)_6^{3-} signal decreased by 36%. This means that the deposited overoxidized pyrrole at the surface of the UME has at least three, 3 ± 1 , units of pyrrole. But the amount of experimental charge that was applied to the system $(7 \pm 2) \times 10^{-5} \text{ C cm}^{-2}$, is enough to produce two monolayers (2.2 ± 0.6) instead of one. Consequently the estimated number of units of pyrrole for each chain is about six (6 ± 2).

Figure 5.6 shows a cartoon representation used to illustrate the polymerization process of OPPy at EPCE. As we previously reported, electrochemical pretreatment of CFE results in a surface of relatively uniform roughness. The roughness factor after ECP increased from 286 ± 44 to 774 ± 74 or by a factor of 2.7 ± 0.6 . The surface is rich in graphite edges with channels between them as illustrated in Figure 5.6.1. A very high number of graphite edge defects which are produced during ECP, are distributed over the entire surface of the electrochemically treated carbon fiber electrode. The defects can act as nucleation sizes for the polymerization process [Noll, et al., 1998; Myrick, et al., 1998]. The topographic structure of the surface allows efficient deposition of the polymer at exposed defect edges rather than in the channels between the edges as

illustrated in Figure 5.6.2. As PPy is overoxidized, the concentration of carbonyl groups increases and the electrical conductivity of OPPy decreases until it is lost, as illustrated in Figure 5.6.3.

We tried to apply a recent model to estimate the growth morphology for the polymerization process [Noll, et al., 1998]. The model is based on information from a potential step experiment analogous to chronocoulometric experiment. A logarithmic plot of current vs. total polymerization charge should produce a straight line as long as a specific type of growth morphology is maintained. Changes in the slope suggest a change in a type of growth morphology. The slope (m) of the line is used to estimate the number of dimensions of the growth (n) using the following relationship:

$$m = (n - 1) n^{-1} \quad (5.4)$$

For planar growth the slope of the line is equal to zero, cylindrical growth presents a slope of one-half, and spherical growth has a slope of two-thirds. Figure 5.7 shows the plot of a logarithm of background subtracted current *versus* logarithm of charge, $\ln(i)$ vs. $\ln(Q)$. The slope of the plot is 0.26 ± 0.02 , $R=0.9892$. The experimentally obtained value can not be used to determine specific growth morphology of polymer because this value is different than the suggested values for the different morphologies. However based on this number, the growth morphology of the polymer is definitively different from a planar growth ($m=0$).

The expected slope values were not obtained because the system may have violated at least two assumptions of the theoretical model. For example: (a) the

polymerization should occur under non-diffusion limited control, but the experimental system is under diffusion control as previously discussed; (b) an electrode material may contain a relatively small number of electroactive sites or defects. However, the EPCFE presents a high number of electroactive sites.

Determination of Diffusion Coefficient of Pyrrole

Figure 5.8 shows a plot of the background-subtracted charge *versus* square root of the polymerization time, Q vs. $t^{1/2}$. The slope of the plot, $2nFAC_0D_0^{1/2}\pi^{1/2}$, was used to determine the diffusion coefficient of pyrrole in TBAP/MeCN solution during the polymerization of PPY.

An experimental diffusion coefficient value of $[8 \pm 2] \times 10^{-10} \text{ cm}^2\text{s}^{-1}$ was obtained by using the projected geometric area of the electrochemically treated CFE. This value is four orders of magnitude lower than the reported value for pyrrole derivatives in TBAP/MeCN ($1 \times 10^{-6} \text{ cm}^2\text{s}^{-1}$) [Saint-Aman, et al., 1997] but is very close to a reported value for organic compounds in TBAP/MeCN ($1.5 \times 10^{-10} \text{ cm}^2\text{s}^{-1}$) [Genies, et al., 1983] at a polypyrrole modified electrode.

Several explanations can be used to justify the value of the experimental diffusion coefficient. First, the experimental D_0 value was calculated assuming the geometric area of the CFEs that were calculated based on $\text{Fe}(\text{CN})_6^{3-}$ response at low scan rate. The proposed OPPy polymerization model assumes that polymerization of OPPy is taking place mainly at the edges rather than the entire surface. Additionally, experimental data suggest that the polymerization took place at only 36 % of the geometric area based on ferricyanide response. Consequently, the “real active” area for

the polymerization process should be lower than the geometric area which produces a larger diffusion coefficient.

Other possible explanation is that pyrrole may be pre-concentrated in very small volumes at the nanostructured surface. Consequently, the concentration of OPPy at the CFE surface may be higher than concentration OPPy in the bulk solution.

Finally, high porosity of the surface of CFE may allow different analytes such as cations and neutral species [Kelly et al., 1999] to penetrate into the CFE surface. This process can produce diffusion coefficients on the order of 1×10^{-6} to $10^{-7} \text{ cm}^2 \text{ s}^{-1}$ [Besenhard and Fritz, 1983] for different analytes. These values are lower (at least one order of magnitude) compared to the determined values in bulk solution.

Thickness of OPPy Layers

In previous work, the thickness of the OPPy film was roughly estimated at about 16 Å (assuming four layers and each layer has a 4 Å). The value of the thickness for each layer is based on the size of Py. The bond lengths of pyrrole are 1.34, 1.48, 1.07 and 1.01 Å for C=C, C-N, C-H, and N-H respectively. Considering the angles between the bonds, the diameter of pyrrole was estimated at ca 4 Å. Using the same geometrical consideration, an OPPy film thickness value of $24 \pm 8 \text{ Å}$ was estimated for six rings (6 ± 2) since each ring has geometric estimated diameter of 4 Å.

Additionally, the thickness of the OPPy films can be estimated from the coulombic charge associated with film formation by using the following equation:

$$D_{\text{thickness}} = (Q_{\text{form}} * (MW)) / nFA\rho \quad (5.5)$$

Where MW is the molar mass of a repeating pyrrole unit (plus dopant); n is the number of electrons associated with the polymer formation (2.25); F is Faraday's constant in C mol^{-1} ; ρ is the estimated density of the film; A is the electrode area which goes under polymerization in cm^2 and Q_{form} is the charge associated with polymer formation in C.

The thickness of the OPPY film was estimated from the assumption that 3 units of pyrrole rings are charge stabilized by one perchlorate ion. The molar mass of the repeating unit (plus dopant) is 98 g mol^{-1} . The ultrathin polymer (with thickness in Å) produced here should have much lower density than the density of thick polymer (with thickness in μm) reported in the literature [Holdcroft and Funt, 1988] (1.5 g cm^{-3}). Therefore, the estimated density (ρ) of the ultrathin film was assumed to be governed by the density of the MeCN (0.7857 g cm^{-3}). An OPPy film thickness value of $12 \pm 2 \text{ Å}$ was estimated by this method.

The second estimated value obtained by coulombic charge is lower than the value estimated from geometrical considerations. However, both estimated reported values are lower than or equal to $24 \pm 8 \text{ Å}$.

Film Stability

Overoxidized polypyrrole film electrodes were used in at least twenty-four UA background subtracted determinations. For each determination two hundred and fifty cycles of the electrolyte without and with UA were performed at a scan rate of 500 Vs^{-1} (for a total number of 12,000 cycles) in a potential window from -1.0 to 1.5 V versus SCE. The response of $\text{Fe}(\text{CN})_6^{3-}$ was used to monitor the presence of the film after the calibration curve. Based on $\text{Fe}(\text{CN})_6^{-3}$ response, the OPPy modified CFE did not show signs of film loss after calibration.

Figure 5.9 shows an improvement in the kinetics of $\text{Fe}(\text{CN})_6^{3-}$ in 0.5 M KCl (pH 6.0) after UA calibration curve was obtained. To study possible changes in kinetics of $\text{Fe}(\text{CN})_6^{3-}$ before and after UA calibration curve, plots of the potential *versus* $\log((i_l - i_a)/i_a)$ were obtained. A plot before the ECP gave a slope of 70 ± 3 mV, indicative of a quasi-reversible wave for a one-electron process. The same plot after UA calibration curve gave a slope of 63 ± 3 mV, indicative of a reversible behavior. After UA calibration curve, the half-wave potential for the oxidation of $\text{Fe}(\text{CN})_6^{3-}$ shifted from 194 ± 8 to 179 ± 6 mV *versus* SCE. Both half-wave potentials are more positive than the half-wave potential reported for a bare electrochemically treated CFE, 166 ± 4 , in Chapter 4. This improvement in the kinetics of $\text{Fe}(\text{CN})_6^{3-}$ can be associated with morphology changes during the calibration curve instead of film loss [Sterson, et al., 1973; Gao, 1994].

Background Current Reduction

At high scan rates, most of the resolution resources of the digital oscilloscope are consumed by the high background current which is associated with all electroanalytical measurements, and which increases proportionally with scan rate. The remaining resolution can not adequately reflect the shape of the analytical signal because of the digitized noise introduced by the lack of resolution of the oscilloscope. This noise can decrease the *signal-to-noise* ratio for low concentrations of analyte, and thus it can yield a poor limit of detection for analytical determinations. In this work, an ultrathin OPPy film was used to decrease the high background which is produced after electrochemical treatment of CFE while the high sensitivity of the electrochemically treated CFE is maintained. Figure 5.10 shows the background current in 70 mM phosphate buffer pH

7.4 before (A) and after modification with OPPY film (B) at scan rate of 10 Vs^{-1} with 50 cycles averaged. The background current after OPPY modification decreased by $24 \pm 4\%$. The background currents were determined at 0.5 V versus SCE as illustrated in Figure 5.10 since UA oxidation potential occurs at the same potential.

Conclusions

Preparation of an ultrathin OPPy film at electrochemically treated CFE was demonstrated in this Chapter. In spite of short time used for the deposition of the film (10ms), a highly reproducible film was achieved using chronocoulometry. The highly reproducible film formation was achieved thanks to the stable nanostructured CFE surface used as template; the use of a fresh pyrrole solution before any modification; and the quality of the potentiostat which allows use of very short pulse techniques.

The effect of the roughness factor, which can be used as an indirect measure of the defect density at CFE surface, was demonstrated studying the effect of $\gamma\text{-Al}_2\text{O}_3$ polishing on film formation. Smooth surfaces may produce a more compact layer, which can block UA response at CFE. Experimental data suggest that the polishing time range with $\gamma\text{-Al}_2\text{O}_3$ should be from 10 to 30 s to keep high sensitivity for UA detection.

Experimental data suggest that the polymerization process is a diffusion-controlled process. Two methods were used to estimate thickness of the film and both methods yield film thickness equal to or lower than $24 \pm 8 \text{ \AA}$. Additionally, a possibility of using the ferricyanide response as an indirect measure of OPPy film formation was demonstrated in this Chapter.

Finally, the presence of an ultrathin OPPy film produces a decrease in background current which can produce an improvement in *signal-to-noise* ratio and a better UA sensitivity. UA detection at OPPy modified CFE is fully discussed in Chapter 6.

Table 5.1. Effect of the polishing time on uric acid signal at a bare electrochemically treated and at an electrochemically treated carbon fiber modified with ultrathin overoxidized polypyrrole film.

Time s	Area ^a $\times 10^7 \text{ cm}^2$	Roughness Factor ^b δ	UA Sensitivity ^c $\text{A mM}^{-1} \text{ cm}^{-2}$		ΔE^d mV		% Decrease Signal ^e Fe(CN)_6^{-3}
			Bare CFE	OPPy CFE	Bare CFE	OPPy CFE	
10	1.7 ± 0.2	774 ± 74	0.65 ± 0.02	1.05 ± 0.02	307 ± 35	394 ± 20	36 ± 10
30	1.2 ± 0.2	699 ± 75	0.65 ± 0.03	1.05 ± 0.03	442 ± 27	447 ± 39	55 ± 6
60	0.9 ± 0.2	623 ± 57	0.65 ± 0.03	0.65 ± 0.03	520 ± 40	547 ± 48	79 ± 7

- $1 \times 10^{-2} \text{ M Fe(CN)}_6^{(-3/-4)}$ in 0.5 M KCl pH 6.0 at 50 mV s^{-1} . After assuming a disk geometric area. Limiting current for ferricyanide was determined at -100 mV versus SCE, potential window from 500 to -100 mV .
- Roughness factor ($\delta = C_{\text{obs}}/[C_{\text{flat}}]^{-1}$) where C_{obs} was determined after electrochemical treatment at 0.5 V in phosphate buffer (pH 7.4) of carbon fiber and $C_{\text{flat}} = 2.7 \mu\text{F cm}^{-2}$ [Frysz et al., 1997].
- Sensitivity was equal to the slope of the calibration curve in the linear dynamic range at 500 Vs^{-1} in 70 mM phosphate buffer (pH 7.4). Three electrodes, five different concentrations and four reading for each concentration were used for data analysis, $n = 60$.
- $5 \times 10^{-6} \text{ M}$ uric acid in 70 mM phosphate buffer pH 7.4. Scan rate 500 Vs^{-1} .
- At OPpy modified electrochemically treated carbon fiber.

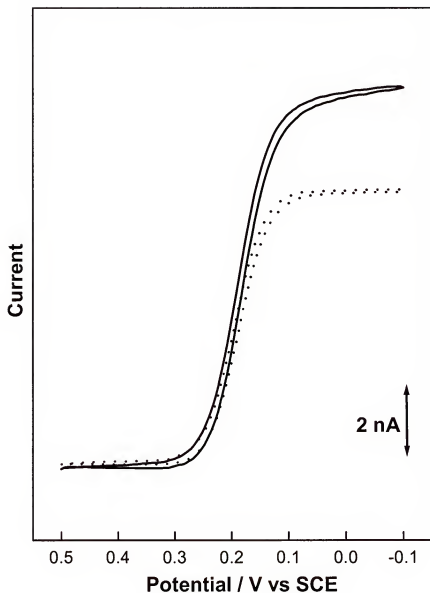


Figure 5.1. Cyclic voltammetry of 1×10^{-2} M $\text{Fe}(\text{CN})_6^{3-}$ in 0.5 M KCl, pH 7.4 at bare electrochemically treated carbon fiber electrode (solid line) and electrochemically treated overoxidized polypyrrole carbon fiber electrode (dashed line), ca $7 \mu\text{m}$ diameter. Scan rate 50 mV s^{-1} . OPPy thickness ca. $24 \pm 8 \text{ \AA}$.

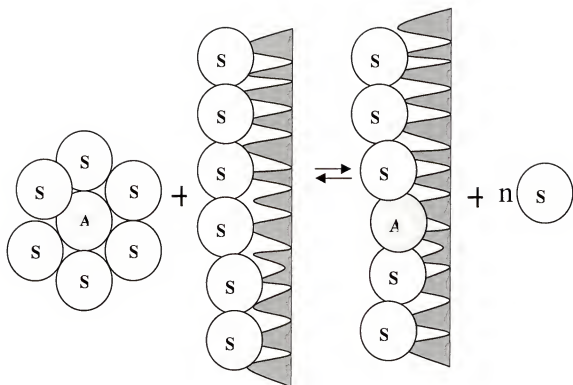


Figure 5.2. Schematic representation of an electrode adsorption process based on equilibrium terms [Anson, 1975].

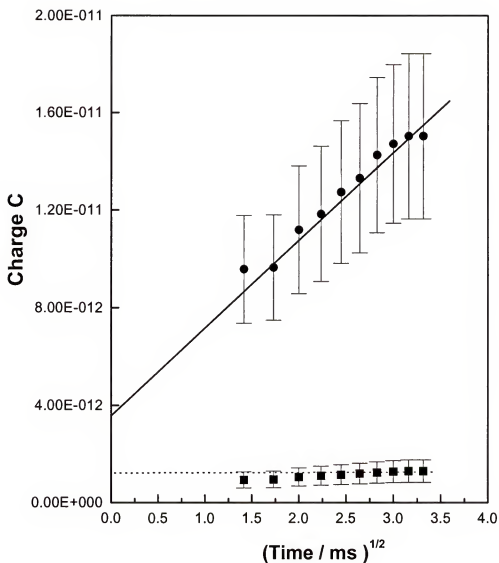


Figure 5.3. Plots of charge versus $t^{1/2}$ of 0.1 M tetrabutylammonium perchlorate in acetonitrile (dashed line) or double layer charge (Q_{dl}) and 2×10^{-2} M pyrrole with 0.1 M tetrabutylammonium perchlorate in acetonitrile (solid line). The responses of eight electrodes were used for data processing. Electrode radius $r = 2.2 \pm 0.3 \mu\text{m}$.

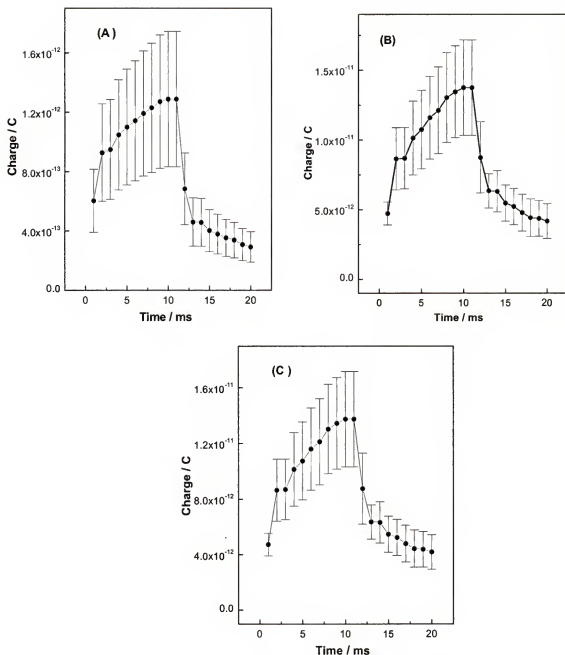


Figure 5.4. Chronocoulometric (CC) formation of OPPy-modified CFEs. (A) Background CC response of 0.1 M tetrabutylammonium perchlorate in acetonitrile; (B) CC response of 2×10^{-2} M pyrrole with 0.1 M tetrabutylammonium perchlorate in acetonitrile; (C) Background corrected CC response (plot A was subtracted from plot B). The plots are the responses of eight averaged electrodes. CC conditions; Potential step from 650 to 950 mV versus Ag wire, pulse 10 ms. Electrode radius $r = 2.2 \pm 0.3 \mu\text{m}$.

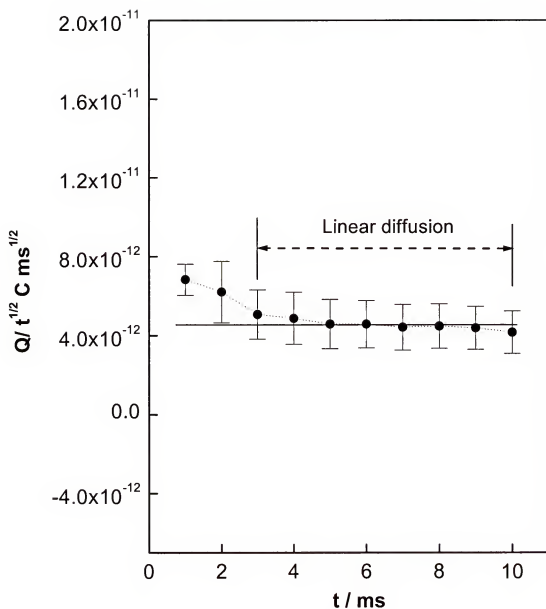


Figure 5.5. Characterization of electrochemical system. Experimental plot of $Q_{pol}t^{-1/2}$ versus t for polypyrrole formation process. The average of eight electrodes were used for data processing.

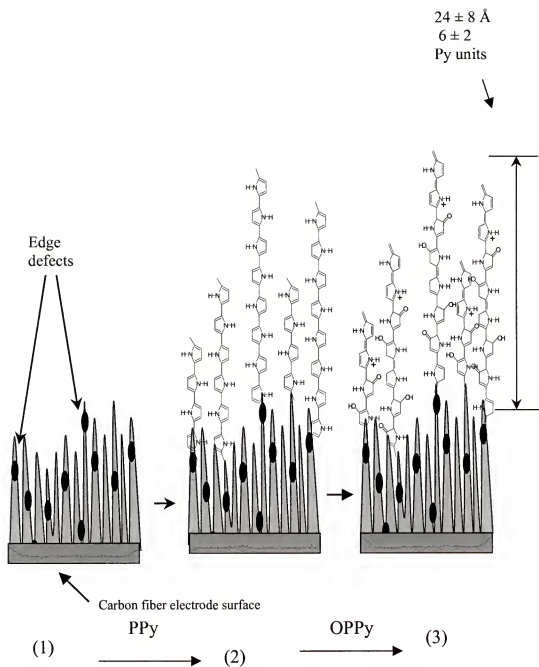


Figure 5.6. Cartoon representation of polypyrrole after polymerization (2) and overoxidation (3) at carbon fiber electrode which has been electrochemically pretreated.

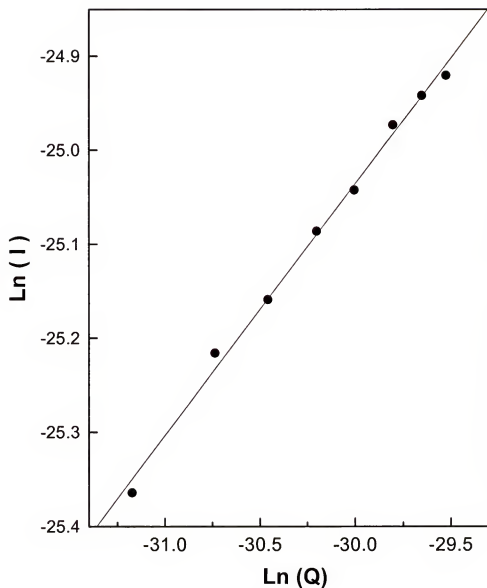


Figure 5.7. Plot of the logarithm of the background subtracted current *versus* the logarithm of the background subtracted charge ($\text{Ln}(I)$ *versus* $\text{Ln}(Q)$) for the experimental (in Figure 5.4.C) data of pyrrole polymerization. Electrode radius $r = 2.2 \pm 0.3 \mu\text{m}$.

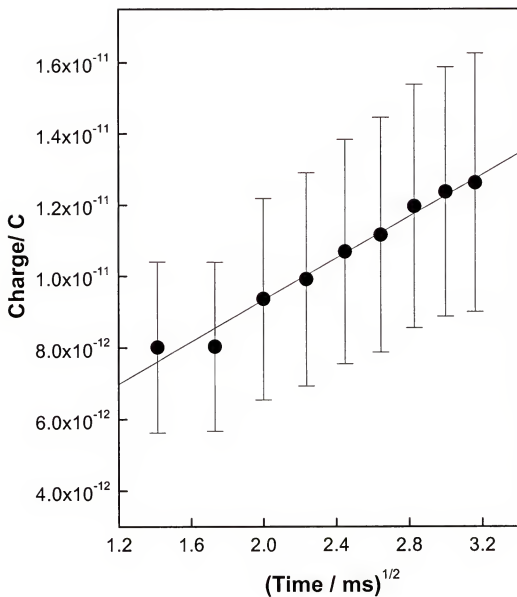


Figure 5.8. Plot of background subtracted charge *versus* $t^{1/2}$ of 2×10^{-2} M pyrrole with 0.1 M tetrabutylammonium perchlorate in acetonitrile. The responses of eight electrodes were used for data processing. Electrode radius $r = 2.2 \pm 0.3 \mu\text{m}$.

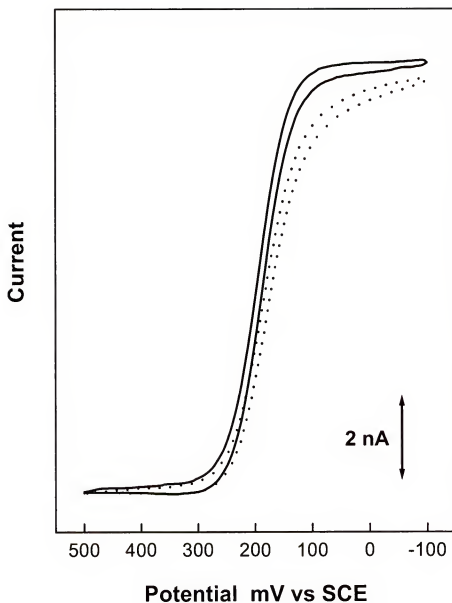


Figure 5.9. Cyclic voltammetry of 1×10^{-2} M $\text{Fe}(\text{CN})_6^{3-}$ in 0.5 M KCl (pH 6.0) at treated OPPy-modified carbon fiber electrode before (dashed line) and after (solid line) uric acid calibration curve. Scan rate 50 mV s^{-1} , ca. $7 \mu\text{m}$ diameter.

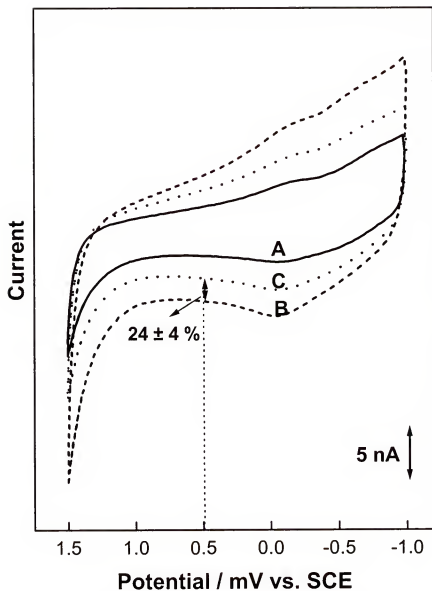


Figure 5.10. Cyclic voltammetry of 7×10^{-2} M phosphate buffer, pH 7.4 at carbon fiber electrode. (A) before electrochemical treatment; (B) after electrochemical treatment; after electrochemical treatment and modification with OPPy film. Scan rate 10 V s^{-1} (ca. $7 \text{ }\mu\text{m}$ diameter). The voltammograms were signal averaged 50 times.

CHAPTER 6

POSSIBILITIES AND LIMITATIONS IN MINIATURIZED SENSOR DESIGNED FOR URIC ACID

Background

Uric acid (UA) is the primary end product of purine metabolism. It has been shown that extreme abnormalities of UA levels are symptoms of several diseases [Harper, 1977; Star, 1995]. Additionally, new hypothesis about the role of UA in biological systems such as brain and heart open new frontiers for the determination of UA in these systems as mentioned in Chapter 1 [Mustard, et al., 1963; Persky, et al., 1979; Brand, et al., 1985; Layton, et al., 1996].

These important areas for UA determinations require selective, rapid determinations with low detection limits of UA. Since biological matrices are complex, the methods should be selective to avoid interferences. Fast determinations are also required because real time monitoring is necessary to determine fast concentration changes; for example, in the myocardial interstitial space, adenosine and its metabolites such as UA are important markers of ischemia, regulators of blood flow, and may produce cardioprotection against ischemia. A fast method to assess the concentration of adenosine and its metabolites is necessary to determine their involvement in mediating these effects [Mei et al., 1996]. Finally, low detection limits are required because of the low concentration of UA in biological systems such as heart microdialysates. Concentrations of UA in samples taken 60 min after implantation of a microdialysis

probe in an isolated rat heart were 1.8×10^{-6} M and in a sample taken 60 min after implantation of a microdialysis probe into the rat liver were $5.4 \pm 2.0 \times 10^{-6}$ M [Layton et al., 1996].

Several common UA detection methods are discussed in Chapter 1 [Haeckel, 1978; Kulys, et al., 1983; Dilella, et al., 1986; Watanabe and Tatsuma, 1991; Gilmartin, et al., 1992; Gilmartin and Hart, 1994; Gilmartin, et al., 1994; Miland, et al., 1996]. In this Chapter, two different approaches are used to detect UA. First, a bare electrochemically treated CFE was used with fast scan voltammetry (FSV). This approach can not only be used in routine analysis such as urine but also in non-conventional systems such as heart perfused preparations. Second, an ultrathin overoxidized polypyrrole (OPPy) modified CFE was used with FSV to improve *signal-to-noise* ratio and sensitivity of the UA detection compared to the bare electrode.

One of the major problems of *in vivo* determinations of UA comes from electrochemical interferences such as ascorbic acid (AA) [Wightman et al., 1988]. Electrodes coated with anion excluding films such as Nafion [Gerhardt et al., 1984] or a thick film of overoxidized polypyrrole [Witkowski and Brajter-Toth, 1992] are not practical for selective determinations of UA (anion) in the presence of interfering anions such as AA because the response of UA and AA is suppressed, since anion excluding films attenuate anion diffusion.

In the first part of this work, we investigate the use of FSV at scan rates above 500 Vs^{-1} to improve the selectivity and sensitivity of UA in the presence of AA at bare electrochemically treated carbon fibers. By pushing scan rates above 500 Vs^{-1} voltammograms of UA in the presence of AA can be resolved because of the kinetic

differences in the response of the two anions and also, simultaneously, improvement in *signal-to-noise* (S/N) ratio is achieved. S/N is improved because of high temporal resolution of FSV, which allows acquisition of a large number of scans that can be signal averaged in a short period of time [Hsueh et al., 1997]. The sensitivity of FSV analysis depends on the stability of the background current [Stamford, 1989; Hsueh, et al., 1997]. We established experimentally that a stable background current can be obtained at carbon fiber electrodes after 30 min of continuous cycling of the electrode in the experimental potential window as previously discussed in Chapter 3 [Hsueh, et al., 1997; Bravo, et. al., 1998; Bravo and Brajter-Toth, 1999].

In the second part of this Chapter, an electrochemically treated CFE with an ultrathin membrane of OPPy was used for the determination of UA to increase the *signal-to-noise* ratio and sensitivity of electrochemically treated CFEs for the detection of UA. The ultrathin OPPy film not only maintains the high sensitivity of the electrochemically treated CFE but also decreases the background current. Therefore, the film enhances the sensitivity of the electrochemically treated CFEs because the electroactive area remains highly activated while the background current is decreased. Additionally, possible interferences of AA in UA detection were studied at OPPy modified CFE.

Results and Discussion

Determination of UA Adsorption in the Oxidation of UA by FSV

Previous work in our group and the shape of the UA wave at low scan rates (see Figure 4.6.1.B) suggest adsorption of UA at the surface of the electrochemically treated CFE. Adsorption of analyte at the surface of the electrode is not apparent at low and moderate scan rates where diffusion current dominates the electrode response [Hsueh and

Brajter-Toth, 1993]. However, weak adsorption can dominate the response at high scan rates ($>100 \text{ Vs}^{-1}$) [Bard and Faulkner, 1980; Freund and Brajter-Toth, 1992; Hsueh and Brajter-Toth, 1993].

The influence of UA adsorption on the oxidation peak current of UA at high scan rates was verified by plotting the logarithm of UA oxidation peak current as a function of the logarithm of scan rate. For weakly adsorbing species the slope of the plot should be between 0.5 to 1 because adsorption and diffusion both contribute to the measured current [Bard and Faulkner, 1980; Freund and Brajter-Toth, 1992; Hsueh and Brajter-Toth, 1993]. Since adsorption-controlled current increases with the scan rate, while the diffusion-controlled current increases with the square root of the scan rate, the slope of the plot should increase as the scan rate increases as the contribution of adsorption to the measured current increases [Freund and Brajter-Toth, 1992; Hsueh and Brajter-Toth, 1993].

The slope of the plot of the logarithm of UA oxidation peak current (bare electrochemically treated CFE) *versus* the logarithm of scan rate in the scan rate from 100 to 2000 Vs^{-1} is 0.5 which is the theoretical value for a diffusion-controlled process as illustrated in Figure 6.1. As expected for a predominantly diffusion-controlled process, the slope of the plot is not significantly different in the low and high scan rate range (0.50 in the range from 100 to 500 Vs^{-1} and 0.506 in the range from 500 to 2000 Vs^{-1}).

Fast Scan Voltammetry (FSV) with Signal Averaging

High temporal resolution, which significantly reduces the time required to complete a voltammogram or scan, is one of the main advantages of FSV. This advantage facilitates signal averaging. Other approaches such as analog and digital filtering to

optimize S/N have been used by Wightman and co-workers [Wiedemann et al., 1991]. Figure 6.2 shows voltammograms that have been obtained as a result of signal averaging of 1, 10, 50, and 250 scans where the signals from each scan were added and divided by the number of scans. As shown in Figure 6.2, the high frequency noise was rapidly reduced as the number of scans increased. However, the low frequency noise tends to remain unchanged after 250 cycles. Table 6.1 summarizes the S/N ratios and current signals as a function of the number of cycles. The results illustrate an improvement in S/N with the increase in the number of scans in spite of the simultaneous increase in the background current. It may account together with non-random noise, for the lower than theoretical ($S/N \propto n^{1/2}$) increase in S/N seen in Table 6.1 with the increase in the number of cycles. A decrease in the noise with the increase in the number of cycles contributes to some decrease in the measured peak signal and a decrease in the standard deviation of current measurements in Table 6.1.

Determination of UA by FSV in Physiological Buffers

Since the detection of uric acid is of interest under physiological conditions [Beck et al., 1981], the activity and the stability of the carbon fiber electrodes was tested following the ECP in different physiological buffers (pH 7.4) used in subsequent determinations of uric acid. It was anticipated that this will improve the stability and will eliminate the need for reequilibration. The buffers tested included sodium phosphate, Krebs, Krebs-Henseleit, trisHCl and KCl.

Ultimately, because of the different background currents at potentials where uric acid was detected, the LOD and the sensitivity varied with the buffer. The best LOD and sensitivity was achieved in 70 mM sodium phosphate (pH 7.4) as illustrated in Table 6.2.

In HEPES, and in other buffers which contained tertiary amines which are electroactive at 1.4 V [Pihel et al., 1994], a high current was observed at positive potentials. In such buffers, uric acid was determined after ECP in the potential window from 1.2 to -1.0 V, which resulted in lower background currents but also resulted in lower sensitivity in the determination of uric acid (Table 6.2).

The method of treatment of carbon fiber electrodes by potential cycling in the experimental potential window and the method of acquisition of background current between each determination of analyte, produce a microdisk carbon fiber electrode surface which allows sensitive and reproducible determinations of uric acid [Hsueh, et al., 1997; Bravo, et al., 1998]. Uric acid anion (urate, $pK_a=5.4$ [Dyhurst 1971]) is not detected under physiological conditions (pH 7.4) at electrodes prepared based on past procedures of electrochemical treatment of carbon fiber electrodes, which have been developed to suppress the response of negatively charged analytes [Hsueh et al., 1997]. Modifications of these procedures to optimize determinations of purines, such as adenosine and urate, have not been straightforward [Chen, et al., 1994; Nowall and Kuhr, 1995; Hsueh, et al., 1997].

As illustrated by results in Figure 6. 3, carbon fiber electrode surfaces that are produced by methods of surface treatment developed here, which include cycling of the electrode potential, show excellent sensitivity in determinations of uric acid.

Panel B in Figure 6.3 shows a response of 12 μ M uric acid at an electrochemically treated CFE obtained by FSV after background subtraction [Hsueh, et al., 1997; Bravo, et al., 1998]. Compared to a response of 300 μ M uric acid in panel A, obtained by slow scan voltammetry, fast scan voltammetric peak of uric acid, at a much

lower concentration of uric acid in solution (12 μM), is well-developed, and *signal-to-noise* ratio [Hsueh, et al., 1997; Bravo, et al., 1998] is high in this measurement.

Table 6.2 summarizes sensitivity values for uric acid that were determined from linear working curves that were obtained from measurements of fast scan voltammetric peak currents at carbon fiber electrodes that were electrochemically treated in different buffers [Bravo, et al., 1998; Bravo and Brajter-Toth, 1999]. Because of high stability of electrochemically treated electrodes, background currents measured in buffer only were easily subtracted from currents measured for uric acid in the same buffer by FSV [Hsueh, et al., 1997; Bravo, et al., 1998]. A peak in background response of electrochemically treated carbon fiber electrode observed in buffer at ca 0.5V has been associated with quinone/hydroquinone groups at the electrode surface [Kepley and Bard, 1988], and was also subtracted.

An important observation from determinations of sensitivity of uric acid in different buffers by FSV is that high sensitivity that is observed for uric acid is largely independent of buffer used in electrode treatment and in determinations of uric acid. This is in agreement with previously discussed results which have shown that surface structure of graphite that is produced as a result of electrochemical treatment is independent of buffer used in treatment. Differences in sensitivity that are observed in different buffers (Table 6.2) are mostly a result of lower potentials (less than 1.2 V vs SCE) that were used to activate electrodes in buffers which contained tertiary amines (Tris-HCl and Krebs) which are electroactive at potentials of ca. 1.4V [Pihel et al., 1994].

Effect of pH in UA Determination at 500 Vs⁻¹

The effect of pH on the electrochemical oxidation of purines has been reported [Owens and Dryhurst, 1977; Ianniello, et al., 1982; Goyal, et al., 1994]. The monoanionic form of UA exists at neutral pH ($pK_a \cong 5.75$). The monoanionic UA is oxidized ($2e^-$, $2H^+$) to a labile diimine anion as previously mentioned in Chapter 1.

Figure 6.4 shows the dependence of the oxidation peak potential E_p (Figure 6.4.A), the peak current i_p (Figure 6.4.B), of UA *versus* pH at bare electrochemically treated CFE at 500 Vs⁻¹ in 70 mM phosphate. Figure 6.4.A shows that the peak potential, E_p , for UA is linearly dependent upon pH, as illustrated by the following equation:

$$E_p (6.6 \text{ to } 8.4) = (0.94 \pm 0.04) - (0.050 \pm 0.005)pH \quad (6.1)$$

Based on the results of previous [Dryhurst, 1972a; 1972b] and this work on the oxidation of UA, the number of electrons and protons in the potential controlling process is constant with pH. The dependence of E_p on pH observed here has a couple differences with the dependence of E_p on pH reported by Dryhurst and co-workers [Wrona et al., 1979]. They found that pH is linearly dependent upon pH and the process follows Equation 1.9 ($E_p (0-11.5) = 0.685 - 0.055pH$). At pH 7.4 (using Dryhurst's equation) the UA oxidation peak should appear at 278 mV. Same pH (using this work's equation) UA oxidation peak should appear at 570 ± 6 mV. This effect can be explained using two different approaches. First, a fast scan rate was used here for this determination in combination with an electrochemically treated CF surface. In contrast, Dryhurst and co-

workers used low scan rate voltammetry of UA in 0.5 M phosphate buffer at rough pyrolytic graphite electrode. Second, the experimental results reported here are not iR compensated which contributes to shifts in E_p [Hsueh and Brajter-Toth, 1993].

Second, the reported slope here 50 ± 5 is slightly lower than the Dryhurst's slope which is 55 mV. This may be an effect of the active CFE surface compared to the RPG surface used by Dryhurst and coworkers.

The 50 ± 5 mV slope of the linear E_p versus pH plot is higher than the theoretical Nernstian value of 30 mV [Bard and Faulkner, 1980] which is expected for two-electron reversible reaction. The higher slope obtained here indicates a quasi-reversible reaction between UA and the active CFE surface.

Figure 6.4.B shows also that the peak (i_p) current depends on pH. The peak current decreases while pH increases. At low pH (6.8), the maximum current is reached however this point presents the biggest error bars in the entire range of pH that was investigated. The lowest peak current was observed at higher pH (8.4). At higher pH the rate of oxidation of the graphite electrode surface is fast which can contribute to a loss of surface activity because of the formation of inert surface oxides [Fagan, et al., 1985; Howell, et al., 1986].

Detection of UA without the Interference from AA

Figure 6.5 shows the cyclic voltammograms of 3×10^{-4} M UA (A) and 3×10^{-3} M AA (B) at scan rate of 50 mV s^{-1} in 7×10^{-2} M phosphate buffer (pH 7.4) at electrochemically treated CFE. It is clear that at this scan rate both compounds have oxidation peaks close to 0.25 V versus SCE. The AA peak is much higher than the UA peak current because of the higher concentration of AA. It means that the current at 250

mV (which will be produced by mixture of AA and UA) must have a contribution from both analytes. Consequently, AA will interfere with UA determinations at this scan rate.

Figure 6.6 shows the cyclic voltammograms of 5×10^{-5} M UA (A), 3×10^{-3} M AA (B), and mixture of 5×10^{-5} M UA with 3×10^{-3} M AA (C) at scan rate of 100 Vs^{-1} under same conditions as Figure 6.4. Using sensitivity values determined for uric acid at electrochemically treated CFEs from Figure 6.5.(A), an accumulation factor, or a sensitivity enhancement factor at scan rate of 100 Vs^{-1} , $f_{a \text{ UA}}$, was determined for uric acid from peak current ratio, $f_{a \text{ UA}} = i_{p \text{ exp}}/i_{p \text{ theor}} = 55 \pm 3$. To calculate $i_{p \text{ theor}}$ electrode radius ($2.4 \pm 0.3 \times 10^{-4} \text{ cm}$) determined at pH 7.4 at electrochemically treated CFEs using ferricyanide was used and the calculation of $i_{p \text{ theor}}$ assumed a purely diffusion-controlled irreversible reaction of urate ($D_o = 1 \times 10^{-6} \text{ cm}^2\text{s}^{-1}$ [Bard and Faulkner, 1980]) at an electrochemically treated CFEs [Bard and Faulkner, 1980].

For ascorbate, accumulation factor, $f_{a \text{ AA}} = i_{p \text{ exp}}/i_{p \text{ theor}} = 0.35 \pm 0.01$, was determined at electrochemically treated CFEs at pH 7.4 at 100Vs^{-1} . A smaller value of accumulation (sensitivity) factor for ascorbate than for uric acid indicates that ascorbate is not accumulated as well as urate at a surface of electrochemically treated CFE at pH 7.4 ($D_o = 1 \times 10^{-6} \text{ cm}^2\text{s}^{-1}$ [Bard and Faulkner, 1980]). As a result, a selectivity factor $f_{a \text{ UA}}/f_{a \text{ AA}} = 157 \pm 9$ at 100Vs^{-1} .

Figure 6.7 shows the cyclic voltammograms of 5×10^{-5} M UA (A) and mixture of 5×10^{-5} M UA with 3×10^{-3} M AA (B) at scan rate of 500 V s^{-1} under same conditions as Figure 6.5. Both voltammograms present only one oxidation peak at 0.5 V versus SCE. The current-to-UA concentration ratios (i_p/C) for UA, and UA, AA mixture are 198 ± 12 and $182 \pm 10 \text{ nA mM}^{-1}$, respectively. The similar values of i_p/C and the

similar peak potential values, E_p , in both voltammograms are a clear indication that the response of AA becomes insignificant relative to the response of UA at 500 Vs^{-1} [Bravo et al., 1998]. Therefore, the peaks that are observed are a result of the oxidation of UA in the presence of slowly reacting AA. Although at 500 Vs^{-1} AA does not show a clear oxidation peak, which is expected at more positive potentials, it may be the principal factor behind the poor background subtraction, that is observed in the solution containing AA, shown in the voltammogram in Figure 6.6.(B).

Figure 6.8 shows voltammograms of $5.0 \times 10^{-5} \text{ M}$ UA (A) and of a mixture of $5 \times 10^{-5} \text{ M}$ UA and $1 \times 10^{-3} \text{ M}$ AA (B) at a scan rate of $1,000 \text{ Vs}^{-1}$ under same conditions as Figure 6.5. The voltammograms are virtually the same, verifying that a very well-defined response of UA can be obtained at low concentrations of UA in the presence of high concentrations of an interfering anion such as AA at the fast scan rate.

Nevertheless, apparent electrode kinetics of ascorbate are fast at electrochemically treated CFE at pH 7.4 and a well-defined peak of ascorbate is detected at low positive potentials at scan rates as high as 100 Vs^{-1} , which does not shift significantly with scan rate [Bravo et al., 1998]. At scan rates of 500 Vs^{-1} and above, voltammetric oxidation peak of ascorbate is not detected and uric acid, which is oxidized at the same potential as ascorbate at electrochemically treated CFE can be detected by fast scan voltammetry without interference from an excess of ascorbate. Even when the concentration of ascorbate exceeds the concentration of uric acid by more than 100 fold ratio [Hsueh, et al., 1997; Bravo, et al., 1998].

Apparent fast electrode kinetics of ascorbate, and an eventual suppression of ascorbate voltammetric response at scan rates of 500 Vs^{-1} , is likely a result of kinetic

effects associated with proton transfer, which follows electron transfer in electrooxidation of ascorbate. Proton transfer can be mediated by surface groups at carbon fiber electrode surfaces and this step can become limiting in electrooxidation of ascorbate at electrolytically treated carbon fiber electrodes at scan rates of 500Vs^{-1} [Hirst et al., 1998].

Determination of UA in Perfused Heart Sample

Preliminary experiments of UA detection in heart perfused samples were performed. The goal of these experiments was to detect the baseline level of uric acid. Hearts were allowed to equilibrate for 30-45 minutes before the sample was taken. Experimental samples were obtained by perfusion of guinea pig heart with modified Krebs-Henseleit buffer (pH 7.4) using standard Langerdorff method of whole heart perfusion [Jennings and Howard,1992]. The perfuse procedure is well documented elsewhere [Grupp 1984; Jennings and Howard,1992]. The Krebs-Henseleit buffer flows through the heart at a flow rate of $20\text{ }\mu\text{L}/\text{min}$ in the standard Langerdorft method of heart perfusion.

Figure 6.9 shows the determination of UA in the perfusate heart sample, by the method of standard additions using FSV at 500 Vs^{-1} . Seventy-five cycles of Krebs-Henseleit (K-H) buffer (pH 7.4) were taken, averaged, recorded at 500 Vs^{-1} , and later used for background subtraction. The same K-H buffer used to perfuse the heart was used to produce the background current. Two hundred and fifty cycles of the perfusate sample (which consisted of K-H buffer and the perfusate metabolites from the pig heart) were taken and averaged. The averaged background signal was subtracted from the averaged perfusate signal. Uric acid concentration of $3.2 \pm 0.3\text{ }\mu\text{M}$ was obtained by this

method in the heart in agreement with the baseline levels of uric acid reported for the samples ($4\text{ }\mu\text{M}$ [Mei et al., 1996]).

A couple of conclusions may be taken from this preliminary experiment. First, the “fat” shape of the cyclic voltammogram suggests a poor background subtraction as illustrated in Figure 6.9.A. This problem may be produced by two factors. First, the presence of “foreign” substances in the perfuse heart sample but non-presence in the background solution can produce the poor background subtraction. The other possible factor is that slight changes in pH during the determination alter the background current and UA determination. Previous experiment suggests that pH is a critical factor for UA detection as discussed previously in this Chapter.

The linearity of the calibration plot suggests that the high activity of the electrode can be maintained during the UA determination in heart perfusate sample. Consequently, lack of poisoning effects from compounds present in the heart perfusate sample were observed. The K-H buffer flows through the heart at a flow rate of 2.0 ml min^{-1} in the standard Langerdorff method of heart perfusion. This may dilute the concentration of interfering compounds in the heart perfusate sample and may avoid poisoning effects.

Determination of UA in Urine Sample

Three human urine samples from laboratory personnel were analyzed for UA content using the bare electrochemically treated CFE. One of the samples belongs to a person who was diagnosed with uric acid elimination problems. First, an UA calibration plot (current *versus* concentration) was performed in the linear range from 0 to $20\text{ }\mu\text{M}$ UA in 70 mM phosphate buffer (pH 7.4), 500 Vs^{-1} , to find the dilution factor of the urine samples. Since the best UA sensitivity was achieved using phosphate buffer (pH 7.4),

this buffer was used to dilute the urine sample. Based on literature reports [Cai, et al., 1994; Zen, et al., 1998], typical values from 2 to 5 mM UA had been reported for urine samples. Therefore, a 1000-fold dilution (100 μ L urine / 100 mL solution) was tested and found to have concentrations around 2 μ M UA. The dilution process can actually help in decreasing the matrix effect of real sample. The diluted urine samples were spiked with small volumes of UA stock standard solution (3×10^{-4} M UA) to double and triple the initial diluted UA concentration.

Figure 6.10 shows the voltammograms of UA in urine before and after spikes. Table 6.3 summarizes the analytical results of UA determination in real samples using standard addition method for all urine samples. These results indicate that the concentration of uric acid obtained using treated carbon fiber electrode at 500 Vs $^{-1}$ are similar to the reported literature values between 2 to 5 mM [Cai, et al., 1994; Hasebec, et al., 1995; Zen, et al., 1998]. The lowest concentration (2.3 ± 0.4 mM) belongs to the person who was diagnosed with UA elimination problems.

Determination of UA at OPPy Modified CFE

Chapter 5 discusses the development of an ultrathin OPPy modified CFE. The film decreases the background current which is produced by the complex interface/solution interactions at high scan rates. In this Chapter, we use an ultrathin OPPY modified the CFE in the detection of UA to increase the *signal-to-noise* (S/N) ratio and to decrease the limited of detection (LOD) compared to the electrochemically treated CFE. The possible problem in this determination is that thick OPPy membranes have been used as permselective membranes against UA because of high concentrations of negative groups introduced during the OPPy overoxidation process [Beck et al., 1987].

However, the ultrathin membranes used here are characterized by high porosity, and thickness ($24 \pm 8 \text{ \AA}$) estimate in Chapter 5. These characteristics allow UA determinations.

Figure 6.11 shows cyclic voltammogram of $5 \text{ }\mu\text{M}$ UA at bare electrochemically treated CFE (A) and at OPPY modified carbon fiber electrode (B) in $7 \times 10^{-2} \text{ M}$ phosphate buffer pH 7.4 at 500 Vs^{-1} . Table 6.4 summarizes different parameters that were evaluated during the determination. By using OPPY modified electrode all three parameters were improved.

The sensitivity enhancement in FSV can occur because the active area remains large while the area that undergoes charging is decreased. The linear dynamic range (LDR) for the OPPY modified electrode is smaller than the LDR of the bare electrode. The biggest improvement is the increased S/N for UA determinations at OPPY modified electrodes as shown in Table 6.4.

Determination of UA in Presence of AA at OPPY Modified Electrodes

In this section, we present the determination of UA in the presence of AA at OPPY modified UME at high scan rates. Figure 6.12 shows the determination of UA, solid line, and a mixture of UA and AA at 500 Vs^{-1} . The experiment results suggest that $25 \text{ }\mu\text{M}$ UA can be detected in the presence of $250 \text{ }\mu\text{M}$ AA (one order of magnitude bigger than UA) at high scan rates, as illustrated in Table 6.5. The determination of UA may be possible thanks to the high porosity morphology of the ultrathin OPPY UME.

In order to compare UA determinations in presence of AA at OPPY modified electrode with previous determinations at bare electrode, the concentrations of AA and UA were increased (from $25 \text{ }\mu\text{M}$ and $250 \text{ }\mu\text{M}$ to $50 \text{ }\mu\text{M}$ and 3 mM , respectively)

and produce the same experimental conditions. In previous work, cyclic voltammograms of 3 mM AA at bare UME did not show clear electrochemical peaks at 1,000 Vs⁻¹. However, voltammograms at 1,000 Vs⁻¹ of the same AA concentration at OPPy modified UME present clear electrochemical peaks as illustrated in Figure 6.13.B. Figure 6.13 shows the determination of 50 µM UA (A), 3 mM AA (B), and mixture of 50 µM UA with 3 mM AA at 1,000 Vs⁻¹. Based on these results, high concentration AA is interfering with UA determination at OPPy modified CFE a high scan rates, above 500 Vs⁻¹. The enhancement in response (compared to bare electrode) of AA suggests a possible interaction between the OPPy membrane and the unwanted AA. By decreasing the scan rate, the interference of AA in the UA determination becomes bigger as illustrated in Figures 6.14. Mao and Pickup reported that AA and ascorbate can diffuse through polypyrrole derivatives (poly [1-methyl-3-(pyrrol-1-ylmethyl)pyridinium]) and the oxidation of AA can be catalyzed by the presence of the polymer via electrostatic interactions [Mao and Pickup, 1989].

Conclusions

In this Chapter, we have demonstrated the analytical utility of FSV at electrochemically pretreated carbon fiber electrodes in the determinations of UA. High selectivity and sensitivity at 500 Vs⁻¹ allows determinations of low concentrations of UA in the presence of high concentrations of AA at electrochemically treated CFE without a permselective film.

While the increases in the magnitude of the signal with an increase in scan rate simplifies signal acquisition, temporal resolution also benefits from fast scan rates. High temporal resolution allows acquisition of many signals for signal-averaging, improving

S/N. However, the method is limited by the enormous background current which are present under the conditions of fast scan. The background current (which consumes high portion of the resolution of oscilloscope) may be the responsible for the non-ideal ($S/N \propto n^{1/2}$) improvement of S/N.

Although the slope of the plot of the logarithm of UA oxidation peak current (bare electrochemically treated CFE) *versus* the logarithm of scan rate in the scan rate from 100 to 2000 Vs^{-1} reveals a diffusion-controlled process (non-adsorption), the high sensitivity enhancement factor, $f_{a\ UA}$, for uric acid, $f_{a\ UA} = i_{p\ exp}/i_{p\ theor} = 55 \pm 3$, suggests a possible accumulation of the UA at the very active electrochemically treated CFE.

Preliminary uric acid determinations in biological systems were achieved using a bare electrochemically treated carbon fiber electrode. These preliminary results suggest that electrochemically treated carbon fiber can be applied to develop a sensor for the detection of uric acid in both systems at fast scan voltammetry.

Modifying the electrochemically treated CFE with an ultrathin OPPy membrane, an improvement in the S/N and sensitivity for UA detection are achieved compared to bare electrochemically treated CFE. However, AA becomes electroactive interference for UA determination at OPPy modified CFE even scan rates above 500 Vs^{-1} .

Table 6.1 Signal-to-noise ratio for uric acid at a scan rate of 500 Vs^{-1} at electrochemically treated carbon fiber electrode.^a

No. of cycles	Peak current ^b $\times 10^9 \text{ A}$	S/N ^c
1	9.4 ± 0.1	2.86 ± 0.06
25	7.76 ± 0.06	8.30 ± 0.09
100	7.71 ± 0.09	9.89 ± 0.06
250	6.38 ± 0.05	13.34 ± 0.05

- a. Electrode diameter $\approx 7 \mu\text{m}$.
- b. $4.11 \times 10^{-5} \text{ M}$ uric acid in $7.0 \times 10^{-2} \text{ M}$ potassium phosphate buffer (pH 7.4). Analytical signals were background subtracted.
- c. Peak-to-peak noise was used rather than N_{rms} .

Table 6.2. Determination of uric acid in different physiological buffer pH 7.4 at electrochemically treated carbon fiber electrode.

Supporting Electrolyte ^a	I _b ^b NA	ΔE_p mV	UA Sensitivity ^c pA μM^{-1}	LOD ^d μM
KCl	25	258 \pm 32	78 \pm 5	25
Tris-HCl	25	628 \pm 16	38 \pm 2	20
Krebs-Henseleit	18	583 \pm 21	346 \pm 2	10
70 mM Sodium Phosphate	10	307 \pm 35	440 \pm 2	5
300 mM Sodium Phosphate	10	450 \pm 35	340 \pm 5	5
Krebs	----	680 \pm 45	57 \pm 9	15

- For composition, see Experimental section (Chapter 2).
- Background current at 0.25 V, 10 Vs⁻¹, 50 cycles, after electrochemical treatment.
- Uric acid (UA). Sensitivity from the slope of the calibration curve at 500 Vs⁻¹. At least 5 points for each calibration curve and 4 determinations for each point. Number of electrodes (n) used ≥ 4 for sodium phosphate and Krebs-Henseleit, $n \leq 3$ for KCl, Tris-KCl, and Krebs.
- Limit of detection (LOD) when S/N = 3. Peak-to-peak noise was used rather than N_{rms} .

Table 6.3. Detection of uric acid in urine samples with a bare electrochemically treated carbon fiber electrode at 500 Vs⁻¹.^a

Sample	Diluted concentration $\times 10^{-6}$ M	Total Concentration ^b	
		$\times 10^{-3}$ M	$\times 10^{-8}$ mg dL ⁻¹
1	3.0 ± 0.7	3.0 ± 0.7	5 ± 1
2	4.3 ± 0.5	4.3 ± 0.5	7 ± 1
3 ^c	2.3 ± 0.4	2.3 ± 0.4	3.9 ± 0.6

- Results were background subtracted. 250 cycles for background and analyte were stored, averaged and used for processing of the data. Electrode diameter $\cong 7 \mu\text{m}$. 7×10^{-2} phosphate buffer (pH 7.4) was used as background.
- Total value obtained by multiplying the diluted concentration value with the dilution factor of 1000.
- Sample belongs to a person who was diagnosed with uric acid elimination problems.

Table 6.4. Relative sensitivities and *signal-to-noise* ratio of uric acid at 500 Vs⁻¹ with bare treated and overoxidized polypyrrole modified treated carbon fiber electrode.

Electrode	UA Sensitivity ^a nA μM^{-1}	S/N ^b	LDR μM
Bare treated CFE	0.44 \pm 0.02	3	1 - 20
OPPy treated CFE	0.70 \pm 0.03	4.8	0.5 - 10

- a. Uric acid (UA). Sensitivity from the slope of the calibration curve at 500 Vs⁻¹. At least 5 points for each calibration curve and 4 determinations for each point. Number of electrodes (n) used \geq 4.
- b. S/N for 5 μM UA in 7×10^{-2} M phosphate buffer (pH 7.4). Peak-to-peak noise was used rather than N_{rms} .

Table 6.5. Determination of uric acid in presence of ascorbic acid at overoxidized polypyrrole modified treated carbon fiber electrode.

Sample ^a	Composition	Concentration μM	Current ^b nA
1	Uric acid	25	6.1 ± 0.3
2	Uric acid	25	6.2 ± 0.6
	Ascorbic acid	25	
3	Uric acid	25	6.0 ± 0.2
	Ascorbic acid	50	
4	Uric acid	25	6.1 ± 0.2
	Ascorbic acid	250	

- a. Samples were prepared in 7×10^{-2} M phosphate buffer (pH 7.4).
- b. Scan rate 500 Vs^{-1} , electrode radius $2.5 \pm 0.3 \mu\text{m}$. Results were background subtracted. 250 cycles for background and analyte were stored, averaged, and used for processing of the data. Three electrodes and four readings for each point were used for data analysis.

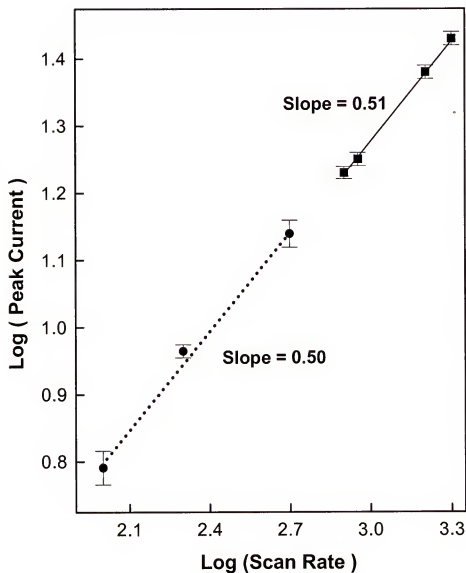


Figure 6.1. Plot of log of 5×10^{-5} M uric acid peak current, log (peak current) *versus* log (scan rate). Scan range is from 100 to 2000 Vs^{-1} . Working electrode is an electrochemical treated carbon fiber (7 μm diameter) and 70 mM phosphate buffer solution pH7.4

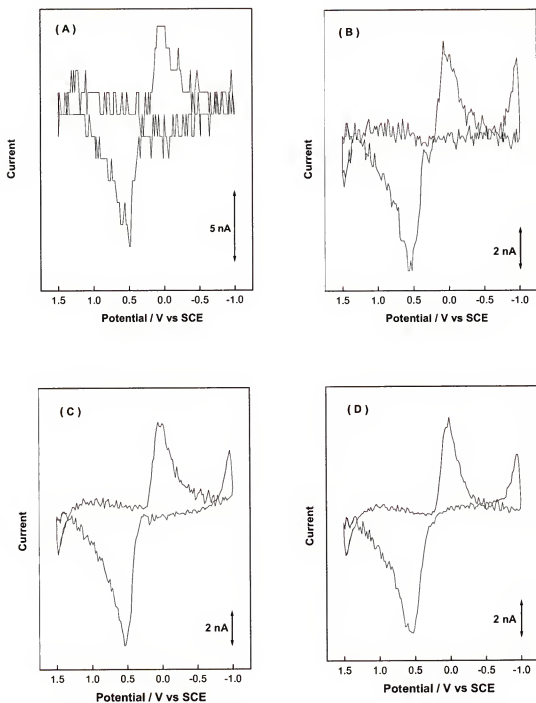


Figure 6.2. Signal averaging cyclic voltammograms of 50 mM uric acid in 70 mM phosphate buffer, scan rate 500 Vs⁻¹. Figures A, B, C, and D are averaged 1, 10, 50, and 250 times, respectively.

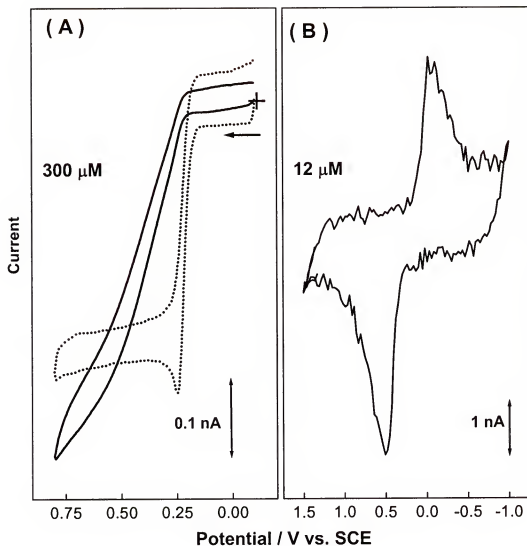


Figure 6.3. Voltammetry of uric acid at carbon fiber electrode at pH 7.4. (A) Slow scan voltammetry at a scan rate of 50 mV s^{-1} before (solid line) and after (small dash) electrochemical treatment. (B) Fast scan voltammetry at 500 V s^{-1} at electrochemically treated carbon fiber electrode. Concentration of uric acid are shown in the Figure. Electrode diameter ca. $7 \text{ } \mu\text{m}$. Fast scan voltammogram in (B) is background subtracted, 250 cycles signal averaged.

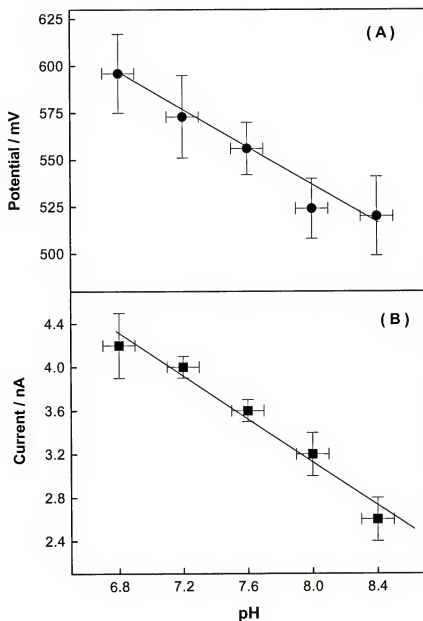


Figure 6.4. Oxidation potential, E_p , (A) and peak current, i_p , (B) dependence on pH of 15 μM uric acid at electrochemically treated carbon fiber, 500 Vs^{-1} , in 70 mM phosphate buffer, electrode diameter ca. 2 μm .

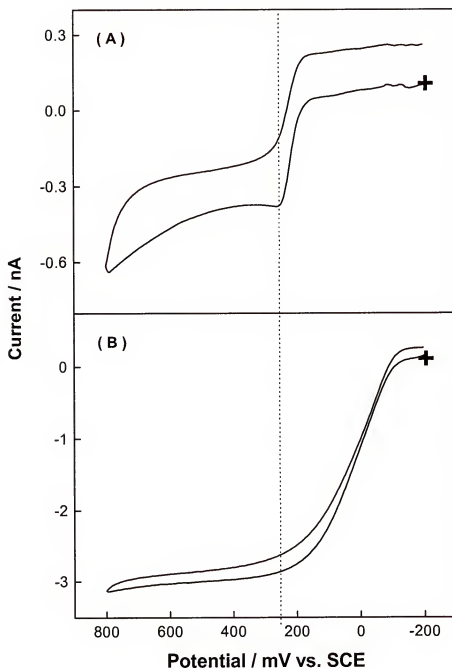


Figure 6.5. Cyclic voltammetry at treated carbon fiber electrode (ca. 7 μm diameter) of (A) 3×10^{-4} M uric acid and (B) 3×10^{-4} M ascorbic acid in 7×10^{-2} M phosphate buffer (pH 7.4). Scan rate 50 mV s^{-1} .

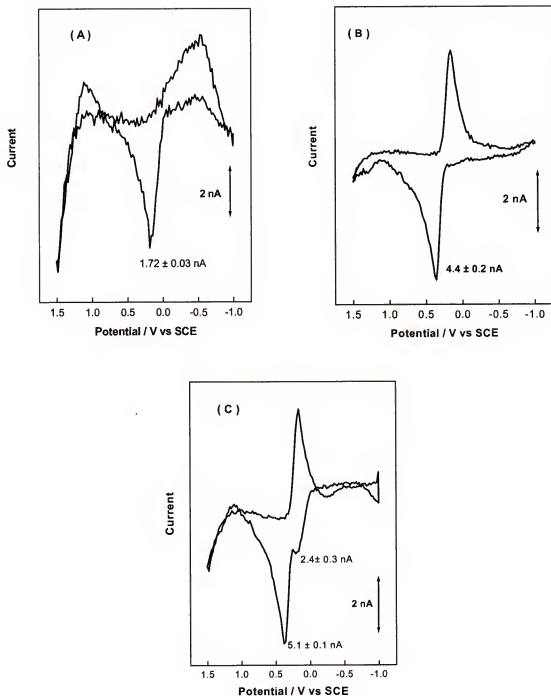


Figure 6.6. Cyclic voltammetry at treated carbon fiber electrode (ca. 7 μm diameter) of (A) 3×10^{-3} M ascorbic acid, (B) 5×10^{-5} M uric acid, and a mixture (C) of 3×10^{-3} M ascorbic acid with 5×10^{-5} M uric acid in 7×10^{-2} M phosphate buffer (pH 7.4). Voltammograms are background subtracted, 250 cycles signal averaged. Scan rate 100 V s^{-1} .

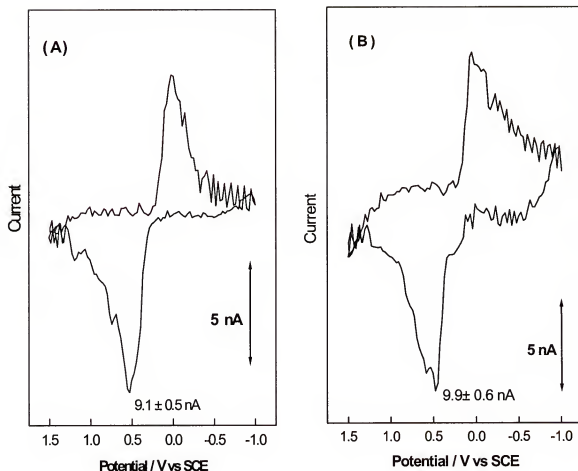


Figure 6.7. Cyclic voltammetry at treated carbon fiber electrode (ca. $7 \mu\text{m}$ diameter) of (A) $5 \times 10^{-5} \text{ M}$ uric acid and a mixture (B) of $3 \times 10^{-3} \text{ M}$ ascorbic acid with $5 \times 10^{-5} \text{ M}$ uric acid in $7 \times 10^{-2} \text{ M}$ phosphate buffer (pH 7.4). Voltammograms are background subtracted, 250 cycles signal averaged. Scan rate 500 V s^{-1} .

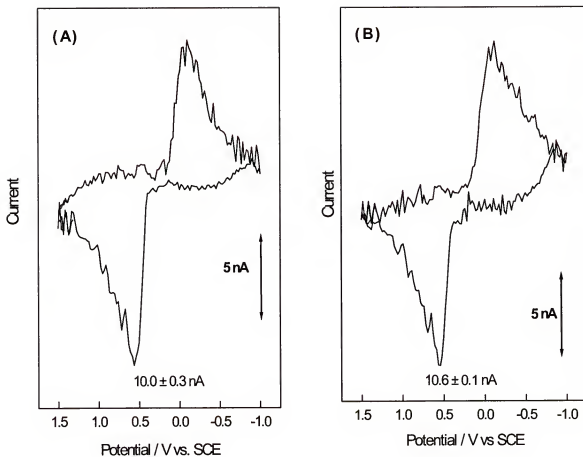


Figure 6.8. Cyclic voltammetry at treated carbon fiber electrode (ca. $7\mu\text{m}$ diameter) of (A) 5×10^{-5} M uric acid and a mixture (B) of 3×10^{-3} M ascorbic acid with 5×10^{-5} M uric acid in 7×10^{-2} M phosphate buffer (pH 7.4). Voltammograms are background subtracted, 250 cycles signal averaged. Scan rate 1000 V s^{-1} .

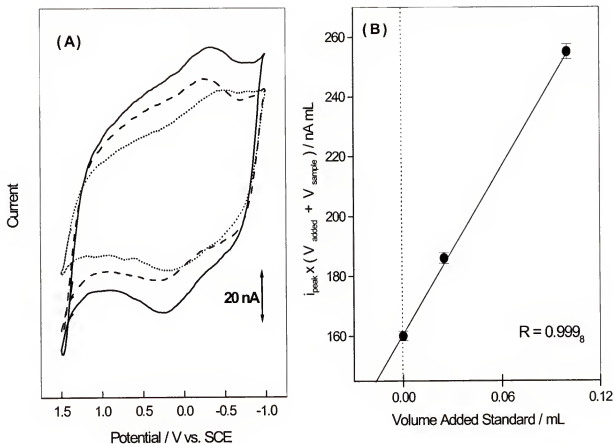


Figure 6.9. Detection of uric acid in perfused heart sample. (A) Fast scan cyclic voltammetry at treated carbon fiber electrode (ca. 7 μ m diameter) of original perfused heart sample (small dot), after spike the original sample with 2.3 μ moles of uric acid (dashed line), and after spike the original sample with 9.5 μ moles of uric acid (solid line). Krebs-Henseleit (KH) buffer (pH 7.4) was used to perfuse the heart. Scan rate 500 V s^{-1} , 75 cycles of KH were averaged and used as background. 250 cycles of the sample were averaged and used for processing of the data. Voltammograms are background subtracted. Figure (B) shows the standard addition plot for the detection of uric acid in heart perfused samples.

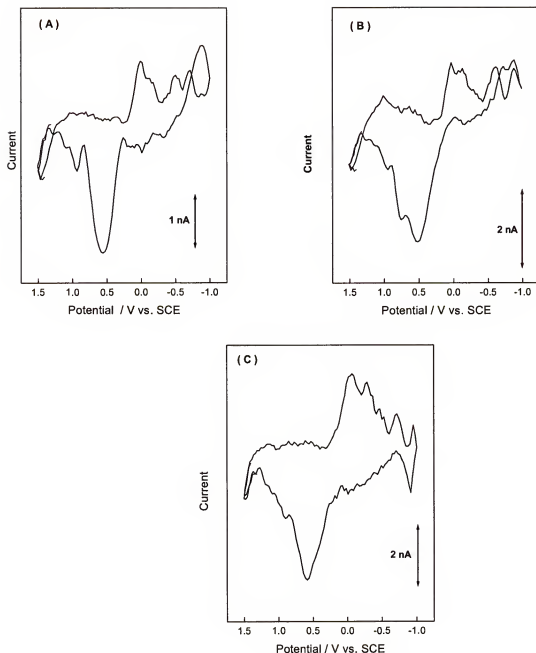


Figure 6.10. Detection of uric acid in urine (A) fast scan voltammetry of 100 μL of urine (without any treatment) in 100 mL of phosphate buffer (pH 7.4) at bare electrochemically treated carbon fiber electrode (7 μm diameter). Figures B and C are after spike the diluted sample (A) with 45 and 90 μmoles , respectively. The voltammograms are background subtracted, 250 cycles for the background and sample were used for data processing.

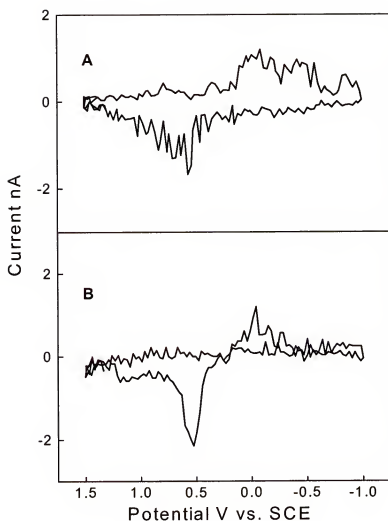


Figure 6.11. Fast scan voltammetry of 4×10^{-6} M uric acid in 7×10^{-2} M phosphate buffer (pH 7.4) at (A) bare electrochemically treated carbon fiber electrode and (B) OPPy-modified treated carbon fiber electrode. Scan rate 500 V s^{-1} . Voltammograms were background subtracted. 250 cycles for the background and uric acid were used for data processing.

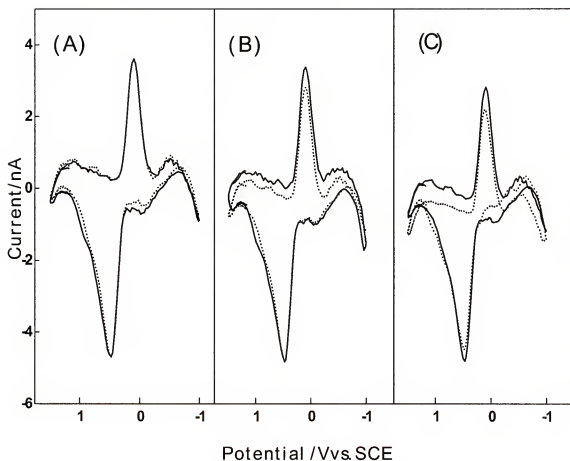


Figure 6.12. Fast scan voltammetry of uric acid in presence of ascorbic acid at OPPy modified electrode in 7×10^{-2} M phosphate (pH 7.4). (A) 25 μ M uric acid (solid line) and a mixture of 25 μ M uric acid with 25 μ M ascorbic acid (dashed line). (B) 25 μ M uric acid (solid line) and a mixture of 25 μ M uric acid with 50 μ M ascorbic acid (dashed line). (C) 25 μ M uric acid (solid line) and a mixture of 25 μ M uric acid with 250 μ M ascorbic acid (dashed line). Scan rate 500 Vs^{-1} , voltammograms were background subtracted. 250 cycles for the background and analyte were used for data processing.

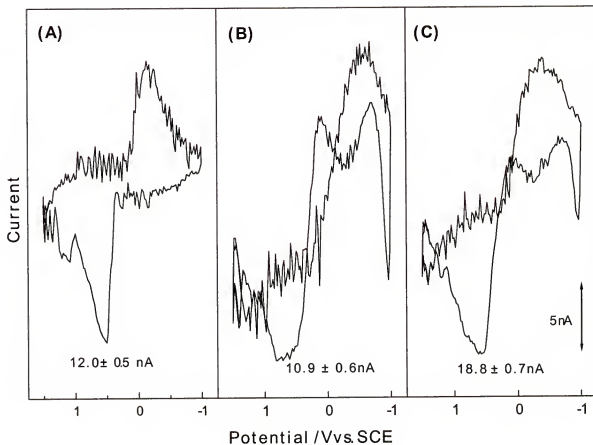


Figure 6.13. Cyclic voltammetry at OPPy-modified treated carbon fiber electrode (ca. 7 μ m diameter) of (A) 3×10^{-3} M ascorbic acid, (B) 5×10^{-5} M uric acid, and a mixture (C) of 3×10^{-3} M ascorbic acid with 5×10^{-5} M uric acid in 7×10^{-2} M phosphate buffer (pH 7.4). Voltammograms are background subtracted, 250 cycles signal averaged. Scan rate 1,000 V s⁻¹.

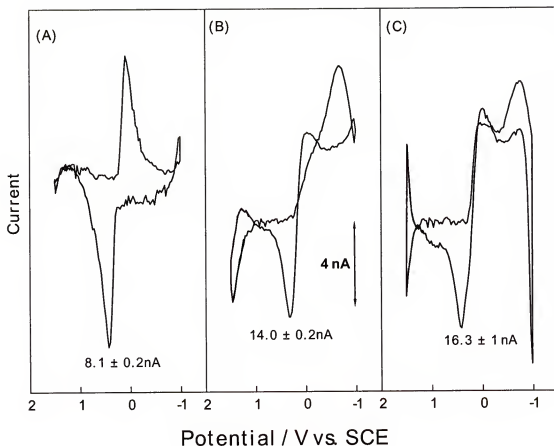


Figure 6.14. Cyclic voltammetry at OPPy-modified treated carbon fiber electrode (ca. $7 \mu\text{m}$ diameter) of (A) 3×10^{-3} M ascorbic acid, (B) 5×10^{-5} M uric acid, and a mixture (C) of 3×10^{-3} M ascorbic acid with 5×10^{-5} M uric acid in 7×10^{-2} M phosphate buffer (pH 7.4). Voltammograms are background subtracted, 250 cycles signal averaged. Scan rate 250 V s^{-1} .

CHAPTER 7

ELECTROCHEMICAL POLYMERIZATION AND CHARACTERIZATION OF PHOSPHOTUNGSTATE FILM

Background

The catalytic redox activity of polyoxometalates has attracted much attention in recent years. The catalytic power of these compounds is related to their reducibility and reoxidizability. The flexibility in applications originates from the possibility of varying the redox potential of polyoxometallates over a wide range by changing composition. The reduced forms can act as donors or acceptors of several electrons while maintaining their structure [Pope and Varga, 1966; Weakly, 1974]. A large number of heteropolyanions (HPO) undergo a series of reversible one and two electron reductions, and the reduced heteropolyanions (so-called "heteropoly blue") are the active species. These compounds are mainly used as reductive electro-catalysts in two ways: homogeneously dissolved in the electrolyte solution and attached to electrode surfaces.

In several reports, it has been demonstrated that HPO can be used to modify electrode surfaces yielding very stable and robust modified surfaces. Electrodes can easily be modified with HPO such as sodium phosphotungstate (SPT) using the following methods: adsorption, entrapment into polymer, and electrodeposition.

Dong and co-workers modified CFE and glassy carbon electrodes by soaking them in an acid solution with HPO such as $\text{PMo}_{12}\text{O}_{40}^{3-}$ [Dong and Jin, 1987; Xi and Dong, 1995; Wang and Dong, 1996], $\text{PMo}_{18}\text{O}_{62}^{6-}$ [Wang and Dong, 1992]. They reported

that the cycle voltammetric waves show the typical symmetry and linear dependence of currents on the scan rate, which is expected for adsorbed species. Rong and Anson also reported that $\text{PMo}_{12}\text{O}_{40}^{3-}$, $\text{PMo}_{18}\text{O}_{62}^{6-}$, $\text{P}_2\text{W}_{18}\text{O}_{62}^{6-}$, $\text{SiW}_{11}\text{O}_{39}\text{Fe}^{\text{III}}(\text{H}_2\text{O})^5$, and $\text{PW}_{11}\text{O}_{39}\text{Fe}^{\text{III}}(\text{H}_2\text{O})^4$ are spontaneously adsorbed on glassy carbon and edge pyrolytic graphite electrodes [Rong and Anson, 1994; 1996].

Electrodes have been modified with a mixture of HPO and polymer such as polypyrrole [Xi and Dong, 1996] to produce stronger binding interactions with the electrode. In many cases, the electrochemical behavior of the HPO incorporated into the polymer is almost the same as the electrochemical behavior of HPO dissolved in solutions [Bidan et al., 1989].

Since Keita and Nadjo reported the electrodeposition of $\text{SiW}_{12}\text{O}_{40}^{4-}$ on electrodes in 1985 [Keita and Nadjo, 1985], an enormous number of publications have been presented in this field due to the ability of these modified electrodes to catalyze hydrogen evolution reactions. The electro-modified electrodes are very stable not only in solution but also in air [Keita and Nadjo, 1990]. Some electrodes can be kept for several years and show the same activity toward the hydrogen evolution reaction.

As mentioned in Chapter 1, the most commonly used colorimetric method for UA determination depends on the reduction of sodium phosphotungstate by uric acid. The reduction of sodium phosphotungstate produces a blue compound which can be detected at 660 and 720 nm. The absorbance at these wavelengths is proportional to UA concentration in the sample. Advantages and disadvantages of this method are discussed in Chapter 1.

The main goal of this part of this work is to fuse the high activity of the electrochemically treated CFE with the catalytic properties of the phosphotungstate species to produce a very sensitive sensor for UA detection. By using the phosphotungstate modified CFE an increase in the UA response due to the catalytic effect of the film may be obtained. In this Chapter, we present preliminary results of the electrodes modified with phosphotungstic acid for UA determination. First, a rough pyrolytic graphite electrode (RPG) (which is characterized by its high activity and high surface roughness and high area) was used to explore the general conditions for the modification and the possible catalytic effect of the film in UA determination. Next, an electrochemically treated CFE was modified with phosphotungstic acid using the parameters optimized for RPG.

Results and Discussion

Experimental Conditions for UA Determination Using the Colorimetric Method.

The phosphotungstic acid procedure is used in most clinical laboratories around the world for UA determinations [Wyngaarden and Kelly, 1976; Kaplan, et al., 1995]. Consequently, we studied the experimental parameters such as pH and concentration of reagents to adopt and to optimize the conditions for UA electrochemical determinations.

Effect of pH

Two vials were marked as blank and UA sample respectively. Three ml of 12.6 mM $\text{H}_3\text{PW}_{12}\text{O}_{40}$ in distilled water were transferred to each vial. One ml of water and 20 μL of 6.0 mM UA in 14% sodium carbonate (pH 8.4) were added to the vial marked as "UA sample" and 1.0 ml of water was added to the "blank". The contents of the vials

were mixed for 5 s. Solution of sodium carbonate (1 ml, 14 %) was added to both containers and the pH was adjusted using 2 M NaOH. After 30 minutes the UA vial changed from colorless to pale blue while the blank solution remained colorless.

Table 7.1 summarizes the results at different pH. The optimum pH for the development of blue color was found to be 9.2. This result agrees with reported literature values [Henry, et al., 1957; Pileggi, et al., 1971].

Effect of Reagent Concentration

The same previously used procedure was followed to determine the effect of concentration of $\text{H}_3\text{PW}_{12}\text{O}_{40}$ on UA determination using the colorimetric method. Five vials were prepared and marked as blank, 1, 2, 3, and 4. Three, 1, 2, 3, and 4 ml of 12.6 mM phosphotungstic acid in distilled water were added to vials blank, 1, 2, 3, and 4 respectively. One ml of water and 20 μL of 6.0 mM UA in 14% sodium carbonate (pH 8.4) were added to the vials marked as 1,2,3, and 4 and 1.0 ml of water was added to the "blank". The contents of the vials were mixed for 5 s. Solution of sodium carbonate (1 ml, 14 %) was added to both containers and the pH was adjusted at 9.2 using 2 M NaOH. After 30 minutes each vial was checked visually for the development of blue color compared to the blank sample.

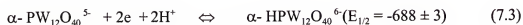
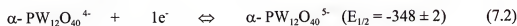
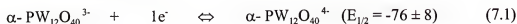
Table 7.2 summarizes the experimental results. We found that the minimum mole ratio of UA to $\text{H}_3\text{PW}_{12}\text{O}_{40}$ was 200 for full development of blue color at pH 9.2 in 14% sodium carbonate. This ratio of UA/ $\text{H}_3\text{PW}_{12}\text{O}_{40}$ can be used as a relative measure of the catalytic power of $\text{H}_3\text{PW}_{12}\text{O}_{40}$ for UA oxidation. The same experiments were repeated using 0.5 M sodium phosphate (pH 8.4) and similar results were obtained.

Electrochemistry of Phosphotungstic Acid at RPG

Electrochemistry in Solution

Figure 7.1 shows the cyclic voltammogram of 0.5 mM $\text{H}_3\text{PW}_{12}\text{O}_{40}$ in 0.5 M H_2SO_4 at RPG, scan rate 50 mVs^{-1} *versus* SCE. Even though a salt bridge was used to avoid contamination of the reference electrode (SCE) with H_2SO_4 , we found evidence of this contamination on the reference electrode at the end of experiments. For future experiments, a quasi-reference such as platinum electrode should be used. Three well-defined reduction peaks are observed. The peaks appear at $E_{1/2}$ ($(E_{pc} + E_{pa}) / 2$) values of -76 ± 8 , -348 ± 2 , and $-688 \pm 3 \text{ mV}$ *versus* SCE. The peak potential separation (ΔE) for the two first peaks ($E_{1/2} = -76 \pm 8$ and -348 ± 2) are 59 ± 3 and $60 \pm 4 \text{ mV}$ respectively. These ΔE values suggest that each redox wave may correspond to a Nernstian reaction with one-electron transfer for each wave. The third potential separation ($E_{1/2} = -688 \pm 3$) is $28 \pm 2 \text{ mV}$ indicating that the redox wave may correspond to a Nernstian reaction with two-electron transfer.

The reduction process may be possibly associated with the following reactions [Sadakane and Steckhan, 1998].



$$0 < \text{pH} < 3$$

Electrochemistry of Phosphotungstate at the RPG Surface

Formation of the Film

A freshly polished (with 600-grit SiC, 1 minute) rough pyrolytic electrode (RPG) was immersed in 0.5 M H_2SO_4 and the cyclic voltammogram of the blank was obtained. Next the RPG was immersed in a solution of 0.5 mM $\text{H}_3\text{PW}_{12}\text{O}_{40}$ in 0.5 M H_2SO_4 and cycled (50 cycles) in a potential window from 200 to -800 mV *versus* SCE at scan rate of 50 mVs^{-1} . The $\text{H}_3\text{PW}_{12}\text{O}_{40}$ modified RPG was rinsed with double distilled water and immersed back into 0.5 M H_2SO_4 and a cyclic voltammogram was taken to verify the electrode modification with $\text{H}_3\text{PW}_{12}\text{O}_{40}$. Figure 7.2 shows the cyclic voltammogram of the modified electrode in 0.5 M H_2SO_4 . The well-defined peaks around -688 and -348 mV are a clear evidence of deposition of phosphotungstate film on the RPG surface after 50 cycles in the experimental potential window.

The quantity of $\text{H}_3\text{PW}_{12}\text{O}_{40}$ electrodeposited on the RPG surface was estimated from the charge under the reduction surface wave at -688 mV. A coverage value for the RPG surface of $(1.8 \pm 0.2) \times 10^{-8} \text{ mol cm}^{-2}$ was obtained. Because the surface wave rides above a high background current, background (which was obtained before modification) subtraction was performed. The RPG electrode areas were obtained from the slope of the chronocoulometric response of 5 mM ferricyanide in 0.5 M KCl (pH 6.0) as discussed in Chapter 2. Typical RPG areas were $0.033 \pm 0.005 \text{ cm}^2$. A value of 120 ± 13 monolayers (50 cycles in a potential window from 200 to -800 mV *versus* SCE) was estimated assuming a typical monolayer value of $1.5 \times 10^{-10} \text{ mol cm}^{-2}$ [Bard and Faulkner, 1980].

Determination of UA Using a Phosphotungstate Modified RPG

Table 7.3 summarizes the UA determination at phosphotungstate modified RPG. The results suggest that the minimum number of cycles needed to produce a good enhancement in UA signal is ten cycles. Results show that improvement in UA determination was achieved in all cases; however, the best improvement was obtained after modification using 50 cycles. All UA determinations were performed at pH 9.2 in phosphate buffer 0.5 M.

Electrochemistry of Phosphotungstic Acid at Electrochemically Treated Carbon Fiber Electrode

Electrochemistry in Solution

Figure 7.3 shows a voltammogram of 0.5 mM $\text{H}_3\text{PW}_{12}\text{O}_{40}$ in 0.5 M H_2SO_4 , scan rate 10 Vs^{-1} . The voltammogram at CFE presents the same features as the voltammogram at RPG. Three well-defined peaks can be associated with Reactions 7.1, 7.2, and 7.3.

Formation of the Film

Modification procedure used for RPG with phosphotungstate was followed to modify the electrochemically treated CFE. Since an electrochemically treated CFE was used for phosphotungstate modification, the same scan rate (10 Vs^{-1}) used for the electrochemical pretreatment was used for modification. Electrochemically treated CFE were cycled 100, 250 and 500 times in a potential window from 200 to -800 mV versus SCE at 10 Vs^{-1} in a solution of 0.5 mM $\text{H}_3\text{PW}_{12}\text{O}_{40}$ in 0.5 M H_2SO_4 . However, only the electrodes that were 500 times cycled presented a clear evidence of phosphotungstate modification. The phosphotungstate modified CFE was immersed in 0.5 M H_2SO_4 and a

voltammogram was taken to verify phosphotungstate modification. Figure 7.4. shows three well-defined peaks at 85, 395, and 634 mV *versus* SCE which are clear evidence of electrodeposition of phosphotungstate on the CFE surface. Preliminary results suggest that phosphotungstate modified CFE may improve UA response, however a more detailed research should be performed.

Conclusions

Experimental results of the colorimetric method for UA determination suggest that the optimum pH for the redox reaction is 9.2 in 14% sodium carbonate buffer and 0.5 M sodium phosphate buffer. Voltammograms of $\text{H}_3\text{PW}_{12}\text{O}_{40}$ in 0.5 M H_2SO_4 show three well-defined Nernstian waves which can be used to verify the formation of phosphotungstate film at rough pyrolytic graphite electrodes.

Preparation of phosphotungstate film at RPG and electrochemically treated CFE has demonstrated in this Chapter. Preliminary experimental determinations of UA at RPG suggest that a minimum amount of phosphotungstate must be used for enhancement of UA signal. Also, promising preliminary results corroborate the catalytic effect of phosphotungstic acid for UA electrochemical oxidation. Finally, these preliminary results open the possibility of using the catalytic redox activity of polyoxometallates to modify electrodes for UA determinations.

Table 7.1. Effect of pH in UA determination using colorimetric method ^a.

PH	Color Evolution ^b
5.0	NCD
7.4	NCD
8.0	PCD
9.2	FCD
9.7 ^c	FCD
10.3 ^c	FCD

- a. 14 % sodium carbonate buffer; basic values of pH were adjusted with 2 M NaOH; UA moles = 1.2×10^{-7} moles; $H_3PW_{12}O_{40}$ moles = 3.78×10^{-5} moles.
- b. NCD = No color developed; PCD = Partial color developed; FCD = Full color developed.
- c. Blue color is not stable after 35 minutes.

Table 7.2. Effect of the reagent concentration in UA determination using colorimetric method.

Amount of $\text{H}_3\text{PW}_{12}\text{O}_{40}$ ^a $\times 10^{-5}$ mol	Color Evolution ^b
1.26	NCD
2.52	NCD
3.78	FCD
5.04	FCD

- a. 14 % sodium carbonate buffer; pH 9.2 (adjusted with 2 M NaOH); UA moles = 1.2×10^{-7} moles.
- b. NCD = No color developed; FCD = Full color developed.

Table 7.3. Determination of UA at phosphotungstate modified RPG.^a

Number of Cycles	UA Response before Modification ^b $\mu\text{A cm}^{-2}$	UA Response after Modification ^b $\mu\text{A cm}^{-2}$	% increase UA signal after modification
1	3.9 ± 0.3	6.1 ± 0.3	40 ± 4
10	4.3 ± 0.3	9.5 ± 0.5	121 ± 13
50	5.1 ± 0.3	11.8 ± 0.5	131 ± 13

- a. Number of electrodes used = 3 and four determinations for each reading was taking ($n = 12$).
- b. Electrode area $0.033 \pm 0.005 \text{ cm}^2$. UA concentration = 0.1 mM in 0.5 M phosphate buffer pH 9.2, scan rate 50 mVs^{-1} . 50 cycles in a solution of 0.5 M $\text{H}_3\text{PW}_{12}\text{O}_{40}$ in 0.5 M H_2SO_4 were used to modify the electrode with phosphotungstate. The UA current before and after modification was determined at $200 \pm 20 \text{ mV}$ versus SCE.

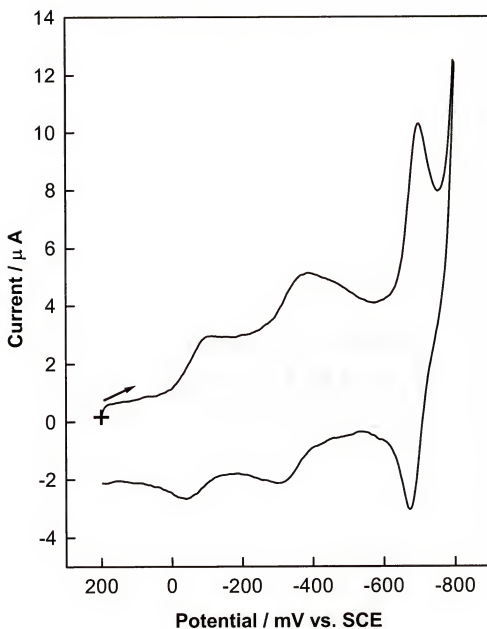


Figure 7.1. Voltammetry of 0.5 mM $\text{H}_3\text{PW}_{12}\text{O}_{40}$ in 0.5 M H_2SO_4 at rough pyrolytic graphite electrode. Electrode area $0.033 \pm 0.002 \text{ cm}^2$; Scan rate 50 mVs^{-1} . Voltammogram is background subtracted.

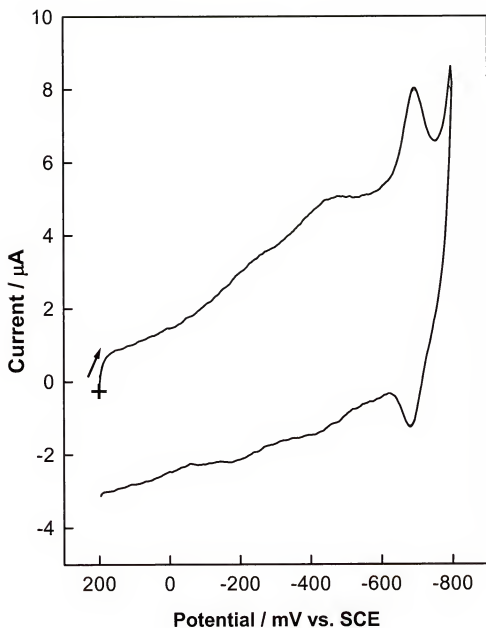


Figure 7.2. Voltammetry of 0.5 M H_2SO_4 at phosphotungstate modified rough pyrolytic graphite electrode. Electrode area $0.033 \pm 0.002 \text{ cm}^2$; Scan rate 50 mVs^{-1} .

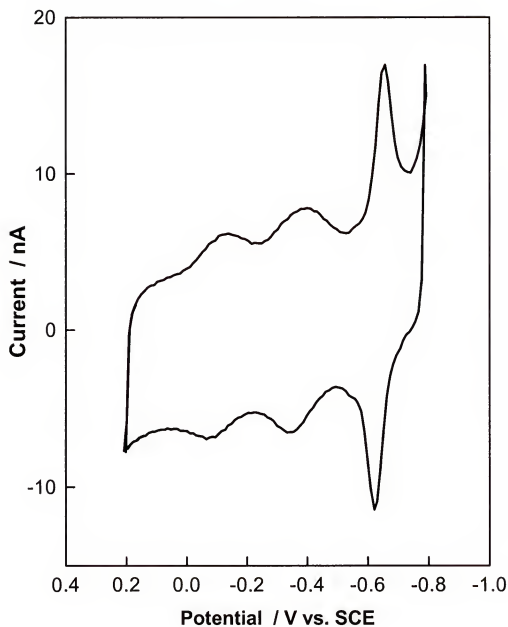


Figure 7.3. Voltammetry of 0.5 mM $\text{H}_3\text{PW}_{12}\text{O}_{40}$ in 0.5 M H_2SO_4 at carbon fiber electrode. Electrode diameter ca. 7 μm ; Scan rate 10 V s^{-1} . 50 cycles signal averaged.

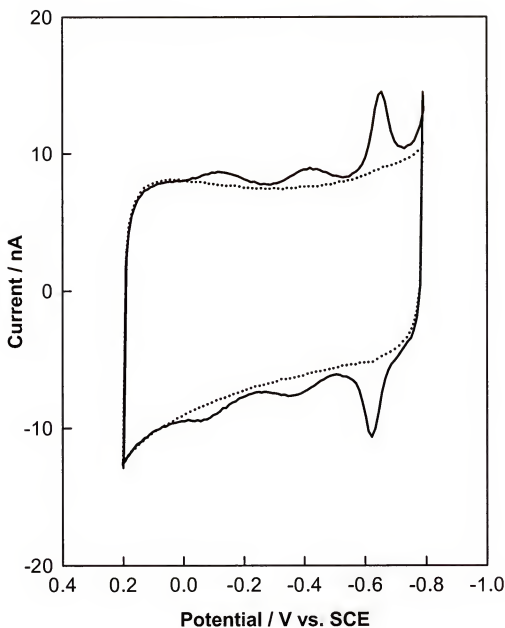


Figure 7.4. Voltammetry of 0.5 M H_2SO_4 before (dotted line) and after (solid line) modification with phosphotungstate at electrochemically treated carbon fiber electrode. Electrode diameter ca. 7 μm ; Scan rate 10 Vs^{-1} . 50 cycles signal averaged.

CHAPTER 8

SUMMARY AND FUTURE DIRECTIONS

Summary

The goal of this research was not only the development of novel surfaces for the enhancement of sensitivity and selectivity of purine determinations but also the characterization of these surfaces using electrochemical parameters and techniques. The work described in this research can be summarized as follows. First, a nanostructured carbon fiber electrode was prepared by a combination of mechanical polishing and electrochemical treatment which involved moderate oxidation of the surface, followed by reduction. The nanostructured carbon fiber electrode exhibits a very stable background current not only in solution but also in air. This stable background current contributes to the high reproducibility of the analytical determinations using fast scan voltammetry presented here. However, the electrochemical treatment increases the background current at the carbon fiber electrode which limits signal detection.

Second, electrochemical characterization of the nanostructured carbon fiber electrode was performed using conventional electrochemical techniques. Cyclic voltammetry at low and fast scan rates was used to determine the projected and microscopic area of the carbon fiber electrodes. Nanostructured carbon fiber electrodes were electrochemically characterized by their high capacitance and their ability to increase the kinetics of different probes. By monitoring experimental parameters (which

were presented here) such as roughness factor, electrode area, and capacitance, more reproducible nanostructured carbon fiber electrode surfaces can be produced.

Third, electrochemically treated carbon fiber electrodes were used as templates to produce an ultrathin OPPy membrane which decreased the background current at fast scan rates while maintaining the high sensitivity of the nanostructured carbon fiber electrode. Even though a short pulse (10 ms) was used to polymerize OPPy at the surface of the NCFE, the formation of this OPPy film was highly reproducible. Also, the chronocoulometry data suggests that OPPy polymerization is controlled by diffusion.

We have demonstrated the analytical utility of FSV with bare nanostructured carbon fiber electrodes and OPPy modified nanostructured carbon fiber electrodes. Both types of carbon fiber electrodes were used for fast scan voltammetry determinations of UA. By using OPPy modified nanostructured carbon fiber electrodes, an improvement in the S/N ratio and limit of detection for UA determinations was achieved. High selectivity and sensitivity at scan rates above 500 Vs⁻¹ allows the determination of low concentrations of UA in the presence of high concentrations of AA. However, at the same scan rates AA can interfere with UA determinations at OPPy modified NCFE. At bare nanostructured carbon fiber electrodes, the dependence of UA response *versus* pH was also investigated and demonstrated that small changes in the pH range of 6.8 to 8.4 can alter UA response.

Finally, preliminary data of the modification of electrode surface with sodium phosphotungstate (STP) were presented. These preliminary results suggest that STP modified electrodes can enhance UA response by catalyzing UA oxidation.

Future Directions

Instrumental Directions

The Lecroy 9310 oscilloscope (used in the FSV) is capable of acquiring 1×10^4 data points per cycle or scan. However, we used only 2500 points per scan or a voltammogram in FSV due to the limitations of the data acquisition software. The Lecroy software (which was developed in our lab) can only acquire one point per each ten points from the oscilloscope. Consequently, the maximum number of points used for each averaged voltammogram with FSV was 250 points. By using commercial acquisition software such as TAL (TAL Technologies, www.taltech.com), which allows to acquire a maximum number of 3.6×10^4 points per scan, an improvement in the S/N ratio due to a decrease in noise could be obtained.

In this work, we demonstrated that the high temporal resolution of FSV allows signal averaging to increase S/N ratio. Other techniques such as digital and analog filtering should be applied to decrease the noise of the system.

Since the background current of different nanostructured carbon fiber electrodes is highly reproducible, dual FSV should be explored [Long and Weber, 1992]. This system will employ two nanostructured carbon fiber electrodes in twin electrochemical cells. In the first cell, the first working carbon fiber will be positioned in buffer solution without electroactive species. The second working carbon fiber electrode will be positioned in the second electrochemical cell in a buffer solution with the electroactive species. The background current from the first working electrode can be subtracted from the signal current from the second a nanostructured carbon fiber electrode.

Applications and New Modified Electrodes

Since high sensitivity and selectivity for purines at a nanostructured carbon fiber electrodes was achieved, nanostructured carbon fiber electrodes should be used in *in vivo* purine determinations. Additionally, future work should be focused on enzyme immobilization at nanostructured carbon fiber electrode using an ultrathin OPPy membrane. These may enhance the sensitivity of enzyme modified electrodes because the high surface area of the nanostructured carbon fiber can permit higher concentrations of enzyme per unit area compared to a non-nanostructured carbon fiber electrode.

Overoxidized polypyrrole should be used to immobilize sodium phosphotungstate and produce a UA sensor due to strong interactions between polymer and heteropolyanions (HPA) such as sodium phosphotungstate. The literature reported [Sadakane and Steckhan, 1998] that the electrochemical behavior of HPA incorporated in a polymer is the same as HPA dissolved in solution. Two advantages could be obtained using this modification. A decrease in the background current will occur due to the presence of OPPy membrane and an increase in the UA signal will also occur due to the catalytic effect of STP for UA oxidation.

REFERENCES

- Adams, N. R. *Anal. Chem.* **1976**, 48, 1126A.
- Amatore, C. In *Physical Electrochemistry Principles, Methods, and Applications*, Rubinstein, I. (Ed.), Marcel Dekker, New York, **1995**, p 131.
- Amatore, C.; Saveant, J. M.; Tessier, D. *J. Electroanal. Chem.* **1983**, 147, 39.
- Ames, B. N.; Cathcar, R.; Schwiers, E. *Proc. Natl. Acad. Scien. USA* **1981**, 78, 6858.
- Andrieux, C. P.; Audebert, P.; Hapiot, P.; Savéant, J. M. *J. Am. Chem. Soc.* **1990**, 112, 2439.
- Andrieux, C. P.; Audebert, P.; Hapiot, P.; Savéant, J. M. *Synth. Met.* **1991**, 41-43, 2877.
- Anjo, M. D.; Kahr, M.; Khodabakhsh, M. M.; Nowinski, S.; Wagner, M. *Anal. Chem.* **1989**, 61, 2603.
- Anson, C. F.; Osteryoung, A. R. *J. Chem. Edu.* **1983**, 60, 4, 293.
- Bard, J. A.; Faulkner, R. L. *Electrochemical Methods, Fundamentals and Applications*, **1980**, Wiley, New York.
- Baur, J. E.; Kristensen, W. E.; May, J. L.; Wiedeman, D. J.; Wightman, M. R. *Anal. Chem.* **1988**, 60, 1268.
- Beck, F.; Braun, P.; Oberst, M. *Ber. Bunsenges. Phys. Chem.* **1987**, 91, 967.
- Beck, F.; Junge, H.; Krohn, H. *Electrochim. Acta* **1981**, 26, 799.
- Becker, F.B.; Gerlach, E. *Topics and Perspectives in Adenosine research*. **1987**, Vol 4, p 180.
- Beilby, L. A.; Carlsson, A. *J. Electroanal. Chem.* **1988**, 243, 283.
- Beilby, L. A.; Sasaki, A. T.; Stern, M. H. *Anal. Chem.* **1995**, 67, 976.
- Benedict, R. *J. Biol. Chem.* **1930**, 86, 179.

- Berne, R. *Am. J. Physiol.* **1963**, 204, 317.
- Besenhard, J. O.; Fritz, H. P. *Angew. Chem. Int. Ed. Engl.* **1983**, 22, 1950.
- Bidan, G.; Laprowski, M.; Travers, J. P. *Synth. Met.* **1989**, 28, C113
- Bindra, P.; Brown, A. P.; Fleischmann, M. *J. Electroanal. Chem.* **1975**, 58, 31.
- Bodalbhai, L.; Brajter-Toth, A. *Anal. Chim. Acta.*, **1990**, 231, 191.
- Bond, A. M. *Electrochem. Newsl.* July **1991**, 70.
- Bond, M. A.; Fleischmann, M.; Robinson, J. *J. Electroanal. Chem.* **1984**, 172, 11.
- Bond, M. A.; Henderson, E. L. T.; Thormann, W. *J. Phys. Chem.* **1986**, 90, 2911.
- Bond, M. A.; Man, F. T. *Electrochim. Acta* **1987**, 32, 863.
- Brajter-Toth, A.; Dryhurst, G. *J. Electroanal. Chem.* **1981**, 122, 205.
- Brand, F.M.; McGee, D. L.; Kannel, W. D. *Am. J. Epidemiol.* **1985**, 121, 11.
- Bravo, R.; Brajter-Toth, A. *Chem. Anal. (Warsaw)* **1999**, 44, 423.
- Bravo, R.; El-Nour, A. K.; Cavalheiro, T. E.; Brajter-Toth, A. *Anal. Chem.*, Submitted.
- Bravo, R.; Hsueh, C. C.; Jaramillo, A.; Brajter-Toth, A. *Analyst* **1998**, 123, 1625.
- Bremle, G.; Persson, B.; Gorton, L. *Electroanalysis* **1991**, 3, 77.
- Cabannis, E. G.; Diamantis, A. A.; Murphy, R. W.; Linton, W. R.; Meyer, J. T. *J. Am. Chem. Soc.* **1985**, 107, 1845.
- Cahill, S. P.; Walker, D. Q.; Finnegan, Q. D.; Mickelson, J. M.; Travis, G. E.; Wightman, R. M. *Anal. Chem.* **1996**, 68, 3180.
- Cai, X.; Kalcher, K.; Neuhold, C.; Oborevc, B. *Talanta* **1994**, 41, 407.
- Capella, P.; Ghasemzadeh, B.; Mitchell, K.; Adams, N. R. *Electroanalysis* **1990**, 2, 175.
- Cavalheiro, T. E.; Brajter-Toth, A. *J. Pharm. Biomed. Anal.* **1999**, 19, 217.
- Chen, G.; Gavin, P. F.; Luo, G.; Ewing, A. G. *J. Neurosci.* **1995**, 15, 7747.
- Chen, K.T.; Strein, G.T.; Abe, T.; Ewing, G. A. *Electroanalysis* **1994**, 6, 746.

- Cheng, H.Y.; Falat, L. *Anal. Chem.* **1982**, 54, 2111.
- Cheng, H.; Falat, L. *J. Electroanal. Chem.* **1983**, 157, 393.
- Cheng, Q.; Brajter-Toth, A. *Anal. Chem.* **1992**, 64, 1998.
- Cheng, Q.; Brajter-Toth, A. *Anal. Chem.* **1995**, 67, 2767.
- Cheng, Q.; Brajter-Toth, A. *Anal. Chem.* **1996**, 68, 4180.
- Cooper, C. J.; Hall, H. A. E. *Biosens. Bioelectron.* **1992**, 7, 85.
- Cosnier, S.; Innocent, C. *J. Electroanal. Chem.* **1992**, 328, 361.
- Cui, Q. C.; Ong, H. L.; Tan, T. C.; Lee, Y. J. *J. Electroanal. Chem.* **1993**, 346, 477.
- Deussen, A.; Bjorst, M.; Kroll, M.; Schrader, J. *Cir. Res.* **1988**, 63, 250.
- Diaz, A.F.; Castillo, J. I. *J. Chem. Soc. Chem. Commun.* **1980**, 397.
- Diaz, A.F.; Kanazawa, K.K.; Gardini, G. P. *J. Chem. Soc. Chem. Commun.* **1979**, 635.
- Dilena, B. A.; Peake, M. J.; Pardue, H. L.; Skorg, J. W. *Clin. Chem.* **1986**, 32, 486.
- Dong, S.; Jin, Z. *J. Chem. Soc., Chem. Commun.* **1987**, 1871.
- Downard, J. A.; Roddick, D. A.; Bond, M. A. *Anal. Chim. Acta* **1995**, 317, 303.
- Dresselhaus, M. S.; Dressalhaus, G.J. *Electrocera.* **1997**, 1, 273.
- Dresselhaus, M. S.; Fung, P. W. A.; Rao, M. A.; DiVittorio, L. S.; Kuriyama, K.; Dresselhaus, G.; Endo, M. *Carbon* **1992**, 30, 1065.
- Dryhurst, G. *Top. Curr. Chem.* **1972(a)**, 34, 47.
- Dryhurst, G. *J. Electrochem. Soc.* **1972(b)**, 119, 1659.
- Duff, A.; O'Neill, R. D. *J. Neurochem.* **1994**, 62, 1496.
- Edison, A. T. *Manufacture of Carbon Filaments* (438,299), Oct. 10, 1890.
- Edison, A. T. *Manufacture of Filaments for Incandescent Electric Lamps* (438,299) Feb. 14, 1891.
- Emr, A. S.; Yacynych, M. A. *Electroanalysis* **1995**, 7, 10, 913.

- Engstrom, C. R.; Strasser, A. V. *Anal. Chem.* **1984**, 56, 136.
- Evans, J. F.; Kuwana, T. *Anal. Chem.* **1977**, 49, 1632.
- Ewing, G. A.; Bigelow, C. J.; Wightman, M. R. *Science* **1983**, 221, 169.
- Ewing, G. A.; Dayton, A. M.; Wightman, M.R. *Anal. Chem.* **1981**, 53, 1842.
- Fagan, D.; Hu, I.; Kuwana, T. *Anal. Chem.* **1985**, 57, 2759.
- Fan, F. R. F.; Kwak, J.; Bard, J. A. *J. Am. Chem. Soc.* **1996**, 118, 9669.
- Feng, X.; Kasser, R.; Brazell, M.; Renner, K. J.; Adams, R. N. *Anal. Chem.* **1987**, 59, 1863.
- Fox, R.; James-Armstrong, M.; Millar, J. *J. Neurosci. Meth.* **1980**, 3, 37.
- Frei, B.; England, L.; Ames, B. N. *Proc. Natl. Acad. Sci. USA* **1989**, 76, 5366.
- Freund, M. S.; Bodalbhai, L.; Brajter-Toth, A. *Talanta* **1991**, 38, 95.
- Freund, M.; Brajter-Toth, A. *J. Phys. Chem.* **1992**, 96, 9400.
- Freund, S. M.; Cotton, M. T.; Henderson, R. E.; Brajter-Toth, A. *Anal. Chem.* **1991**, 63, 1047.
- Frysz, C.; Shui, X.; Chung, L. D. *Carbon*, **1997**, 35, 893.
- Funt, B. L. In *Encyclopedia of Polymer Science and Engineering*, Vol 5, John Wiley, New York, **1986**, p 587.
- Gagnon, G. E.; Austin, G. L. *J. Electrochem. Soc.* **1973**, 120, 2, 251.
- Gao, Z.; Ivaska, A. *Anal. Chim. Acta* **1993**, 284, 393.
- Gao, Z.; Zi, M.; Chen, B. *J. Electroanal. Chem.* **1994**, 373, 141.
- Geise, R. J.; Adams, M. J.; Barone, J. N.; Yacynych, M. A. *Biosens. Bioelectron.* **1991**, 6, 151.
- Genies, E. M.; Bidan, G.; Diaz, A. F. *J. Electroanal. Chem.* **1983**, 149, 101.
- Gerhardt, A. G.; Oke, F. A.; Nagy, G.; Moghaddam, B.; Adams, N. R. *Brain Res.* **1984**, 290, 390.
- Gilmartin, T. A. M.; Hart P. J.; Birch, J. B. *Analyst* **1994**, 119, 243.

- Gilmartin, T. A. M.; Hart, P. J. *Analyst* **1994**, 119, 833.
- Gilmartin, T. A. M.; Hart, P. J.; Birch, J. B. *Analyst* **1992**, 117, 1299.
- Gomathi, H.; Rao, P.G. *J. Electroanal. Chem.* **1985**, 190, 85.
- Gonon, F. *Neurosci.* **1988**, 24, 19.
- Gonon, F.; Cespuglio, R.; Ponchon, J-L; Buda, M.; Jouvet, M.; Adams, R.N.; Pujol, J-F. *Compte Rendus.* **1978**, 286, 1203.
- Gonon, F.; Navane, F.; Buda, M. *Anal. Chem.* **1984**, 56, 573.
- Gonon, F.; Ponchon, J. L.; Cespuglio, R.; Jouvet, M.; Pujol, J. F. *Anal. Chem.* **1979**, 51, 1483.
- Gonon, F.G.; Fombarlet, C.M.; Buda, M. J. Pujol F. J. *Anal. Chem.* 1981, 53, 1386.
- Gonon, G.; Buda, J. M., *Neurosci.* **1985**, vol 14, No 3, 765.
- Gorton, L.; Karan, H. I.; Hale, P. D.; Inagaki, T.; Okamoto, Y.; Skotheim, A. T. *Anal. Chem. Acta* **1990**, 228, 23.
- Goss, C. A.; Brumfield, J. C.; Irene, E. A.; Murray, R. W. *Anal. Chem.* **1993**, 65, 1378.
- Goyal, N. E.; Mittal, A.; Sharma, S. *Electroanalysis* **1994**, 6, 609.
- Grupp, G. In *Methods in Pharmacology*, vol. 5, Schwartz, A. (ed.), Plenum Press, New York, 1984.
- Guadalupe, A. R.; Abruña, H. D. *Anal. Chem.* **1986**, 58, 3257.
- Haeckel, H. *Clin. Chem. Acta* **1978**, 24, 1846.
- Harper, H. A. *Review of Physiological Chemistry* **1977**, Lange Medical Publications, CA, 16th edn., p.406.
- Hartwick, R. A.; Assenza, S. P.; Brown, P. R. *J. Chromatog.* **1979**, 186, 659.
- Hathcock, W. K.; Brumfield, C. J.; Goss, A. C.; Irene, A. E.; Murray, W. R. *Anal. Chem.*, 1995, 67, 2201.
- Heineman, R. W. *Current Separation* **1985**, 7, 58.
- Henry, J. R.; Sobel, C.; Kim, J. *Amer. J. Clin. Pathol.* **1957**, 28, 152.

- Heyrovsky, J. *Recl. Trav. Chim. Pays-Bas* **1925**, 44, 488.
- Hirst, J.; Duff, J. L. C.; Jameson, G. N. L.; Kemper, M. A.; Burgess, B. K.; Armstrong, F. A. *J. Am. Chem. Soc.* **1998**, 120, 7085.
- Holdcroft, S.; Funt, B. L. *J. Appl. Electrochem.* **1988**, 135, 3106.
- Howel, R. M.; Wightman, M. R. *Anal. Chem.* **1984**, 56, 524.
- Howell, O. J.; Kurh, G. W.; Ensman, E. R.; Wightman, R. M. *J. Electroanal. Chem. Interfacial Electrochem.* **1986**, 209, 77.
- Hsueh, C. C. New Strategies to Improve Selectivity and sensitivity with Ultramicroelectrodes, Ph. D. Thesis, University of Florida, 1994.
- Hsueh, C. C.; Brajter-Toth, A. *Anal. Chim. Acta* **1996**, 321, 209.
- Hsueh, C.; Brajter-Toth, A. *Anal. Chem.* **1994**, 66, 2458.
- Hsueh, C.C., Bravo, R., Jaramillo, A., and Brajter-Toth, A. *Anal. Chim. Acta* **1997**, 349, 67.
- Hsueh, C.C.; Brajter-Toth, A. *Anal. Chem.* **1993**, 65, 1570.
- Hu, F.I.; Karweik, D. H.; Kuwana, T. *J. Electroanal. Chem.* **1985**, 188, 59.
- Hu, F.I.; Karweik, D. H.; Kuwana T. *Anal. Chem.* **1985**, 57, 545.
- Hua, C.; Walsh, S.; Smyth, R. M.; Svancara, I.; Vytros, K. *Electroanalysis* **1992**, 4, 107.
- Huang, H.; He, P.; Faulkner, L. *Anal. Chem.* **1986**, 58, 2889.
- Ianniello, M. R.; Lindsay, J. T.; Yacynych, M. A. *Anal. Chem.* **1982**, 54, 1980.
- Ikeda, O.; Yoneyama, H. *J. Electroanal. Chem.* **1989**, 265, 323.
- Imisides, D. M.; John, R.; Wallace, G. G. *Chemtech*, May **1996**, 19.
- Iwamoto, T.; Yoshiura, M.; Iriyama, K. *J Chromatogr.* **1983**, 278, 156.
- Jankowski, J. A.; Schroeder, C.; E. L.; Wightman, R. M. *J. Biol. Chem* **1993**, 268, 14694.
- Jennings, R. B.; Morgan, H. E. In *The Heart and Cardiovascular System*, 2nd Ed., Fozzard, H.A., et. al. (Ed), Raven Press, Ltd., New York, 1992.

- John, R.; John, M. S.; Wallace, G. G.; Zhao, H. In *Electrochemistry in Colloids and Dispersions*, Mackay, R.A., Texter, J. Eds; VCR, New York, 1992.
- John, R.; Wallace, G. G. *J. Electroanal. Chem.* **1991a**, 306, 157.
- John, R.; Wallace, G. G. *J. Electroanal. Chem.* **1991b**, 354, 145.
- Jung, H. D.; Parekh, C.A. *Clin. Chem.* **1970**, 16, 247.
- Kamau, G. N.; Willis, S. W.; Rusling, F. *Anal. Chem.* **1985**, **57**, 545.
- Kanemitsu, H.; Tamura, A.; Sano, K. *J. Neurochem.* **1986**, 46, 851.
- Kaplan, A.; Jack, R.; Opheim E. K.; Toivola, b.; Lyon, W. A. *Clinical Chemistry*, Fourth Edition, Williams & Wilkins, Malvern, PA, 1995.
- Kashyap, R.; Gratzl, M. *Anal. Chem.* **1998**, 70, 8, 1468-1476.
- Kawagoe, P. A., Garriss, A. P.; Wightman, M. R. *J. Electroanal. Chem.* **1993**, 359, 193.
- Keita, B.; Essaadi, K.; Nadjo, L. *J. Electroanal. Chem.* **1989**, 259, 127.
- Keita, B.; Nadjo, L. *J. Electroanal. Chem.* **1985**, 191, 441.
- Keita, B.; Nadjo, L. *J. Electroanal. Chem.* **1988**, 243, 87.
- Keita, B.; Nadjo, L. *J. Electroanal. Chem.* **1990**, 287, 149.
- Keita, B.; Nadjo, L.; Savèant, M. J. *J. Electroanal. Chem.* **1988**, 243, 105.
- Kelly, R. S.; Weiss, D. J.; Chong, S.H.; Kuwana, T. *Anal. Chem.* **1999**, 71, 413.
- Kelly, R.; Wightman, R. M. *Anal. Chim. Acta.* **1986**, 187, 79.
- Kepley, L. J.; Bard, A. J. *Anal. Chem.* **1988**, 60, 1459.
- Kinoshita, K. *Carbon: Electrochemical and Physical Properties*, Wiley & Son's; New York, **1988**.
- Kissinger, P.T.; Felice, L. J.; Riggin, R. M.; Pachla, L. A.; Wenke, D. C. *Clin. Chem.* **1974**, 20, 992.
- Koopal, C. G. J.; Deruiter, B.; Nolte, R. J. M. *J. Chem. Soc. Chem. Comm.* **1991**, 23, 1691.

- Kovach, M. P.; Deakin, R. M.; Wightman, R. M. *J. Phys. Chem.* **1986**, 90, 4612.
- Kozlowski, C.; Sherwood, P. M. A. *J. Chem. Soc. Faraday Trans.* **1985**, 81, 2745.
- Kristensen, W. E.; Kuhr, G. W.; Wightman, R. M. *Anal. Chem.* **1987**, 59, 1751.
- Kuhr, G. W.; Barrett, L. V.; Gagnon, R. M.; Hopper, P.; Pantano, P. *Anal. Chem.* **1993**, 65, 617.
- Kuhr, G. W.; Wightman, R. M. *Brain Res.* **1986**, 381, 168.
- Kulesza, P. J.; Faulkner, R. L. *J. Electroanal. Chem.* **1988a**, 248, 305.
- Kulesza, P. J.; Faulkner, R. L. *J. Am. Chem. Soc.* **1988b**, 110, 4905.
- Kulesza, P. J.; Faulkner, R. L. *J. Electroanal. Chem.* **1989a**, 259, 81.
- Kulesza, P. J.; Faulkner, R. L. *J. Electrochem. Soc.* **1989b**, 136, 707.
- Kulys, J. J.; Laurinavicius, A. S. V.; Pesliakienė, V. M.; Gureviciene, V. U. *Anal. Chim. Acta.* **1983**, 141, 13.
- Kwak, J.; Bard, J. A. *Anal. Chem.* **1989a**, 61, 1221.
- Kwak, J.; Bard, J. A. *Anal. Chem.* **1989b**, 61, 1794.
- Lawrence, A. P.; Reynolds, D. L.; Wright, D. S.; Kissinger, P. *J. Assoc. Off. Anal. Chem.* **1987**, 70, 1.
- Layton, E. M.; Wood, G. J.; Yan, Y. Z.; Forster, J. *J. Surgical Res.* **1996**, 64, 1.
- Leszczyszyn, D. J.; Jankowski, J. A.; Viveros, O. H.; Diliberto, E. J.; Near, J. A.; Wightman, R. M. *J. Biol. Chem.* **1990**, 265, 14736.
- Long, T. L.; Weber, G. S. *Electroanalysis*, **1992**, 4, 429.
- Lord, S. S.; Rogers, L. B. *Anal. Chem.* **1954**, 56, 284.
- Lowen, S. V.; Van Dike, J. D. *J. Pol. Sci. Pol. Chem.* **1990**, 28, 451.
- Lyons, G. E. M.; Breen, W.; Cassidy, J. *J. Chem. Soc. Faraday trans* **1991**, 87, 115.
- Mao, H.; Pickup, G. P. *J. Electroanal. Chem.* **1989**, 265, 127.
- Marino, A.; Brajter-Toth, A. *Anal. Chem.* **1993**, 65, 370-374.

Marsden, C. A.; Joseph, H. M.; Kruk, L. Z.; Maidment, N. T.; O'Neill, D. R.; Schenk, O.; Stamford, A. J. *Neuroscience* **1988**, 25, 389.

Marsh, H. A.; Dryhurst, G. *J. Electroanal. Chem.* **1979**, 95, 81.

Matsue, T. *Denki Kagaku*, **1991**, 59, 92.

McCreery, L. R. In *Electroanalytical Chemistry*, Bard, A. J. (ed), Dekker, New York, vol 17, 1991.

McCreery, L. R.; Cline, K. K. In *Laboratory Techniques in Electroanalytical Chemistry*, Kissinger, T. P.; Heineman, R.W.(ed), 2nd ed, Dekker, New York, 1996.

Mei, A. D.; Garrett, J. G.; Nithipatikom, K. *Anal. Biochem.* **1996**, 238, 34.

Michael, A. C.; Ikeda, M.; Justice, J. B. Jr. *Brain Res.* **1987**, 421, 325.

Michael, A. C.; Justice, J. B. *Anal. Chem.* **1987**, 59, 405.

Miland, E.; Ordieres, M. J. A.; Blanco, T. P.; Smyth, R. M.; Fagain, O.C. *Talanta* **1996**, 43, 785.

Miller, J. M.; Armstrong-James, M.; Kruk, L. Z. *Brain Res.* **1981**, 205, 419.

Mueller, K.; Palmour, R.; Andrews, C. D.; Knott, P. J. *Brain Res.* **1985**, 335, 231.

Murray, W. R. *Acc. Chem. Res.* **1980**, 13, 135.

Murray, W. R. In *Electroanalytical Chemistry*, A. J. Bard (ed.); Marcel Dekker: New York; Vol. 13, 1984.

Mustard, J. F.; Murphy, E. A.; Ogryzlo, M. A. *Can. Med. Assoc. J.* **1963**, 89, 1207.

Myrick, L. M.; Noll, D. J.; Nicholson, A. M. *J. Electrochem. Soc.* **1998**, 145, 179.

Nakazato, T.; Hosada, S.; Akiyama, A. *J. Neurosci. Meth.* **1993**, 46, 69.

Netchiporouk L. I.; Shulga A. A.; Jaffrezic-Renault N.; Martelet C.; Olier R.; Cespuglio R. *Anal. Chim. Acta* **1995**, 303, 275.

Noll, D. J.; Nicholson, A. M.; Van Patten, G. P.; Chung, W. C.; Myrick, L. M. *J. Electrochem. Soc.* **1998**, 145, 3320.

Nowall, W. B.; Kuhr, W. G. *Anal. Chem.* **1995**, 67, 3583.

O'Brien, C. J.; Shumaker-Parry, J.; Engstrom, C. R. *Anal. Chem.* **1998**, 70, 1307.

Oldham, B. K.; Myland, C. J. *Fundamental of Electrochemistry Science* Acad.Press, INC: San Diego, CA, 1994.

Owens, J.; Henry, A.; Dryhurst, G. *J. Electroanal. Chem.* **1978**, 231.

Owens, L. J.; Dryhurst, G. *Anal. Chim. Acta* **1977**, 89, 93.

Palmisano, F.; Guerrieri, A.; Quinto M.; Zambonin, G. P. *Anal. Chem.* **1995**, 67, 2084.

Pantano, P.; Kuhr, G. W. *Anal. Chem.* **1993**, 65, 623.

Paras, D. C.; Kennedy, T. R. *Anal. Chem.* **1995**, 67, 3633.

Persky, V. W.; Dyer, A. R.; Idris-Sovene, A. *Circulation* **1979**, 59, 969.

Pihel, K.; Hsieh, S.; Jorgenson, W. J.; Wightman, M. R. *Anal. Chem.* **1995**, 67, 4514.

Pihel, K.; Schroeder, J. T.; Wightman, R. M. *Anal. Chem.* **1994**, 66, 4532.

Pihel, K.; Walker, D. Q.; Wightman, M. R. *Anal. Chem.* **1996**, 68, 2084.

Pilleggi, J. V.; DiGiorgio, J.; Wybenga, R. D. *Clinica Chim Acta.* **1971**, 37,141.

Pishko, V. M.; Michael, C. A.; Heller, A. *Anal. Chem.* **1991**, 63, 2268.

Pope, M. T.; Varga, G. M. *Inorg. Chem.* **1966**, 5, 1249.

Raymond, D.E.; Harrison, D. J. *J. Electroanal. Chem.* **1993**, 361,65.

Reynolds, R. E.; Yacynych, M. *Electroanalysis* **1993**, 5, 405.

Rhode, E. E.; Dempsey, E.; Smyth, R. M.; Vos, G. J. *Anal. Chim. Acta.* **1993**, 278,

Rice, M. E.; Nicholson, C. *Anal. Chem.*, **1989**, 61, 1805.

Rojo, A.; Rosenstratten, A.; Anjo, M. D. *Anal. Chem.* **1986**, 58, 2988.

Rong, C.; Anson, F. C. *Anal. Chem.* **1994**, 66, 3124.

Rong, C.; Anson, F. C. *Inorg. Chim. Acta* **1996**, 242, 11.

Sadakne, M.; Steckhan, E. *Chem. Rev.* **1998**, 1, 219.

Sadik, O. A.; Wallace, G. G. *Electroanalysis* **1994**, 6, 860.

- Saint-Aman, E.; Ungureanu, M.; Visan, T.; Moutet, J. C. *Electrochim. Acta* **1997**, *42*, 1829.
- Saruceno, A. R.; Pack, G. J.; Ewing, G. A. *J. Electroanal. Chem.* **1986**, *197*, 265.
- Saunders, R. B.; Fleming, J. R.; Murray, S. K. *Chem. Mater.* **1995**, *7*, 1082.
- Scharifker, B. R.; Garcia-Pastoriza, E.; Marino, W. J. *J. Electroanal. Chem.* **1991**, *300*, 85.
- Schroeder, T. J.; Jankowski, J. A.; Kawagoe, K. T.; Wightman, R. M.; Lefrou, C.; Amatore, C. *Anal. Chem.* **1992**, *64*, 3077.
- Senftleber, F. C.; Halline, A. G.; Veening, H.; Dayton, D. *Clin. Chem.* **1976**, *22*, 1522.
- Shirakawa, H.; Louis, E. J.; MacDiarmid, A. G.; Chiang, C. K.; Heeger, A. J. *J. Chem. Soc. Chem. Commun.* **1977**, 578.
- Snider, K. E.; Merzbacher, C. I.; Hagus, P. L.; Rolison, D. R. *Chem. Mater.* **1997**, *9*, 1248.
- Stackelberg, M.; Pilgram, M.; Toome, V. *Z. Electrochim.* **1953**, *57*, 342-447.
- Stamford, J. *J. Neurosci. Meth.* **1986**, *17*, 1.
- Stamford, J. *J. Neurosci. Meth.* **1990**, *34*, 67.
- Stamford, J. *Trends in Neurosc.* **1989**, *12*, 10, 407.
- Stamford, J. A.; Kruk, L. Z.; Miller, J. M. *Brain Res.* **1986**, *381*, 351.
- Star, L. V. *Hospital Medicine* **1995**, November, 25.
- Strein, G. T.; Ewing, G. A. *Anal. Chem.* **1991**, *63*, 194.
- Swain, M. G.; Kuwana, T. *Anal. Chem.* **1992**, *64*, 565.
- Tanaka, K.; Shichiri, T.; Wang, S.; Yananbe, T. *Synth. Met.* **1988**, *24*, 203.
- Tayag, E.; Nair, N.S.; Wahhab, S.; Katsetos, D. C.; Lighthall, J. W.; Lehmann, C. J. *Brain Research*, **1996**, *733*, 287.
- Thorp, H. M. *J. Chem. Ed.* **1992**, *69*, 250.
- Tietz, N. W.; In *Fundamentals of Clinical Chemistry*, 2nd. ed., Saunders B. W. Co., Philadelphia, Pa, 1974.

- Tschuncky, P.; Heintze, J. *Anal. Chem.* **1995**, 67, 4020.
- Unwin, P. R.; Bard, J. A. *Anal. Chem.* **1992**, 64, 113.
- Van Wylen, L. G. D.; Schmit, J. T.; Lasley, D. R.; Gingell, L.R.; Mentzer, M. R. *Am. J. Physiol.* **1992**, H1934.
- Wang, B.; Dong, S. *Electrochim. Acta* **1996**, 41, 895.
- Wang, B.; Dong, S. *J. Electroanal. Chem.* **1992**, 328, 245.
- Wang, J.; Leech, D.; Ozsoz, M.; Martinesz, S.; Smyth, R. M. *Anal. Chim. Acta.* **1991**, 245, 139.
- Wang, J.; Tuzhi, P. *Anal. Chem.* **1986**, 58, 3257.
- Wang, J.; Tuzhi, P.; Villa, V. *J. Electroanal. Chem.* **1987**, 234, 119.
- Watanabe, T.; Tatsuma, T. *Anal. Chim. Acta.* **1991**, 242, 85.
- Wehmeyer, R. M.; Wightman, R. M. *J. Electroanal. Chem.* **1995**, 196, 417.
- Wen, J.; Baranski, J.; Cassidy, R. *Anal. Chem.* **1998**, 70, 8, 2504.
- Whiteley, D. L.; Martin, R. C. *Anal. Chem.* **1987**, 59, 1746.
- Whiteley, L.; Martin, C. *Mol. Cryst. Liq. Cryst.* **1988**, 160, 359.
- Wiedemann, D. J.; Kawagoe, T. K.; Kennedy, T. R.; Ciolkowski, E.; Wightman, R. M. *Anal. Chem.* **1991**, 63, 2965.
- Wightman M. R.; Wipf, O. D. In *Electroanalytical Chemistry*, A. J. Bard (Ed.); Marcel Dekker: New York, Vol. 15, 1989.
- Wightman, R. M.; Dayton, A. M.; Brown, K. J.; Stutts, J. K. *Anal. Chem.* **1980**, 52, 946.
- Wightman, M. R.; Weltmeyer, K. R.; Deakin, M. R. *Anal. Chem.* **1985**, 57, 1913.
- Wightman, R. M.; May, J. L.; Michael, C. A. *Anal. Chem.* **1988**, 60, 769A-779A.
- Wightman, R. M.; Deakin, R. M.; Kovach, M. P.; Kuhr, G. W.; Stutts, J. K. L. *Electrochem. Soc.* **1984**, 131, 1578.
- Winsatt, H. J. In *Gout, Hyperuricemia, and other Crystal-Associated Arthropathies*, Eds Smyth, J. C.; Holers, M. V., Marcel Dekker, New York, 1999.

- Wipf, O. D.; Kristensen, W. E.; Deakin, M. R.; Wightman, R. M. *Anal. Chem.* **1988**, 60, 306.
- Witkowski, A.; Brajter-Toth, A. *Anal. Chem.* **1992**, 64, 635.
- Witkowski, A.; Freund, M. S.; Brajter-Toth, A. *Anal. Chem.* **1991**, 63, 622.
- Wood, A. G.; Iroh, O. J. *Synthetic Met.* **1996**, 80, 73.
- Wrona, M.Z.; Owens, J. L.; Dryhurst, G. J. *Electroanal. Chem.* **1979**, 105, 295.
- Wun, W. E.; Howell, S. B. *Clin. Chem.* **1980**, 26, 1704.
- Wyngaarden, B. J.; Kelley, N. W. *Gout and Hyperuricemia*, Grune & Statton Inc, 1976.
- Xi, X.; Dong, S. *Electrochim. Acta* **1995**, 40, 2785.
- Xi, X.; Dong, S. *J. Mol. Cata. A: Chemical* **1996**, 114, 257.
- Zagorska, M.; Pron, A.; Lefrant, S.; Kucharski, Z.; Suwalski, J.; Bernier, P. *Synth. Met.* **1987**, 18, 43.
- Zak, J.; Kuwana, T. *J. Am. Chem. Soc.* **1982**, 104, 5514.
- Zen, M. J.; Jou, J. J.; Ilangoan, G. *Analyst* **1998**, 123, 1345.
- Zhang, J.; Wang, E. *J. Electroanal. Chem.* **1995**, 399, 83.
- Zhang, Z.; Lei, C.; Sun, W.; Liu, H.; Deng, J. *J. Electroanal. Chem.* **1996**, 419, 85.
- Zoski, C. G.; Bond, A. M.; Allinson, E. T.; Oldham, K. B. *Anal. Chem.* **1990**, 62, 37.


BIOGRAPHICAL SKETCH

Robert Bravo was born in Santiago de Cali, Colombia on August 14, 1962, to Manuel Bravo and Maria Teresa Cardenas. In August 1978, he graduated from secondary school from Colegio Guillermo Valencia. In the winter of 1979, he began his undergraduate education in Biology and Chemistry at Universidad Santiago de Cali. In 1984, he obtained a B. Ed. in Biology and Chemistry. In 1981, Roberto was also accepted to Universidad del Valle (Univalle) for the fall of 1982. He received his B. S. in Chemistry from Univalle in September of 1987 after a six-month internship at Americana de Grasas y Aceites, Cali, Colombia. During his undergraduate days at Univalle, Roberto started dating his lovely fiancé, Maria Ospina.

Roberto worked at Varela for about three years as a research assistant. He worked also as chemist in quality control of pharmaceutical products at Bristol-Myers Squibb, Cali, for one year. At that time, his fiancé was offered the opportunity of working as a research assistant in the Spectroscopic Service Laboratory of the University of Florida doing mass spectrometry. Roberto decided to come with his fiancé to the U. S. even though he spoke no English at all. Roberto studied English at the English Language Institute of the University of Florida for one semester. He also took classes at Santa Fe Community College for one year until he was able to fulfill the requirements for graduate school. Roberto began graduate school in August of 1994. He investigated the development of surfaces for enhancement of selectivity and sensitivity with carbon fiber

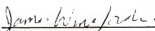
electrodes under the direction of Dr. Anna Brajter-Toth. Upon graduation, Roberto will move to Atlanta, Georgia, to join his sweetheart Maria.

I certify that I have read this study and that in my opinion it conforms to acceptable standards of scholarly presentation and is fully adequate, in scope and quality, as a thesis for the degree of Doctor of Philosophy.



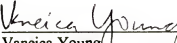
Anna Brajter-Toth
Associate Professor of Chemistry

I certify that I have read this study and that in my opinion it conforms to acceptable standards of scholarly presentation and is fully adequate, in scope and quality, as a thesis for the degree of Doctor of Philosophy.




James Winefordner
Graduate Research Professor of
Chemistry

I certify that I have read this study and that in my opinion it conforms to acceptable standards of scholarly presentation and is fully adequate, in scope and quality, as a thesis for the degree of Doctor of Philosophy.



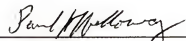
Vaneica Young
Associate Professor of Chemistry

I certify that I have read this study and that in my opinion it conforms to acceptable standards of scholarly presentation and is fully adequate, in scope and quality, as a thesis for the degree of Doctor of Philosophy.



John Reynolds
Professor of Chemistry

I certify that I have read this study and that in my opinion it conforms to acceptable standards of scholarly presentation and is fully adequate, in scope and quality, as a thesis for the degree of Doctor of Philosophy.



Paul Holloway
Professor of Materials Science
and Engineering

This thesis was submitted to the Graduate Faculty of the Department of Chemistry in the College of Liberal Arts and Sciences and to the Graduate School and was accepted as partial fulfillment of the requirements for the degree of Doctor of Philosophy.

August 1999

Dean, Graduate School